



UNIVERSIDAD DE INVESTIGACIÓN DE TECNOLOGÍA EXPERIMENTAL YACHAY

Escuela de Ciencias Químicas e Ingeniería

TÍTULO: Synthesis and characterization of fluorescent carbon quantum dots from citric acid as potential optical sensor for the detection of metal cations

Trabajo de integración curricular presentado como requisito para la obtención del título de Magíster en Ciencias Químicas con mención en Ciencia e Ingeniería de los Materiales

Autor:

Cánchig Rodríguez María Belén

Tutor:

Ph.D. Saucedo Juan Pablo

Co-tutor:

Ph.D. Caetano Manuel

Urcuquí, Julio 2024

AUTORÍA

Yo, **CÁNCHIG RODRÍGUEZ MARÍA BELÉN**, con cédula de identidad 1725031635, declaro que las ideas, juicios, valoraciones, interpretaciones, consultas bibliográficas, definiciones y conceptualizaciones expuestas en el presente trabajo; así cómo, los procedimientos y herramientas utilizadas en la investigación, son de absoluta responsabilidad de el/la autor (a) del trabajo de integración curricular. Así mismo, me acojo a los reglamentos internos de la Universidad de Investigación de Tecnología Experimental Yachay.

Urcuquí, Julio 2024

María Belén Cánchig Rodríguez CI: 1725031635

Autorización de publicación

Yo, **CÁNCHIG RODRÍGUEZ MARÍA BELÉN**, con cédula de identidad 1725031635, cedo a la Universidad de Investigación de Tecnología Experimental Yachay, los derechos de publicación de la presente obra, sin que deba haber un reconocimiento económico por este concepto. Declaro además que el texto del presente trabajo de titulación no podrá ser cedido a ninguna empresa editorial para su publicación u otros fines, sin contar previamente con la autorización escrita de la Universidad.

Asimismo, autorizo a la Universidad que realice la digitalización y publicación de este trabajo de titulación en el repositorio virtual, de conformidad a lo que dispone la Ley Orgánica de Educación Superior

San Miguel de Urcuquí, Julio 2024

María Belén Cánchig Rodríguez

CI: 1725031635

Dedication

A mis padres, Nancy y Jorge, por todo su amor y apoyo.

A mi hermano, Stalin, por cuidar de mí desde que tengo uso de razón.

A mi prima, María Gabriela, por ser como mi hermana mayor, tan incondicional y a la vez ser mi confidente.

A mi sobrina Yuyu.

Acknowledgments

I would like to express my deepest gratitude to my supervisors and advisors for their invaluable support throughout my academic journey. I extend special thanks to **Juan Pablo Saucedo, Ph.D.** and **Manuel Caetano, Ph.D.** for their scientific guidance and enlightening discussions that significantly enhanced my knowledge. Their patience and practical assistance in the laboratory were essential to my progress.

I am particularly grateful to **Thibault Terencio, Ph.D.**, whose shared expertise was crucial for my research and the presentation of my results. His insights and mentorship were fundamental to the success of this work.

I wish to express my most sincere gratitude to Senescyt for the financial support provided through the national postgraduate scholarship program 416 “Fortalecete 2022” ARSEQ-BEC-006913-2022 for the realization of this research.

My sincere appreciation goes to the jury members, especially **Floralba Lopez, Ph.D.**, **Joan Vera, Ph.D.**, and **Juan Pablo Saucedo, Ph.D.** for their valuable revisions and constructive feedback. Their contributions have substantially improved the quality of my work.

I am profoundly thankful to Yachay Tech University, particularly the School of Chemical Sciences and Engineering, for providing an excellent educational foundation. I extend my heartfelt gratitude to all my professors for their unwavering motivation and support throughout my master’s studies.

Lastly, I am deeply grateful to my **parents** and **brother** for their unconditional love, care, and sacrifices to support my education and daily life. I also want to express my appreciation to everyone who has supported me, both directly and indirectly, in the completion of my research work. Your collective encouragement and assistance have been invaluable to my academic journey. Thanks to them, my smile is brighter and my laugh is louder.

Abstract

Carbon Quantum Dots (CQDs), as fluorescent nanomaterials based on carbon, have garnered significant interest due to their small size, high chemical stability, excellent water solubility, low cost, and intriguing optical properties. These nanoparticles and their modified versions have applications in nanotechnology, such as light sources for televisions and LED lamps, and in biomedical fields, guiding surgeons during tumor removal.

This study aims to synthesize citric acid CQDs functionalized with N, S, and O donors via hydrothermal synthesis, comparing the effects of such different heteroatoms on their properties, evaluating the influence of constituent components and synthesis parameters. CQDs were synthesized using six different precursors: cinnamic acid, allicin, 2-mercaptoethanol, L-cysteine (L-CQDs), ethylenediamine (E-CQDs), and diethylenetriamine (D-CQDs).

TEM analysis revealed that the size of L-CQDs ranged between 3 and 5 nm. UV-Vis spectroscopy confirmed the characteristic transitions for L-CQDs, E-CQDs, and D-CQDs, while FT-IR results confirmed the incorporation of each precursor into the CQDs, revealing structural differences in the heteroatoms. Concentration studies showed that L-CQDs and D-CQDs suffered from aggregation-induced quenching, while E-CQDs exhibited aggregation-induced emission. To stabilize CQDs over time, they were incorporated into polymer matrices (VCL-PEGDA and NIPA), which demonstrated an increase in fluorescent properties over time.

An optical sensor based on CQDs was developed for the selective and sensitive detection of metal ions in aqueous media. Selectivity studies revealed sensitivity to Cd^{2+} for L-CQDs and to Hg^{2+} for E-CQDs and D-CQDs. Theoretical models using Time-Dependent Density Functional Theory (TD-DFT) were employed to elucidate the underlying photophysical mechanisms, revealing that the functional groups in the carbon structures affect the optical properties of the CQDs.

Keywords: *Carbon Quantum Dots, doped, quenching, mercury detection, polyethylene glycol diacrylate, cations detection .*

Resumen

Los puntos cuánticos de carbono (CQDs) como nanomateriales fluorescentes basados en el carbono, han despertado un gran interés debido a su pequeño tamaño, alta estabilidad química, excelente solubilidad en agua, bajo costo y propiedades ópticas fascinantes. El reciente Premio Nobel de Química 2023, otorgado a Mounji G. Bawendi, Louis E. Brus y Aleksey Yakimov por el descubrimiento y síntesis de los puntos cuánticos, que han sido objeto de cientos de investigaciones desde su descubrimiento, resalta el potencial de estos materiales. Estas nanopartículas y sus versiones modificadas tienen aplicaciones en nanotecnología, como fuentes de luz para televisores y lámparas LED, y en biomedicina, guiando a los cirujanos durante la extirpación de tumores.

El objetivo de este estudio es sintetizar CQDs de ácido cítrico funcionalizados con donadores de N, S y O mediante síntesis hidrotermal, haciendo una comparación de los efectos de los diferentes heteroátomos sobre sus propiedades, evaluando la influencia de los componentes y los parámetros de síntesis. Los CQDs se sintetizaron utilizando seis precursores diferentes: ácido cinámico, alicina, 2-mercaptoetanol, L-cisteína (L-CQDs), etilendiamina (E-CQDs) y dietilentriamina (D-CQDs).

El análisis morfológico realizado por TEM reveló que el tamaño de los L-CQDs oscilan entre 3 y 5 nm. La espectroscopia UV-Vis confirmó las transiciones características de los L-CQDs, E-CQDs y D-CQDs, mientras que los resultados de FT-IR confirmaron la incorporación de cada precursor, revelando diferencias estructurales en los heteroátomos. Los estudios de concentración mostraron que los L-CQDs y los D-CQDs sufrían un apagamiento inducido por agregación, mientras que los E-CQDs presentaban una emisión inducida por agregación. Para estabilizar los CQDs a lo largo del tiempo, se incorporaron a matrices poliméricas (VCL-PEGDA y NIPA), que demostraron un aumento de las propiedades fluorescentes con el tiempo.

Se desarrolló un sensor óptico basado en CQDs para la detección selectiva y sensible de iones metálicos en medios acuosos. Los estudios de selectividad revelaron sensibilidad a

Cd^{2+} para L-CQDs y a Hg^{2+} para E-CQDs y D-CQDs. Se emplearon modelos teóricos utilizando la Teoría del Funcional de la Densidad Dependiente del Tiempo (TD-DFT) para dilucidar los mecanismos fotofísicos subyacentes, revelando que los grupos funcionales en las estructuras de carbono afectan a las propiedades ópticas de los CQDs.

Palabras Clave: Puntos cuánticos de carbono, dopamiento, quencheo, detección de mercurio, diacrilato de polietilenglicol, detección de cationes.

Contents

Dedication	iii
Acknowledgments	iv
Abstract	v
Resumen	vi
Contents	viii
List of Tables	xii
List of Figures	xiii
Abbreviations	xvi
1 Introduction	1
1.1 Problem statement	1
1.2 Justification	2
1.3 Objectives	2
1.3.1 General objective	2
1.3.2 Specific objectives	2

2	Theoretical Background	4
2.1	Carbon Quantum Dots	7
2.1.1	Structural Properties	7
2.1.2	Electrochemical properties	8
2.1.3	Optical and electronic properties of CQDs	9
2.2	Synthesis Methods of CQDs	12
2.3	Surface Modification and Doping	13
2.3.1	Surface Oxidation	13
2.3.2	Passivation	14
2.3.3	Doping Heteroatoms	14
2.4	Applications of CQDs	16
2.4.1	Bioimaging	16
2.4.2	Photocatalysis	16
2.4.3	Sensors	16
2.4.4	Optoelectronic Devices	18
2.5	CQDs in Composites	19
2.5.1	Carbon Quantum Dots - Polymer Composites	19
2.5.2	CQDs-Polymeric Hydrogels	20
3	Methodology	21
3.1	Reagents	21
3.2	Equipment	21
3.3	Synthesis of CQDs	22
3.3.1	Preparation of the L-CQDs Polycaprolactone nanofibers	23
3.3.2	Preparation of Hydrogel Optical with D-CQDs	25

3.4	Structural and Spectroscopic Characterization	25
3.4.1	Fluorescence spectroscopy analysis	25
3.4.2	FT-IR spectroscopy analysis	26
3.4.3	UV-Vis Absorbance	26
3.4.4	Transmission Electron Microscope (TEM)	26
3.4.5	High Resolution Transmission Electron Microscope (HRTEM)	26
3.5	Metal Sensing from CQDs-Hydrogel	27
3.5.1	Sensitivity to metal ions	27
3.5.2	Selectivite sensing	27
3.6	Computational Methods to estimate the properties of CQDs	29
3.6.1	Geometry Optimization	29
3.6.2	Spectroscopy Properties Calculations	29
4	Results and Discussion	31
4.1	Optical Properties of CQDs	31
4.1.1	Emission Photoluminescence Properties	31
4.1.2	UV-Vis Absorption Spectroscopy	34
4.2	Structural Analysis of CQDs	37
4.2.1	Transmission Electron Microscopy Analysis	37
4.2.2	Structural Analysis of CQDs by FT-IR	38
4.3	Stability of CQDs	44
4.3.1	Stability with concentration of CQDs	44
4.3.2	Stability with Time	47
4.4	Selectivity and Sensing Study of CQDs	49
4.4.1	Selectivity Study	49

4.4.2	Sensing with different metals	52
4.5	Computational Chemical Calculations	59
4.5.1	Geometry optimization of CQDs and CQDs with Hg ²⁺	59
4.5.2	UV-Vis calculations	63
4.5.3	Fluorescence analysis	67
4.6	Stability of CQDs with Polymers	71
4.6.1	Stability of LCQDs with polymers into a 1:1 ratio	71
4.6.2	Stability of L-CQDs and D-CQDs with VCL-co-PEGDA into 1:150 ratio polymer: CQDs	72
4.6.3	TEM Analysis of L-CQDs nanofibers	73
4.6.4	D-CQDs-Incorporated PEGDA Film for Selective Sensing of Hg ²⁺ ions	74
4.6.5	Characterization of D-CQDs-PEGDA Film	76
5	Conclusions and Recommendations	78
5.1	Conclusions	78
5.2	Recommendations for future work	79
	Bibliography	81

List of Tables

3.1	Amounts of precursors used in the synthesis of CQDs, their structures and the appearance of the dispersion obtained.	24
3.2	Metal concentration in Selectivity tests for each CQDs samples and Hydrogel	28
4.1	Assignments of IR bands spectra of L-CQDs	39
4.2	Assignments of IR spectra of E-CQDs	42
4.3	Assignments of IR spectra bands of D-CQDs	44
4.4	Distances between Hg and CQDs model structure	61
4.5	HOMO-LUMO energy levels and band gaps for different CQDs with and without Hg ²⁺ ions	62
4.6	Energy of Interaction for different CQDs with and without Hg ²⁺ ions	63

List of Figures

2.1	Applications of Carbon Quantum Dots	5
2.2	Schematic representation of carbon dot quenching in the presence of metal ions	17
3.1	Synthesis for L-CQDs, E-CQDs and D-CQDs	23
3.2	Structure of Poly(ethylene glycol) diacrylate	25
3.3	Structure of 2,2-Dimethoxy-2-phenylacetophenone	25
3.4	Input for Geometry optimization	29
3.5	Input for TDDFT calculations	30
4.1	PL spectra of CQDs obtained from L-cysteine (L-CQDs), ethylenediamine (E-CQDs), and Diethylenetriamine (D-CQDs) at the excitation wavelengths of 365, 465, and 635 nm	32
4.2	UV-Vis absorption spectra of synthesized carbon dots with l-cysteine	35
4.3	UV-Vis absorption spectra of synthesized carbon dots with ethylenediamine	36
4.4	UV-Vis absorption spectra of synthesized carbon dots with diethylenetriamine	37
4.5	TEM of CQDs obtained from a) L-cysteine (L-CQDs), b) ethylenediamine (ECQDs), and c) Diethylenetriamine (D-CQDs)	38
4.6	FT-IR spectra of a) L-Cysteine reference, b) citric acid reference and c) L-Cysteine CQDs	40
4.7	FT-IR Spectra of a) ethylenediamine reference, b) citric acid reference and c) ethylenediamine CQDs	41

4.8	FT-IR Spectra of a) diethylenetriamine reference, b) citric acid reference and c) diethylenetriamine CQDs	43
4.9	Fluorescence spectra of L-CQDs at different dilutions	45
4.10	Fluorescence Spectroscopy to different dilutions of Diethylenetriamine CQDs	45
4.11	Fluorescence Spectroscopy to different dilutions of Ethylenediamine CQDs	47
4.12	PL spectra of L-CQDs at different days	48
4.13	PL spectra of D-CQDs at different days	49
4.14	I/I ₀ ratio of L-CQDs in the presence of 50 ppm of various metal ions . . .	50
4.15	I/I ₀ ratio of E-CQDs in the presence of 50 ppm of various metal ions . . .	51
4.16	I/I ₀ ratio of D-CQDs in the presence of 50 ppm of various metal ions . . .	51
4.17	PL spectra of L-CQDs in the presence of Pb ²⁺ ion in a concentration range of 0-66 ppm	53
4.18	Fluorescence Spectroscopy to different dilutions of Ethylenediamine CQDs	54
4.19	PL spectra of L-CQDs in the presence of Cd ²⁺ ion (0-100 ppm)	54
4.20	Fluorescence Spectroscopy to different dilutions of L-CQDs in a concentration range of 1-100 ppm	55
4.21	PL spectra of E-CQDs in the presence of Hg ²⁺ ion in a range of 0-100 ppm	56
4.22	The relationship between fluorescence intensity ratio Log(I _o -I) of E-CQDs and mercury (II) concentration	57
4.23	PL spectra D-CQDs in the presence of Hg ²⁺ ion in a concentration range 0-300 ppm	58
4.24	Fluorescence Spectroscopy to different dilutions of Diethylenetriamine CQDs	59
4.25	The 4 CQDs models with different structural features a) Only Carbon (C) b) N-Modifier (N-CQDs) c) O-Modifier (O-CQDs) and d) S-Modifier (S-CQDs) optimized by CAM B3LYP	60
4.26	The 4 CQDs models with Hg ²⁺ a) Only Carbon b) N-Modifier c) O-Modifier and d) S-Modifier optimized by CAM B3LYP	61

4.27 UV-Vis spectra for L-CQDS a) experimental result b) nitrogen, c) carbon, d) oxygen and e) sulfur in structure	64
4.28 UV-Vis spectra for E-CQDS a) experimental result b) nitrogen, c) carbon and d) oxygen in structure	65
4.29 UV-Vis spectra for D-CQDS a) experimental result b) nitrogen, c) carbon and d) oxygen in structure	66
4.30 PL spectra for L-CQDS a) experimental result b) nitrogen, c) carbon, d) oxygen and e) sulfur in structure	68
4.31 PL spectra for E-CQDS a) experimental result b) nitrogen, c) carbon and d) oxygen in structure	69
4.32 PL spectra for D-CQDS a) experimental result b) nitrogen, c) carbon and d) oxygen in structure	70
4.33 Effect of concentration in L-Cysteine-CQDs: Relation 1:1 (left) and 1:150 (right) during 8 days	72
4.34 Effect of concentration on a ratio 1:150 with L-CQDs (left) and D-CQDs (right) in VCL-co-PEGDA	73
4.35 Transmission electron microscope (TEM) image Polycaprolactone embedded L-CQDs	74
4.36 a) Fluorescence response of D-CQDs PEGDA Film and b) D-CQDs PEGDA Film with Hg^{2+} under 365 nm light	75
4.37 The fluorescence intensity spectra of D-CQDs with Polyethylene Glycol diacrylate in the presence of Hg^{2+} ion (0-10 ppm)	76
4.38 FTIR spectra of D-CQDs, PEGDA and D-CQDs-PEGDA film	77

Abbreviations

PL Photoluminescence

QDs Quantum Dots

CQDs Carbon Quantum Dots

L-CQDs Carbon Quantum Dots of L-Cystein

E-CQDs Carbon Quantum Dots of Ethylenediamine

D-CQDs Carbon Quantum Dots of Diethylenetriamine

CnnA Cinnamic acid

ALLI Allicin

MPET 2- MercaptoethanoL

LCYS L-cysteine

EDA Ethylenediamine

DETA Diethylenetriamine

PEGDA Poly(ethylene glycol) diacrylate

DMPA 2,2- dimethoxy-2-phenylacetophenon

LOD Limit of Detection

LOQ Limit of Cuantification

C-CQDs Model Simulated of Carbon Quantum Dots only carbon

N-CQDs Model Simulated of Carbon Quantum Dots with nitrogen

O-CQDs Model Simulated of Carbon Quantum Dots with oxygen

S-CQDs Model Simulated of Carbon Quantum Dots with sulfur

FT-IR Fourier-transform infrared spectroscopy

HRTEM High Resolution Transmission Electron Microscope

TEM Transmission Electron Microscope

Chapter 1

Introduction

1.1 Problem statement

The rapid acceleration of economic development, urbanization, and population expansion have led to an increased demand for resources to support routine functions, creating significant challenges for both natural and human systems, including industrial, agricultural, and mining activities, as they endeavor to meet this growing demand. Consequently, an inevitable consequence of this scenario is a notable rise in environmental pollution, particularly water pollution, due to waste produced during the execution of diverse activities. [1, 2].

The contamination of water sources with heavy metals poses a significant threat to environmental and human health. Conventional methods for detecting heavy metal ions, such as atomic absorption spectroscopy and inductively coupled plasma mass spectrometry, though effective, are often expensive, time-consuming, and require sophisticated instrumentation [3, 4, 5]. As a result, there is an urgent need for the development of cost-effective, rapid, and sensitive detection methods. Carbon quantum dots (CQDs), a class of zero-dimensional nanomaterials, have emerged as promising candidates for sensing applications due to their unique optical properties, excellent biocompatibility, and ease of functionalization. Despite their potential, the synthesis of CQDs with high sensitivity and selectivity towards specific metal cations remains a challenge.

This thesis aims to address this gap by exploring novel synthetic routes to produce CQDs with tailored surface functionalities for the selective and sensitive detection of heavy metal ions in water. The research is focused on optimizing synthesis parameters, understanding the interaction mechanisms between CQDs and metal cations, and evaluating the perfor-

mance of these CQDs as fluorescent sensors for real-world water samples.

1.2 Justification

Environmental water pollution from toxic metal ions has become a severe and significant environmental issue. Analytical detection methods of metal ions involve toxic elements or or complex devices. Carbon Quantum Dots (CQDs), are a new type of carbon-based nano-materials that have attracted considerable interest because unlike organic dyes, which can easily lose their fluorescence over time (tendency to photobleaching) [6, 7], CQDs exhibit remarkable resistance to this process. Since their discovery, CQDs have been extensively studied by researchers due to these particles have the ability to produce different colors of light, and they are also very compatible with living organisms, making them suitable for a wide range of applications such as optical sensors, solar cells, drug delivery, and bio-imaging [8]. By advancing the understanding and development of CQD-based sensors, this work seeks to contribute to the field of environmental monitoring and provide a practical solution for the detection and mitigation of metal contamination in water resources.

1.3 Objectives

1.3.1 General objective

This study is aimed to produce functionalized (N, S, O) carbon quantum dots from citric acid via hydrothermal synthesis and evaluate the effects of the different heteroatoms on their properties in metal ions detection.

1.3.2 Specific objectives

- To elucidate the structure-property relationships governing the photoluminescence properties of doped CQDs by systematically evaluating the influence of constituent components and synthesis parameters.
- To conduct comprehensive physicochemical characterization of the synthesized CQDs utilizing a multi-analytical approach: Fourier Transform Infrared (FT-IR) Spectroscopy for functional group identification, Ultraviolet-Visible (UV-Vis) Spectroscopy to determine optical properties and electronic transitions and Transmission Electron Microscopy for morphological and structural analysis at the nanoscale and finally, Fluorescence Spectroscopy to probe optical properties.

- Develop an optical sensor based on CQDs for the selective and sensitive detection of metal ions in aqueous media, demonstrating how the surface structure of CQDs affects their selectivity.
- To employ Time-Dependent Density Functional Theory (TD-DFT) computational methods to elucidate the underlying photophysical mechanisms and correlate theoretical predictions with experimental observations, in order to improve the fundamental understanding of CQDs fluorescence phenomena.
- To develop a new composite material incorporated with CQDs that acts as a fluorescence sensor for the selective detection of mercury ions.

Chapter 2

Theoretical Background

Nanostructured materials can be defined as those whose structural units, such as clusters, crystallites, or molecules, have dimensions in the range of 1 to 100 nm. Some properties such as solubility, reactivity, spectroscopic behavior, electrical and magnetic properties among others, generally differ from those of the same materials with larger particle sizes [9]. Due to the increase in surface area and quantum effects, nanostructured materials can produce significant changes in their properties compared to their bulk counterparts, leading to the consideration that reducing dimensionality results in a new material [10]. They have various shapes, sizes, and structures, including spherical, cylindrical, conical, tubular, hollow core, spiral, or irregular forms.

According to Ealia and Saravanakumar [11], the nanoparticles usually classified into three classes :

- **Carbon-based nanoparticles** include fullerenes, black carbon, and carbon quantum dots. They are notable for their electrical, optical, and thermal properties, and are used in bioimaging, energy storage, and photovoltaic devices [12, 13] .
- **Organic nanoparticles** : They are made from organic compounds such as proteins and lipids. They are biodegradable and are primarily used in targeted drug delivery and cancer therapy [14].
- **Inorganic nanoparticles** encompass metallic, ceramic, and semiconductor nanoparticles. Quantum dots generally fall under the category of nanomaterials. They are typically composed of inorganic semiconductor compounds such as cadmium selenide (CdSe), cadmium telluride (CdTe), and lead sulfide (PbS). These nanocrystalline structures exhibit unique optical and electronic properties due to quantum confine-

ment effects at the nanoscale. They are known for their unique optical, electrical, and biological properties and are employed in nanodevices, catalysis, and biomedical applications (Figure 2.1) [15, 16, 17, 18].

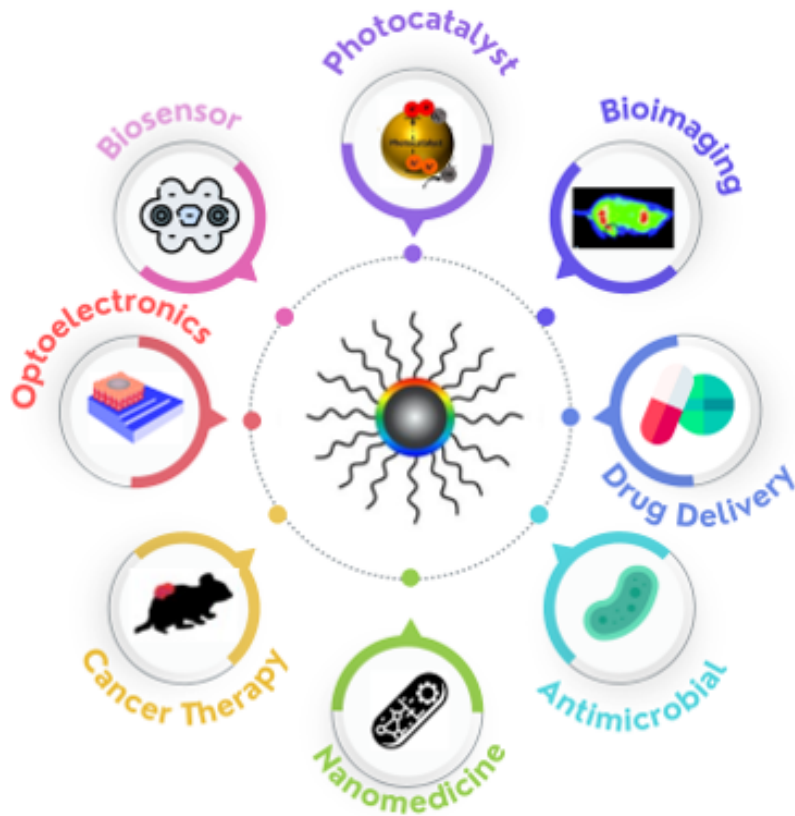


Figure 2.1: Applications of Carbon Quantum Dots

However, the above-mentioned classifications can be somewhat unhelpful since the same material can belong to more than one category. Therefore, a generic and most used classification is based on their dimensions. Based on this characteristic nanomaterials can be classified into 0D, 1D, 2D, and 3D [19].

- **0D:** All dimensions are on the nanoscale (metallic nanoparticles, quantum dots, nanoclusters).
- **1D:** One dimension is on the micro or macroscale (nanowires, nanofibers, nanotubes).
- **2D:** Two dimensions are on the micro or macroscale (surface nanocoatings, thin nanolayer films).
- **3D:** Assemblies of 0D, 1D, or 2D nanomaterials with all three dimensions larger than 100 nm

In particular, Quantum Dots (QDs), which belong to the 0D category, have captured

the attention of the scientific community due to their electronic and optical properties. These small semiconductors exhibit discrete quantized energy levels and a different density of states compared to bulk materials and those confined in fewer dimensions. The size at which a material becomes quantum confined can vary significantly between different materials and is determined by the quantum mechanical nature of the electrons and holes in those materials [20].

QDs have been a research area developed over the last 40 years, representing a concerted effort in Chemistry, Quantum Physics, and Nanotechnology. It corresponds to field that the Nobel Prize 2023 laureates [21], namely Alexei Ekimov, Louis Brus, and Moungi Bawendi, have made their significant contributions. Since their discovery, the broad absorption spectrum, narrow tunable emission, and enhanced photostability compared to organic dyes make them attractive materials for bioimaging. QDs represent a class of materials that are distinct from both molecular and bulk materials. Although they share the same structure and atomic composition as bulk materials, their properties can be precisely tuned by adjusting a single parameter: the particle size [22].

Alexei Ekimov and Onushenko discovered quantum dots in 1981 [23]. Subsequently, Efros and Efros theorized that quantum size effects are responsible for the changes in the optical and optoelectronic properties of nanoparticles [24]. Building upon this foundation, in 1983, Brus dedicated his research to investigating the effect of nanoparticle size on the color of light they absorbed [25]. Despite these developments, there was no control over the wide variety of different particle sizes until 1993. At that time, Moungi Bawendi made a discovery: a synthesis technique based on growing "seeds" of the crystals in a controlled manner. Through this method, which involved using an appropriate solvent and varying the solution temperature, it became possible to grow nanocrystals of a given size [26].

Due to their tiny size, QDs suffer a series of quantum effects, such as the discretization of their energy bands. As an interesting property, these semiconductor nanoparticles exhibit quantum confinement in three spatial directions, because the electrons are restricted to move in very small regions, smaller than 10 nm. Quantum confinement occurs when the crystal diameter is smaller than its Bohr radius and influences the properties of QDs, making them very different from those of macroscopic materials [27].

An innovative discovery in this area was made serendipitously in 2004 during the purification procedure of carbon nanotubes [28], opening new possibilities for CQDs. Compared to traditional quantum dots, CQDs offer a solution characterized by reduced toxicity and improved biocompatibility.

2.1 Carbon Quantum Dots

Carbon Quantum Dots (CQDs) as they are frequently called, represent an advanced class of carbon nanomaterials that have captured significant scientific interest because of their exceptional properties and applications. Part of the broader category of nanostructured carbon allotropes, CQDs are quasi-spherical nanometer-sized particles that may exhibit amorphous or nanocrystalline structures [29]. In the field of research concerning to CQDs, the principal objects of study are graphene quantum dots (GQDs), carbon nanodots (CNDs), and polymer dots (PDs). They show similar size and photoelectrochemical properties, although they differ in their internal structure and the chemical groups found on their surfaces [30].

Renowned for their luminescent properties, low cytotoxicity, and quantum confinement abilities, CQDs exhibit exceptional electrical and optical characteristics. The synthesis of CQDs has been achieved through both top-down and bottom-up approaches, similar to other nanomaterials, ensuring their suitability for a variety of scientific and technological applications. Their attributes, including water solubility, biocompatibility, non-toxicity, ease of functionalization, and chemical stability, make them suitable for applications in photocatalysis [31, 32], bioimaging [33], sensing [34, 35], drug delivery [36], and energy storage [37].

2.1.1 Structural Properties

Carbon dots are zero-dimensional (0D) nanocarbons with a typical size of less than 10 nm. They can exist as nanocrystallites or amorphous nanoparticles interconnected through sp^2 bonding [38]. They have been reported in a shape of circular or elliptical; some possess quadrate, triangular, and hexagonal structures. However, the most reported structure is the spherical with diameters generally below 10 nm [30]. Spherical graphitic carbon dots are likely the most prevalent type documented in academic literature, as indicated by numerous references [39, 40, 41]. However, it's important to acknowledge that only a handful of studies have conclusively demonstrated the presence of a graphitic monocrystalline structure in carbon dots through high-resolution transmission electron microscopy (HR-TEM) investigations. It should be noted that only a handful of studies have conclusively demonstrated the mono-crystalline graphitic structure of carbon dots through HR-TEM investigations [42].

The core of these quantum dots can be either crystalline or amorphous, this is indicated by techniques mentioned above like HR-TEM and X-ray diffraction (XRD), which reveal structured lattice spacing and crystallinity. The carbon content and synthesis conditions,

such as temperature, influence whether the structure is more sp^2 -hybridized graphitic or sp^3 -hybridized amorphous [43]. Typically, the presence of a graphitic crystalline core is predominantly made of sp^2 carbon. Graphene is a two-dimensional material composed of a single layer of carbon atoms bonded through sp^2 hybridization, whereas the core of graphitic carbon dots consists of multiple layers of sp^2 hybridized carbon stacked together. In addition to these crystalline graphitic cores, some researchers have identified carbon dots with a high degree of nitrogen doping, featuring cores composed of carbon nitride structures arranged in either graphitic or β -crystalline configurations [42]. In contrast, CQDs exhibit a more mixed hybridization, incorporating in the core sp^2 and sp^3 carbon in different proportions, leading to disorder in the structure and resulting in spherical amorphous carbon quantum dots with size less than 10 nm [44].

Beyond the core, the structure of carbon dots can be segmented into two distinct regions known as the surface state and the molecular state. The surface state specifically encompasses the outermost area of the sp^2 hybridized core which supports functionalization with various groups like hydroxyl, carboxyl, and amino groups [45]. These surface modifications significantly enhance the photoluminescent properties of CQDs, unlike unmodified carbon nanoparticles which lack inherent luminescence. Such functional groups not only contribute to the luminescence but also enhance the CQDs compatibility with both hydrophilic and hydrophobic environments, thereby broadening their application spectrum across different mediums, particularly in aqueous solutions [46]. The categorization of these nanostructures extends beyond just their core composition to include the nature and arrangement of functional groups on their surface, which can range from simple atomic attachments to complex, lengthy chains [44, 47].

2.1.2 Electrochemical properties

Carbon quantum dots represent a significant innovation in the field of electrochemistry, above traditional materials. These CQDs stand out for their economic accessibility and ease of acquisition compared to the precious metals commonly used in electrocatalysis, offering enhanced performance through the promotion of electronic transfer via internal interactions. CQDs improve electronic conductivity and increase the sites of active catalytic reaction, resulting in more effective charge transfer during electrocatalytic processes [48, 49, 50].

Compared to other carbon-based nanomaterials, CQDs exhibit charge transferable, increased electroconductivity, and a efficient surface area, along with reduced toxicity, making them more economical and efficient. These characteristics allow CQDs to offer multiple

binding sites for molecules such as DNA, due to their extensive surface area and functional diversity [51].

The functionality of CQDs extends to sensitivity in detection, where the precision of sensors is improved by the ability of CQDs to immobilize receptor molecules on electrode surfaces through abundant functional groups such as hydroxyl, carboxyl, and amine. These groups not only provide numerous sites for surface modification but also accelerate inter-molecular electroconductivity, thereby improving electrocatalytic activity [48, 52].

In the context of specific electrochemical reactions, such as hydrogen evolution reaction, oxygen reduction reaction, and oxygen evolution reaction, CQDs have verified to be effective catalysts. They reduce activation energy and over-potential, offering significant advantages over noble metal-based catalysts in terms of cost, stability, reduced toxicity, corrosion resistance, and catalyst poisoning [37, 53, 54, 55].

Furthermore, the presence of heteroatoms such as nitrogen, phosphorous, sulfur, and bismuth in CQDs plays a crucial role in modulating the electronic properties of carbon atoms through intramolecular charge transfer, improving their utility in various electrochemical applications [37, 55]. During electrochemical reactions, CQDs act as efficient active centers due to their excellent electroconductivity, numerous defect sites, and active edges, as well as their large surface-to-volume ratio. When combined with conductive materials, CQDs can improve performance and electrochemical characteristics, exhibiting superior properties for applications such as super-capacitors compared to traditional precursors like lignite [56].

2.1.3 Optical and electronic properties of CQDs

The optical and electronic properties of CQDs are determined by the band gap of sp^2 domains, and are significantly influenced by surface conditions, fluorophores, and the doping with various elements [39, 57]. Quantum confinement effect plays a crucial role in defining these properties, it explains the electron behavior using concepts such as energy levels, potential wells, valence and conduction bands, and the gaps between electron energy bands [58]. This effect becomes evident when the particle size is small enough to be comparable to the wavelength of electrons. These materials lead to a transition in the conduction and valence bands from continuous to discrete energy levels, as materials near this radius, the band gap becomes inversely proportional to their size [59, 60].

The optical properties of carbon quantum dots have acquired attention due to their potential in various scientific and technological applications. These nanomaterials have char-

acteristics such as absorption, photoluminescence, phosphorescence, chemiluminescence, electrochemiluminescence, and upconversion photoluminescence, which are highly tunable through synthesis methods and surface modifications.

Optical Absorption

CQDs exhibit strong absorption in the ultraviolet region, extending into the visible region. This absorption is primarily attributed to $\pi - \pi^*$ transitions of C=C bonds and $n - \pi^*$ transitions of C=O bonds [8, 31, 39, 52, 61, 62]. The absorption spectrum can be altered through surface engineering and heteroatom doping [63]. The ability of CQDs to absorb light in these regions makes them suitable for applications requiring strong UV-visible responses, such as sensors and photocatalytic devices [61, 64]. The optical absorption of CQDs is fundamental to their performance in optoelectronic and catalytic devices, as it determines the efficiency with which these materials can interact with light.

Photoluminescence (PL)

Photoluminescence is one of the most notable properties of CQDs. The PL of CQDs is significantly dependent on the excitation wavelength, meaning the emission wavelength and intensity can vary based on the excitation wavelength used [52]. This phenomenon is due to the presence of emissive traps on the surface of CQDs and the quantum confinement effect. The size of CQDs determines the bandgap energy. Smaller dots have larger bandgaps, leading to blue shifts in emission, while larger dots have smaller bandgaps, resulting in red shifts [65, 66]. Surface functionalization with various groups (e.g., hydroxyl, carboxyl, amino) significantly influences the PL behavior [63]. This surface passivation improves photoluminescence quantum yield by minimizing non-radiative recombination [67]. This excitation-dependent PL is especially useful in imaging and sensor applications, where the ability to tune the emission wavelength allows for the detection of different signals or biological processes [8].

Phosphorescence (PhL)

CQDs also exhibit phosphorescence, particularly when dispersed in a polyvinyl alcohol (PVA) matrix and excited with UV light. This phosphorescence is attributed to the triplet excited states of aromatic carbonyls on the CQDs surface, protected by hydrogen bonds with PVA molecules [52].

Chemiluminescence (CL)

The chemiluminescence of CQDs occurs when they coexist with oxidants such as potassium permanganate (KMnO_4) or Ce^{4+} [63]. The oxidants inject holes into CQDs, increasing hole population and accelerating electron-hole annihilation, resulting in CL emission. The intensity of CL is concentration-dependent and influenced by temperature, allowing its use in chemical sensors and detection applications.

Electrochemical luminescence (ECL)

Electrochemiluminescence (ECL) involves the electrochemical generation of excited states. The ECL response of CQDs is influenced by the oxidation state of their surface, with highly oxidized CQDs showing significant ECL activity. Highly oxidized CQDs (o-CQDs) exhibit substantial ECL activity, related to the direct oxidation of o-CQDs and subsequent reactions involving strong oxidizing agents such as SO_4 radicals. This property is of great interest for the development of advanced electrochemical detection devices and sensors [52].

Upconversion Photoluminescence (UCPL)

Upconversion photoluminescence (UCPL) is the emission of light at a shorter wavelength than the excitation wavelength, attributed to multiphoton activation processes. However, recent studies have questioned the existence of UCPL in CQDs, suggesting that previously observed phenomena might be normal fluorescence excited by filtered components of the spectrophotometer's monochromator. Despite these controversies, UCPL remains a property investigated for live imaging applications, allowing deeper tissue penetration and reduced background autofluorescence [8, 46, 48].

Fluorescence Emission Mechanisms

CQDs exhibit various fluorescence emission mechanisms, including bandgap transitions in π -conjugated domains and defect-derived emissions. Bandgap transitions in π -conjugated domains are formed by sp^2 -hybridized carbon atoms, and the emission can originate from these transitions. Surface defects, such as imperfect sp^2 domains and functionalized sites, create localized energy states that emit multicolor fluorescence. These defects act as energy traps, where the recombination of electron-hole pairs in the localized electronic levels of sp^2 sites leads to visible emissions [30, 46, 48, 55, 57].

The fluorescence intensity of CQDs can vary with the pH of the solution. These changes in pH affect the protonation states of surface groups, such as carboxyls, altering the electronic environment and fluorescence characteristics. This behavior is valuable for detecting pH

changes in biological and environmental systems, where fluorescence variation can monitor local conditions.

2.2 Synthesis Methods of CQDs

CQDs are synthesized using two principal approaches: top-down and bottom-up methods, each giving distinct physicochemical properties to the CQDs such as size, crystallinity, and fluorescence characteristics. The top-down approach involves deconstructing larger carbon structures into smaller ones through methods such as chemical oxidation, discharge, electrochemical oxidation, ultrasonic methods, arc-discharge, laser ablation, and acidic oxidation [68]. These methods, though effective, often require expensive materials, harsh reaction conditions, and extended reaction times [52].

On the other hand, the bottom-up approach synthesizes CQDs from smaller carbon structures or organic molecules through hydrothermal treatment, ultrasonic treatment, thermal decomposition, pyrolysis, carbonization, microwave synthesis, solvothermal methods, microwave pyrolysis, combustion routes, and electrochemical methods [69, 70, 71]. This approach allows for the construction of CQDs with specific desired properties, including the ability to control their oxygen/nitrogen content and colloidal stability. Additionally, the bottom-up method can lead to enhanced fluorescence qualities and quantum yields due to more controlled synthesis conditions [47, 66].

Each synthesis technique can impart unique properties to CQDs such as size-dependent photoluminescence, photo-blinking, excitation-dependent photoluminescence, and variations in hydrophilicity and surface ligands [72]. These properties significantly broaden the potential applications of CQDs, making it crucial to understand the effects of the complex structures resulting from different synthesis routes. Overall, the choice of synthesis approach and specific methods within each approach influences the functionality and application of carbon quantum dots.

Hydrothermal synthesis is one of the most common methods for preparing CQDs. It provides a low-cost, green, non-toxic route to new carbon-based materials from a wide range of precursor systems [52]. Essentially, this approach involves reactions in a solution phase wherein synthesis occurs over a wide range of temperatures, from room temperature to very high temperatures. The morphology of the resulting CQDs can be controlled by changing the pressure conditions, whether low or high, by the vapor pressure of the significant reactant in the reaction. Therefore, it gives a very flexible platform for synthesizing a wide range of these nanomaterials with desired properties [73]. Under these conditions, water

becomes more reactive and behaves like a non-polar solvent due to its high ionic product and low dielectric constant [74]. Due to, hydrolysis occurs, and the resulting products undergo simultaneous processes, including dehydration, decarboxylation, condensation, and polymerization. The end result is the formation of cross-linked polymeric materials [75, 76]. Besides, although carbonization and polymerization primarily affect the average size of CQDs, these activities cannot be observed inside the black box/hydrothermal reactor [77].

2.3 Surface Modification and Doping

One of the most effective ways to adjust the optical properties of CQDs is through surface modification and doping with heteroatoms. Surface modification involves coating CQDs with polymers or other molecules that can passivate surface defects and enhance photoluminescence stability [67]. Doping with heteroatoms such as nitrogen, sulfur, phosphorus, and boron introduces new electronic states in CQDs, altering their absorption and emission properties [55]. For instance, nitrogen-doped CQDs often show a red shift in emission and an enhancement in photoluminescence quantum yield due to the creation of new energy states [48].

The core-shell structure of carbon quantum dots offers a versatile platform for precisely adjusting their optical properties. The existence of surface states can modify the band gap and the radiative energy states of carbon quantum dots (CQDs) [78]. Various techniques, such as surface oxidation, passivation, and heteroatom doping, have been developed to fine-tune the surface states of CQDs. Surface oxidation, typically the initial step in passivation, generates oxygen-containing groups and surface defects, facilitating the attachment of passivation agents. Passivation is crucial for preventing the escape of photoinduced carriers from the surface, thus enhancing radiative recombination efficiency and improving photoluminescent properties. Additionally, integrating heteroatoms into CQDs structures enhances control over size, shape, and surface chemistry [79].

2.3.1 Surface Oxidation

Surface oxidation has several influence in the photoluminescence CQDs, resulting in excitation independent surface state PL emissions, enabling full-color luminescence. This effect primarily stems from surface oxygenated groups such as hydroxyl, carboxyl, ether, and epoxy. Different groups of CQDs, despite similar size distributions and graphitic structures, can exhibit a spectrum of PL colors from blue to red, linked primarily to increased carboxyl groups on the surface. The quantity of oxygen-containing groups formed dur-

ing C=C bond decomposition correlates directly with surface oxidation level [80, 81]. At the same time, extensive surface oxidation introduces more structural defects, narrowing the band gap and causing a redshift in photoluminescence, because of higher potentials may reduce CQDs size but also increase surface oxidation, further leading to red-shifted photoluminescence [82, 83]. The types of oxygen-containing groups significantly affect CQDs properties; C=O and COOH groups enhance photocatalytic activity by promoting electron-hole separation, while C-OH groups facilitate recombination, resulting in intense PL emission. Overall, understanding the relationship between surface oxidation, oxygen-containing groups, and PL behavior is essential for adapting CQD properties for various applications.

2.3.2 Passivation

Passivation often utilizes organic molecules to adjust the surface states controlling electron-hole recombination. For example, CQDs are commonly passivated with groups like amino, epoxy, and carboxyl to increase their solubility and interaction with biological molecules. This is particularly important for creating specific biosensors and targeted imaging agents in biomedical applications. By modification of the surface, CQDs achieve higher quantum yields and improved environmental stability. The passivation process also includes the use of heteroatoms as additional agents, which provide new pathways for electron-hole recombination, further enhancing the photoluminescent efficiency [79, 41].

2.3.3 Doping Heteroatoms

Doping CQDs with heteroatoms like nitrogen, sulfur, phosphorus, among others, significantly alters their electronic and optical properties. This alteration is primarily due to the introduction of new energy levels within the carbon dot matrix, enhancing optical absorption and emission capabilities. Introducing dopant atoms into the structure can create additional n-state energy levels within the $\pi - \pi^*$ band, resulting in multiple photoluminescence emissions. Adding more heteroatoms to CQDs generates additional surface states and defects. These defects effectively capture more electrons, there by promotion fluorescence [78]. Therefore, the selection of an appropriate dopant is crucial for successful atom doping . Depending on the application, different doping strategies are employed. For example, the functionalization is vital for creating specific biosensors and targeted imaging agents [52].

Doping with heteroatoms is a key strategy for optimizing the optical properties of CQDs. Nitrogen doping introduces additional electronic states in the CQD structure, enhanc-

ing photoluminescence efficiency and enabling emission in the near-infrared (NIR) range. Doping with sulfur (S) and phosphorus (P) also improves optical properties by creating new emissive states and increasing charge transfer efficiency. CQDs doped with multiple heteroatoms, such as N and S, can exhibit synergistic effects that further enhance photoluminescence properties.

Nitrogen doping

The nitrogen atom doping improves luminescence due to shifts in the Fermi level, introducing p-type carriers, and enhancing conductivity. It is commonly used in optoelectronic devices due to improved electron mobility and photoluminescence. Nitrogen doping is noted for causing a red shift in emission wavelength and an increase in fluorescence intensity [41, 55, 57, 54]. The process of in-situ doping during synthesis integrates heteroatoms during the CQDs formation, ensuring a uniform distribution and precise control over doping levels [52]. Additionally, post-synthesis modifications allow for further adjustments in doping levels and distributions, a step crucial for customizing CQDs properties to meet specific needs. On a more complex level, multi-heteroatom doping influences the co-doping of multiple heteroatoms to produce synergistic effects that significantly alter electronic interactions and enhance the multifunctionality of CQDs, thus allowing for finely tuned optical properties. Moreover, the enhanced surface reactivity observed in doped CQDs improves interactions with surrounding molecules, which is particularly advantageous in sensing applications where this reactivity can detect specific molecules based on changes in luminescence [31]

Sulfur and Phosphorous doping

These elements create localized states in the electronic structure of CDs, shifting the photoluminescence and affecting the band gap. They introduce n-type characteristics and create new luminescent centers, which can either enhance PL intensity or shift emission wavelengths [84, 85].

Metal Doping

Although less common due to potential toxicity, metals can be used to modify the band structure and introduce properties like magnetism or improved catalytic activity [86].

2.4 Applications of CQDs

2.4.1 Bioimaging

Researchers currently employ CQDs widely, primarily because of their biocompatibility and minimal toxicity against nanoparticles and quantum dots [87]. The high biocompatibility and tunable emission capability of CQDs allow their use in cell labeling, tracking biological processes, and detecting biomolecules with high sensitivity, demonstrating their ability to fulfill the two essential criteria for clinical application in diagnosis and cancer therapy [88]. CQDs have been utilized in various applications such as enhancing photoacoustic imaging contrast, serving as photosensitizers in photodynamic therapy, and contributing to photothermal therapy. Their large surface area and the presence of carboxylic functional groups on their surface facilitate the creation of versatile probes and therapeutic combinations [33, 89, 40].

2.4.2 Photocatalysis

An effective photocatalyst would have two important characteristics: resistance to photo-corrosion and near-UV working ability and/or visible light. In other words, CQDs with controlled sizes can show different emissions that go from blue to near-infrared wavelengths, turning them very versatile [47]. The superior water solubility, chemical stability, and low toxicity made CQDs attractive compared with typical photocatalysts compared by ZnO, TiO₂, and QDs. The absorbance and photoluminescence, after surface modification. This feature enables wide bandgap semiconductors to provide an absorption edge that extends into the visible and near-infrared region of light [80]. In addition, the photoexcited CQDs become excellent electron donors and acceptors, due to which recombination of electron-hole pairs is minimized [32]. Thus, the CQDs can perform multiple roles in the design of photocatalysts: electron mediators, photosensitizers, spectral converters, or even sole photocatalysts. Most often, multiple functions occur simultaneously [90].

2.4.3 Sensors

Theoretically, any change in fluorescence intensity, wavelength, anisotropy, or lifetime connected to the different concentration of analytes develops as a potential sensor [91]. The most common method for the fluorescent detection of metals is fluorescence quenching ("turn-off") 2.2. In this context, it is crucial to consider the potential interference of other species present in the matrix, as multiple species can interact with CQDs and cause fluorescence quenching.

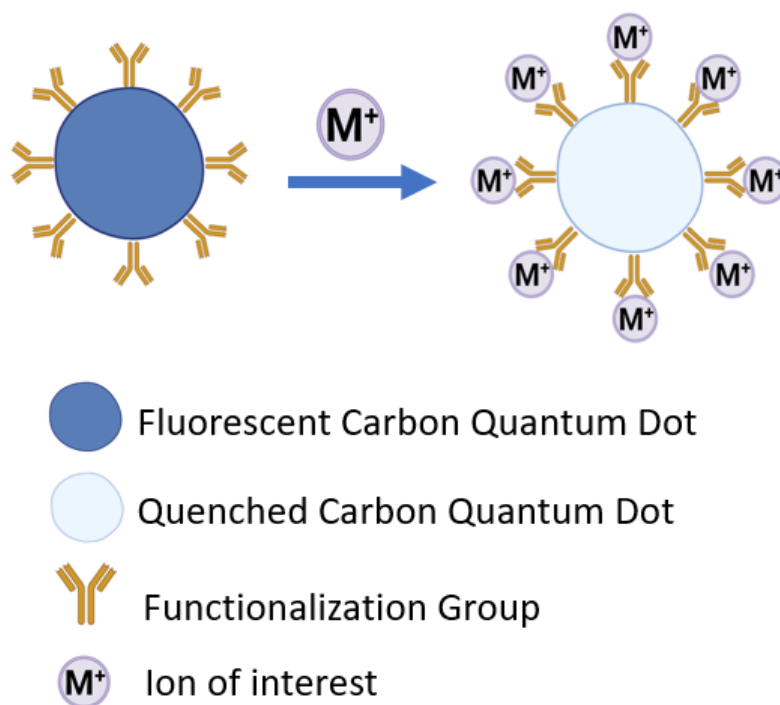


Figure 2.2: Schematic representation of carbon dot quenching in the presence of metal ions

Therefore, the selectivity of the detection process is a critical aspect to consider. CQDs with surface functional groups that are soft bases can detect soft metal acids, whereas the opposite is expected for pairs of hard acids and bases. Recent research has demonstrated that carbon dots (CDs) can detect Hg^{2+} , Fe^{3+} , Cu^{2+} , $\text{Cr}_2\text{O}_7^{2-}$, CrO_4^{2-} , Zn^{2+} , Cd^{2+} , Ag^+ , Au^{3+} , Pb^{2+} , Al^{3+} , As^{3+} , Co^{2+} , Ni^{2+} , MnO_4^- , VO_4^{3-} , and MoO_4^{2-} ions [92]. The use of CDs for the detection of metal cations is significantly more common than for the detection of anions. The mechanisms responsible for the fluorescence changes of CQDs are as follows:

- **Photo-induced electron transfer (PET):** This process is an internal redox deactivation process between the excited state of fluorophores and an analyte capable of donating or accepting an electron. In this process, a complex between the electron donor and electron acceptor is formed. On many occasions, this complex returns to the ground state in a nonradiative process. Ultimately, this extra electron on the acceptor gets transferred back to the electron donor [93].
- **Resonance energy transfer (RET):** In Förster Resonance Energy Transfer, when the donor molecule is first excited by returning to the ground state, it must simultaneously provide energy to the acceptor molecule, elevating it to an excited state. This occurs because of long-range dipole-dipole interactions between the excited donor and the acceptor.

The efficiency of FRET is dependent upon many variables, including the relative orientation of the dipoles of the donor and acceptor, the overlap between the fluorescence emission spectrum of the donor and the absorption spectrum of the acceptor, and the distance between the donor and the acceptor [94]. Additionally, dynamic quenching usually dominates the quenching process in energy transfer, where the fluorescence lifetime decreases with increasing concentration of a quencher [95].

- **Photo-induced charge transfer (PCT):** This mechanism involves the electron transfer between electron donor and electron acceptor functionalities to promote fluorescence. PCT sensors function by partial charge transfer within a fully conjugated system. Unlike PET sensors, where an electron donor moiety is separated from the fluorophores by a spacer. PCT sensors operate based on partial charge transfer within a fully conjugated π system. This interaction between the donor and acceptor alters the energy levels of the electrons, resulting in changes in fluorescence signals [95].
- **Inner filter effect (IFE):** This mechanism for non-irradiative energy conversion involves the absorption of excitation/emission radiation by absorbers within the detection system. This phenomenon occurs when their spectra overlap with the excitation or emission bands of a fluorophore. IFE is useful for converting absorption signals into fluorescence signals. The resulting fluorescence intensity is proportional to the excitation light intensity, although the quantum yield is somewhat lower than that of an infinitely dilute solution. This reduction in either excitation intensity or observed fluorescence due to absorption is termed the inner filter effect. In contrast, CQDs in sensing applications utilize the inner filter effect. Different energy transfer, quenching based on the inner filter effect does not significantly alter the fluorescence lifetime, despite affecting the overall intensity [35, 96].

2.4.4 Optoelectronic Devices

CQDs have demonstrated great potential in the development of optoelectronic devices such as LEDs and photovoltaic cells. Their tunable emission capability and strong UV-visible absorption make them suitable for applications requiring high energy conversion efficiency. Integrating CQDs into optoelectronic devices can significantly improve performance and stability, providing a platform for developing advanced light conversion technologies.

2.5 CQDs in Composites

Carbon quantum dots exhibit remarkable potential as viable alternatives to conventional semiconductor quantum dots in diverse applications, including energy conversion systems, sensing technologies, bioimaging modalities, and biodiagnostic platforms [48, 54, 39, 52], however it is crucial to stabilize CQDs in a medium to hold their fluorescent properties. To optimize the stability and enhance the optical performance of CQDs, it is necessary to incorporate into an appropriate solid-state matrix or to fabricate them as solid-state nanocomposites. Such integration can be achieved through various physicochemical interactions, including electrostatic forces, covalent bonding, non-covalent associations, or hydrogen bonding networks [97].

2.5.1 Carbon Quantum Dots - Polymer Composites

Polymer matrix are often selected for this purpose because they can sterically hinder CQDs from agglomerating or growing. Tomczak et al. [98] report that polymers act as stabilizers for QDs or provide a confined spatial environment to control particle size and size distribution. The reaction site can be controlled to some extent through the proper engineering of functional groups, morphology, and the self-assembly of the polymer. In particular, several polymer precursors have been used to prepare CQDs/polymer composites, polymers naturals such as chitosan, cellulose acetate, and alginate, as well as synthetic precursors like APTES, polysulfone, polyethyleneimine, polydopamine, polystyrene, and polyvinyl alcohol, among others [34, 99, 100, 101, 102, 103, 104, 105].

The objective of incorporating CQDs into polymers is due to their structure and composition of the final material (composites) can be easily controlled. In the case of natural precursors have been recommended for the production of eco-friendly nanomaterials due to their cost-effective preparation [106]. On the other hand, the synthetic precursors are chosen due to easy designability, adjustability, and compositional control through their synthesis procedures by their specific composition [107]. Researchers do not understand the photoluminescence process by CQDs making the effects of polymers on their optoelectronic properties are unclear too. The complexity and variability in the synthesis of carbon dots make it difficult to predict their properties with precision.

Polymers play a crucial role in the adherence of CQDs-composites to specific application. As a result, the development of membranes modified with CQDs has been investigated to significantly enhance their properties, leading to substantial improvements in various aspects of performance such as dispersedly anchoring CQDs to effectively avoid the aggregation-induced photoluminescence self-quenching of CQDs [101]

2.5.2 CQDs-Polymeric Hydrogels

Hydrogels based polymer are materials with viscoelastic properties and network structure caused by cross-linker and the solvent, respectively [108]. In general, hydrogels can be classified based on various characteristics, such as the nature of groups (cationic, anionic, or neutral), the method of fabrication (homo or copolymer), structural and mechanical properties (amorphous, semicrystalline, hydrogen-bonded, supramolecular, or hydrocolloid), and their ability to respond to environmental stimuli. Other characteristics for classifying hydrogels include their water absorption capacity. Additionally, the chemical or physical nature of the crosslinking bonds further categorizes hydrogels into two additional groups: physically and chemically crosslinked hydrogels [109].

With the increasing application of CQDs in biological diagnosis in imaging, optoelectronics, and sensors, the methods to create CQDs/hydrogel composite with tunable optical properties have gained relevant attention from researchers. The formation of the two components individually involves distinct processes: the synthesis of CQDs includes carbon nucleation and growth, while the construction of hydrogel involves creating a 3D network structure through physical or chemical cross-linking of polymeric chains [110].

Chapter 3

Methodology

This chapter presents in detail the CQDs synthesis methodologies with the different precursors, microscopy analysis by TEM, structural analysis by FT-IR spectrum, spectroscopic studies by fluorescence spectroscopy, computational studies and finally the application studies from synthesized CQDs.

3.1 Reagents

All the reagents in this study were of analytical grade and used without additional purification. Table 3.1 lists the chemicals used in this research. Ultrapure water was used for dilution throughout the entire experiment.

All reactives were acquired from different distributors:

- From Fisher Chemical: Citric acid (99%), Diethylenetriamine, Ethylenediamine, L-Cysteine, 2-Mercaptoethanol (99%), cadmium nitrate tetrahydrate (99%), potassium nitrate, lead nitrate 2, iron nitrate 3, cobalt nitrate hexahydrate, mercury nitrate 2, poly(ethylene glycol) diacrylate (average Mn 700), 2,2-dimethoxy-2-phenylacetophenon (99%).
- From SIGMA-Aldrich: Cinnamic Acid, , aluminum nitrate nonahydrate

3.2 Equipment

- Diode array UV-Vis spectrophotometer Analytik Jena Specord S200.
- Spectrophotometer model Ocean Optics QEPro series High Sensitivity Spectrometer

- UV/VIS/NIR spectrophotometer lambda 1050 (Perkin Elmer, EEUU).
- Balance Cobos precision HR-150A
- Drying stove SLW 115 (POL-EKO APARATURA, Poland).
- FTIR Spectrometer Perkin Elmer Cary 630
- UV-Vis Lamp

3.3 Synthesis of CQDs

In this work, the CQDs were synthesized using citric acid (CA) as the carbon source, along with various precursors. The objective was to evaluate the functionality of CQDs in the presence of different heteroatoms (S, O, N) contained in the precursors. Six initial options for precursors were selected:

- Cinnamic acid (CnnA) → Source of O
Contains carboxyl groups (-COOH) that can serve as a source of oxygen. The water solubility. Also, the oxygen can provide better hydro solubility as well as reactive sites for additional modifications.
- Allicin (ALLI) → Source of S and O
Sulfur can enhance charge transfer efficiency and the luminescent properties of CQDs. Oxygen, similar to cinnamic acid, can improve the solubility and reactivity of CQDs.
- 2- Mercaptoethanol (MPET) → Source of S and O
Mercaptoethanol, with its thiol group (-SH) and hydroxyl group (-OH), provides a combined source of sulfur and oxygen.
- L-cysteine (LCYS) → Source of S and O.
L-cysteine contains both a thiol group (-SH) and an amino group (-NH₂) able not only for the sulfur and oxygen it provides but also because the presence of the amino group can enhance dispersion in aqueous media.
- Ethylenediamine (EDA) → Source of N.
It contains two amino groups, is an excellent source of nitrogen. The incorporation of nitrogen into CQDs can enhance their electronic properties, such as charge mobility and luminescence. Additionally, the amino groups facilitate further functionalization and solubility in aqueous media.
- Diethylenetriamine (DETA) → source of N.

With two amino groups being a favorable source of nitrogen, their incorporation into CDs is expected to improve electronic properties, especially charge mobility and luminescence

For the synthesis, CDQs 1.0 g of citric acid (CA) were dissolved in 50 mL of ultrapure water, and then the surface modification precursor was included according the amount indicated in Table 3.1. Subsequently, the mixture was transferred and sealed into 100 mL autoclave, and additionally heated at 180 °C for 6 hours. The synthesized CQDs were collected in a container appropriately coded according to the precursor and stored under refrigeration. In the Figure 3.1, the final synthesis of L-CQDs, E-CQDs and D-CQDs is exhibited.



Figure 3.1: Synthesis for L-CQDs, E-CQDs and D-CQDs

3.3.1 Preparation of the L-CQDs Polycaprolactone nanofibers

In order to facilitate the visualization of the CQDs by electron microscopy, they were incorporated into a polymeric matrix of polycaprolactone, and nanofibers of the resulting composite (LCQDs) were subsequently generated by electrospinning.

Initially, a solution of chloroform and N,N-dimethylformamide was prepared in an 80/20 ratio, and 200 μL of L-CQDs were added. The mixture was stirred for 24 hours at a speed of 200 rpm. Afterward, the solution was sonicated for 30 minutes. Next, 4 mL of the solution was drawn into a syringe. The syringe was placed in the electrospinning apparatus, and electrospinning was performed at a constant flow rate of 0.05 mL/h, a voltage of 7.7 kV, and room temperature. The scaffolds were collected on aluminum foil and stored at room temperature until TEM analysis was performed.

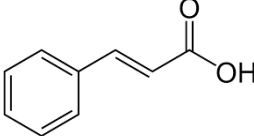
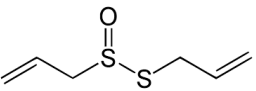
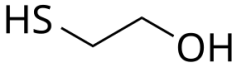
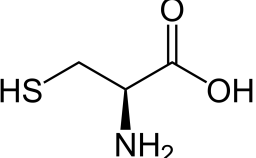
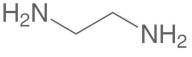
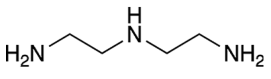
Sample Code	Precursor Species Amount	Precursor Structure	Color
CN-CQDs	CnA = 0.5 g		Colorless Transparent
A-CQDs	ALL = 0.335 mL		White color Opaque
M-CQDs	MOH = 0.5 g		Yellow
L-CQDs	CYS = 0.5 g		Pale Yellow
E-CQDs	EDA = 0.333 mL		Brown-black well-dispersed
D-CQDs	DETA = 0.333 mL		Light yellow

Table 3.1: Amounts of precursors used in the synthesis of CQDs, their structures and the appearance of the dispersion obtained.

3.3.2 Preparation of Hydrogel Optical with D-CQDs

The hydrogel synthesis was accomplished via a photocrosslinking process employing ultraviolet radiation ($\lambda = 366$ nm). A typical synthesis procedure involved the initial preparation of 3 mL poly(ethylene glycol) acrylate (PEGDA) solution, which was agitated for 10 minutes in an amber vessel to minimize light exposure. Subsequently, 15 mg of 2,2-dimethoxy-2-phenylacetophenone (DMPA), serving as the photoinitiator, was introduced into the solution. Immediately thereafter, 3 mL of a 1:150 dilution of D-CQDs solution was added dropwise. The resulting mixture was homogenized with the precursor solution for 5 minutes, followed by ultrasonication at 25 °C for 10 minutes. All reagent quantities were calculated based on a final volume of 6 mL. Post-sonication, the solution was UV-irradiated to 365 nm under dark conditions for 10 minutes. The synthesized hydrogel samples, denoted as DCQDs-Hydrogel, were then stored at room temperature. The chemical structures of the PEGDA monomer and DMPA are shown in Figure 3.2 and 3.3, respectively.

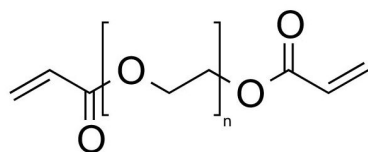


Figure 3.2: Structure of Poly(ethylene glycol) diacrylate

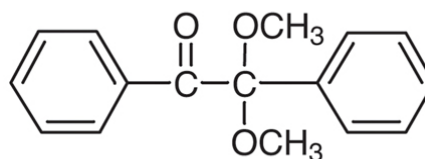


Figure 3.3: Structure of 2,2-Dimethoxy-2-phenylacetophenone

3.4 Structural and Spectroscopic Characterization

3.4.1 Fluorescence spectroscopy analysis

The photoluminescence (PL) of CQDs can be characterized by fluorescence spectroscopy (FS) using an Ocean Optics QEPro series High Sensitivity Spectrometer. Fluorescence spectroscopy was used to investigate the study of the emission properties of CQDs, such as the emission spectrum and fluorescence intensity, is essential for understanding how CQDs interact with light. Furthermore, investigating the stability of CQDs over time and across different dilutions is crucial because fluorescence stability serves as an indicator of

the robustness of CQDs for practical applications. Finally, this technique helps evaluate the sensitivity and selectivity of CQDs in detecting various ion metallic, providing the information about their behavior and utility in sensor applications. In this study, the M-CQDs, CN-CQDs, and A-CQDs samples were excluded from further analysis due to their insufficient fluorescence properties. The observed weak fluorescence intensity precluded meaningful investigation of these samples photo-luminescent characteristics.

3.4.2 FT-IR spectroscopy analysis

Fourier transform infrared spectra of freeze dried samples of D-CQDs, E-CQDs and L-CQDs were obtained in the middle infrared region, between 4000 cm^{-1} and 400 cm^{-1} through a Cary 630 FT-IR Spectrometer with ATR sampling mode.

3.4.3 UV-Vis Absorbance

The optical properties of D-CQDs, E-CQDs, and L-CQDs samples were characterized by measuring their absorbance spectra in the ultraviolet-visible (UV-Vis) range. Samples were diluted 1:150 in ultrapure deionized water, which also served as the reference. Spectral measurements were performed using a Shimadzu UV-2600 spectrophotometer over a wavelength range of 200-1000 nm.

3.4.4 Transmission Electron Microscope (TEM)

The shape and structure of the CQDs in solution were determined by Transmission Electron Microscopy (TEM) using a microscope model Tecnai G2 Spirit Twin equipped with an Eagle 4k HR camera, on a Copper F/C TEM grid.

3.4.5 High Resolution Transmission Electron Microscope (HRTEM)

HRTEM was employed to examine morphology and microstructure of the polycaprolactone nanofibers. It was analyzed using a (JEOL-JEM 2200FS) equipped with a spherical aberration corrector in the condenser lens and operated at 200 kV. The samples were prepared by alcohol dispersion and then deposited on a lacey carbon copper grid.

3.5 Metal Sensing from CQDs-Hydrogel

3.5.1 Sensitivity to metal ions

To evaluate ion sensitivity through fluorescence, 50 ppm solutions of $\text{Hg}(\text{NO}_3)_2$, $\text{Pb}(\text{NO}_3)_2$, $\text{Cd}(\text{NO}_3)_2$, $\text{Co}(\text{NO}_3)_2$, $\text{Al}(\text{NO}_3)_3$, $\text{Fe}(\text{NO}_3)_3$ were used to observe the fluorescence quenching of CQDs in water. A 100 μL aliquot of diluted CQDs solution (comprising 0.6 μL CQDs and 99.4 μL desionizade deionized ultrapure water) was placed in each test tube, and 3 mL of each solution was added to the respective tube. After a 30-minute incubation at room temperature, fluorescence was measured at 365 nm using a Ocean Optics QEPro spectrofluorometer. The comparison of the fluorescence intensities obtained with the added ions against the control without ions allowed for the evaluation of fluorescence quenching and the determination of CQDs selectivity against the different ions.

3.5.2 Selectivite sensing

The selectivity test for each CQDs and CQDs hydrogel was conducted by mixing the CQDs with each metal ion as listed in Table 3.2. It was used the method of Wang et. al. with some modifications [111]. Fluorescence emission intensities of CQDs and CQDs hydrogel were measured in the presence (I) and absence (I_0) of interference at $\lambda_{ex} = 365$ nm (excitation wavelength). The detection of each ion by CQDs and CQDs hydrogel was performed in an aqueous solution. A 100 μL aliquot of diluted CQDs solution (comprising 0.6 μL CQDs and 99.4 μL deionized ultrapure water) was mixed with 3 mL of different concentrations of each ion (Table 3.2). After a 30-minute incubation at room temperature, the measurements were recorded to evaluate the linear concentration range and the limit of detection. The fluorescence spectra at the emission wavelength were recorded for each CQDs sample, and all experiments were performed at room temperature.

In the case of hydrogel with D-CQDs, a 5 mm \times 5 mm probes were immersed in different test Hg^{2+} solutions at different concentration, for a duration of 96 hours (4 days). Upon completion of the immersion period, the samples exhibited significant swelling, with dimensions increasing to approximately 10 mm \times 7 mm.

Stern and Volmer have considered that the quenching process is a bimolecular reaction that competes with the radiative process and other molecular processes [112]. Based on this, they derived an equation that can be expressed in the following form:

$$\frac{I_0}{I} = 1 + K_{SV}[Q] \quad (3.1)$$

Table 3.2: Metal concentration in Selectivity tests for each CQDs samples and Hydrogel

Sample name	Sensing Ion	Solution Concentration (ppm)
L-CQDs	Pb ²⁺	0, 0.03, 0.10, 0.20, 0.33, 1.66, 3.30, 10.00, 16.56, 23.18, 66.0
L-CQDs	Cd ²⁺	0, 0.5, 1.0, 2.0, 5.0, 10, 30, 50, 100
E-CQDs	Hg ²⁺	0, 0.5, 1.0, 2.0, 5.0, 10, 30, 50, 100
D-CQDs	Hg ²⁺	0, 0.5, 1.0, 2.0, 5.0, 10, 30, 50, 100, 200, 300
DCQDs-Hydrogel with D-CQDs	Hg ²⁺	0, 0.5, 1, 2, 5, 10

where I_0 is the fluorescence intensity in the absence of the quencher, I is the fluorescence intensity in the presence of the quencher, K_{SV} is the Stern-Volmer constant, and $[Q]$ is the concentration of the quencher. If the emission intensity is measured in the absence of the quencher and then in the presence of increasing amounts of the quencher, and the ratio of the emission intensities (I_0/I) is plotted against the concentration of the quencher ($[Q]$), the resulting plot (Stern-Volmer plot) will intersect at 1 and have a slope referred to as the Stern-Volmer constant [113]. The fluorescence spectra were recorded to estimate the limit of detection (LOD) (eq. 3.2) and limit of quantification (LOQ) (eq. 3.3) by using Stern-Volmer graphs.

$$\text{LOD} = \frac{3 \sigma}{K_{sv}}, \quad (3.2)$$

$$\text{LOQ} = \frac{10 \sigma}{K_{sv}}, \quad (3.3)$$

where K_{sv} is the slope of the graph and σ is the error of the intercept.

3.6 Computational Methods to estimate the properties of CQDs

In this work, a computational study of the CQDs was conducted. ORCA 5.1 software was used to execute theoretical studies [114]. The steps performed in this computational stage are described below.

3.6.1 Geometry Optimization

Initially, Avogadro was used to draw the initial structures of CQDs. Four structures were created based on ordered graphene layered structures, incorporating different modifiers: NH₂, OH, SH₂, and one without modifiers. Then, mercury was incorporated to these structures optimized to compare the different interaction it has with each selected heteroatom. The Avogadro tool was then used to generate Orca input files. All compounds were optimized using the CAM-B3LYP method with the def2-TZVP basis set and including D4 (dispersion correction to improve the accuracy of van der Waals interaction calculations). The specific input used for geometry optimization is detailed in the following Figure 3.4.

```
# avogadro generated ORCA input file
# Basic Mode

! CAM-B3LYP OPT D4 def2-TZVP PAL6
```

Figure 3.4: Input for Geometry optimization

3.6.2 Spectroscopy Properties Calculations

The UV-Vis and fluorescence spectra were calculated using the coordinates of the optimized structures. For the UV-VIS analysis, additional calculation parameters were introduced, specifically the def2-TZVP basis set, the D4 dispersion correction, and the calculation of 30 excited states. For fluorescence analysis, addition parameter was to specify that the optimization would be carried out in the first excited state, IROOT 1. The ORCA input used in this work is shown in the Figure 3.5a and Figure 3.5b, for UV-Vis and fluorescence spectra respectively.

```
# avogadro generated ORCA input file
# Basic Mode
#
! CAM-B3LYP def2-TZVP D4 PAL6
%TDDFT
  NROOTS 30
END
```

(a) Input for UV-VIS Calculation

```
# avogadro generated ORCA input file
# Basic Mode
#
! CAM-B3LYP def2-TZVP D4 PAL6 OPT
%TDDFT
  NROOTS 30
  IROOT 1
END
```

(b) Input for Fluorescence Calculation

Figure 3.5: Input for TDDFT calculations

Chapter 4

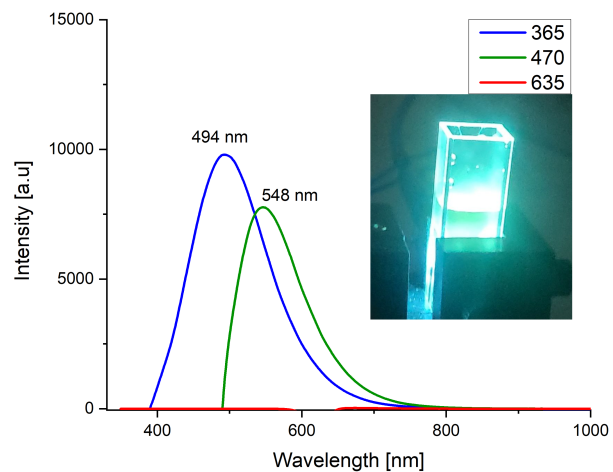
Results and Discussion

4.1 Optical Properties of CQDs

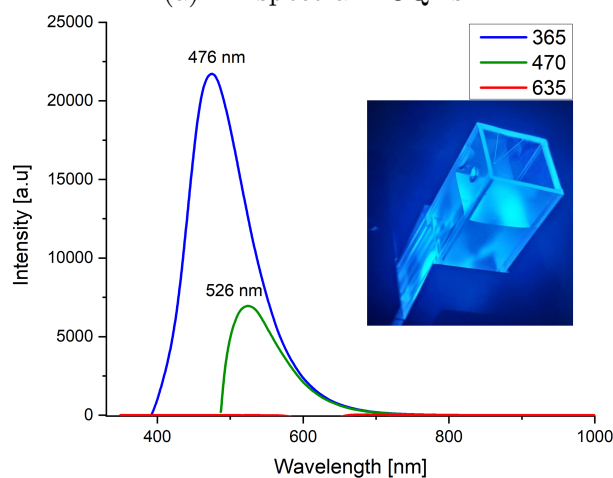
To understand the structure-function relationship between heteroatoms and carbon quantum dots, functionalization was performed using six different precursors molecules. After synthesis processes were completed, properties of obtained CQDs were analyzed and their emission spectra at different excitation wavelengths were recorded.

4.1.1 Emission Photoluminescence Properties

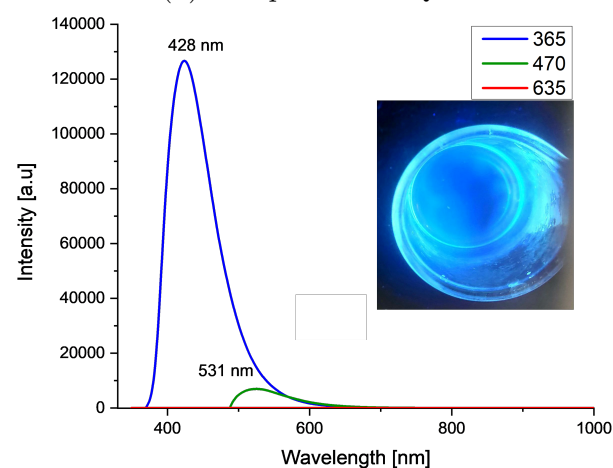
The photoluminescence (PL) spectra of the CQDs synthesized from citric acid in combination with the different surface modification precursors (SMP) were determined. However, only the CQDs synthesized that exhibited fluorescence (L-CQDS, ECQDs, and D-CQDS) are shown in the Figure 4.1. In contrast to the materials obtained from the other precursors for surface modification, the material obtained from cinnamic acid and 2-mercaptoethanol exhibited emission peaks that coincide with the excitation wavelengths, suggesting that the electronic states responsible for emission are light incident. This can be observed in Appendix 5.2. Only A-CQDs show a emission peak at 470 nm but with low intensity. These PL spectra does not revel a shift as the following precursors. For this reason, CQDs obtained from this synthesis process were discarded for the subsequent studies.



(a) PL spectra L-CQDs



(b) PL spectra E-CQDs



(c) PL spectra D-CQDs

Figure 4.1: PL spectra of CQDs obtained from L-cysteine (L-CQDs), ethylenediamine (E-CQDs), and Diethylenetriamine (D-CQDs) at the excitation wavelengths of 365, 465, and 635 nm

The maxima of the two prominent emission bands identified in the PL spectra of L-CQDs, shown in Figure 4.1a located at 494 nm (under $\lambda_{ex} = 365$ nm) and 548 nm (under $\lambda_{ex} = 470$ nm) are consistent with the expected red shift from the fluorescence phenomenon. Although the intensity of the longer wavelength band is lower, this is still a prominent and well-defined emission band. On the other hand, diethylenetriamine presents a sharp and intense peak at 428 nm when excited at 365 nm, indicating strong blue fluorescence. Another much smaller peak is observed at 531 nm under $\lambda_{ex} = 470$ nm, indicating a minimal response in the yellow region. The last one, ethylenediamine demonstrates a single sharp peak at 476 nm under 365 nm excitation, displaying bright blue fluorescence. A smaller peak at 526 nm under 465 nm excitation indicates a transition to green fluorescence under a slightly longer excitation wavelength.

According to Xiao et al. [115], CQDs synthesized using L-cysteine exhibited strong and stable photoluminescence with a high fluorescence intensities. The emission peak was obtained at 461 nm when excited at 390 nm, indicating that fluorescent substances or structures dominate the fluorescence of CQDs in this excitation range. This suggests that under these specific excitation conditions, the CQDs exhibit robust fluorescent properties, which is consistent with findings in related studies. Similarly, Kim et al. [116], supports the strong blue and green emissions observed in their study. The peak excitation at 370 nm results in the highest emission at 445 nm. Notably, the maximum fluorescence emission of CQDs remains constant regardless of changes in the excitation wavelength. These studies collectively validate the observed optical properties of L-cysteine synthesized CQDs in the present study.

In the spectra shown in Figure 4.1b, carbon quantum dots synthesized with ethylenediamine E-CQDs showed distinct emission peaks under various excitation wavelengths. Notably, at 365 nm excitation, a prominent emission peak was observed at 473 nm with a high intensity. At 465 nm excitation, a significant emission peak appeared at 524 nm with an intensity of around 8000 a.u., indicating excitation-dependent photoluminescence. According to the literature, the CQDs emission maximum at 454 nm, is observed when the excitation occurs at 360 nm of synthesized by microwave-assisted reaction of citric acid and ethylenediamine [117]. In another study, it was demonstrated that fluorescent carbon dot from citric acid and ethylenediamine revealed an emission maximum at 441 nm (the emission region is mainly concentrated at 400–550 nm) [118].

A fluorescence emission spectrum was employed to investigate the typical optical properties of carbon quantum dots (CQDs) synthesized using diethylenetriamine. In the fluorescence emission spectra, the CQDs exhibited distinct emission peaks under different excitation wavelengths. Specifically, under 365 nm excitation, a notable emission peak appeared at

423 nm with a high intensity. Under 470 nm excitation, a significant emission peak was observed at 525 nm with a lower intensity. These observed maximum emissions at 428 nm and 531 nm, suggest enhanced blue and green emission properties due to the specific synthesis conditions. According to the literature, graphene carbon dots with blue emission through reflux treatment of citric acid in the presence of diethylenetriamine demonstrates strong photoluminescence emission peak obtained at 461 nm when excited at 440 nm [119].

4.1.2 UV–Vis Absorption Spectroscopy

As seen in the previous study, the CQDs synthesized using cinnamic acid (CnnA), allicin (ALLI), and 2-mercaptoethanol (MPET) did not exhibit fluorescence and were therefore excluded from subsequent studies. From this characterization, only L-CQDS, E-CQDS, and D-CQDS are considered in further work.

L-CQDs

The UV-Vis absorbance spectrum of L-CQDs is presented in Figure 4.2. The spectrum exhibits a distinctive absorption peak in the 200-250 nm range, attributed to $\pi - \pi^*$ transitions of C=C and C=O bonds present in the CQDs. Beyond this peak, the absorbance decreases markedly, maintaining a low and relatively constant profile within the 300-600 nm range [120]. This spectral behavior suggests the absence of significant electronic transitions in the latter region, which is characteristic of CQDs lacking extensively conjugated functional groups [121].

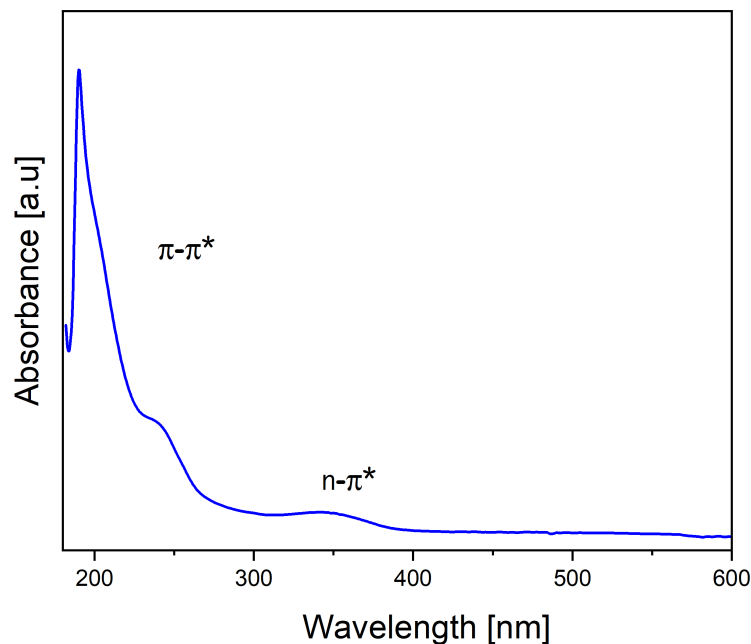


Figure 4.2: UV-Vis absorption spectra of synthesized carbon dots with l-cysteine

E-CQDs

The UV-Vis absorbance spectra of CQDs synthesized from EDA and CA (Figure 4.3 exhibits two distinct absorption peaks. The first peak, centered at approximately 270-280 nm, corresponds to $\pi - \pi^*$ transition of the conjugated carbon-carbon units associated with the carbon core [122]. A second, less intense peak in the 350-380 nm region suggests the presence of surface states or defects, likely originating from functional groups on the CQDs surface that suggest nonbonding orbital to antibonding pi orbital $n - \pi^*$ transitions of the carbonyl/amine functional groups present on E-CQDs [123]. These spectral characteristics align with previous literature reports on CQDs synthesized from similar precursors. Additionally, these CQDs demonstrate strong blue fluorescence under UV excitation, suggesting the successful synthesis of fluorescent E-CQDs.

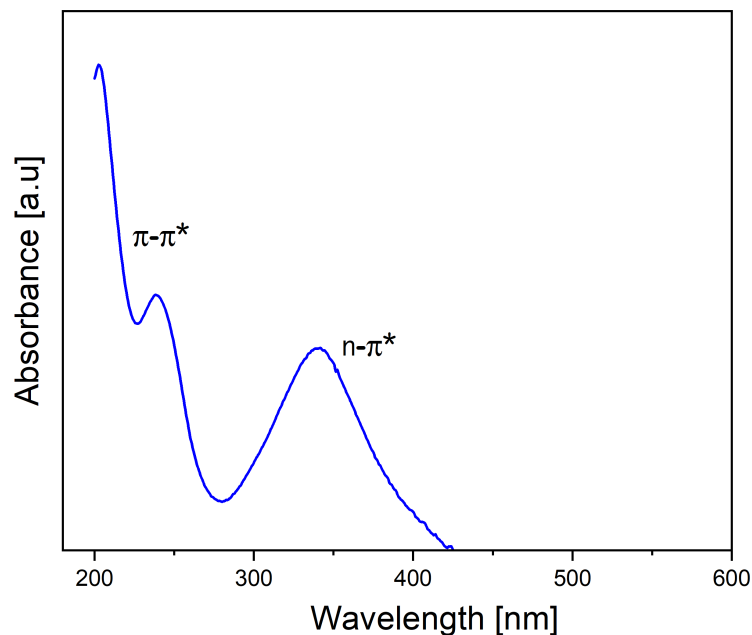


Figure 4.3: UV-Vis absorption spectra of synthesized carbon dots with ethylenediamine

D-CQDs

The UV-Vis absorbance spectrum of D-CQDs synthesized is presented in Figure 4.4. The spectrum exhibits two distinct absorption peaks. The first peak, observed in the range of 200-250 nm, is attributed to $\pi - \pi^*$ transitions of C=C and C=O bonds present in the CQDs. The second peak, located in the 350-400 nm range, corresponds to $n - \pi^*$ transitions of C=O or C-OH bonds within the CQDs structure. Fluorescence spectroscopy reveals that these CQDs exhibit optimal emission in the blue region of the visible spectrum. Notably, neither the citric acid nor the diethylenetriamine precursor solutions display luminescence in the visible region when excited at the wavelength used for CQDs analysis. This observation confirms that the observed bright blue fluorescence originates exclusively from the synthesized CQDs [124].

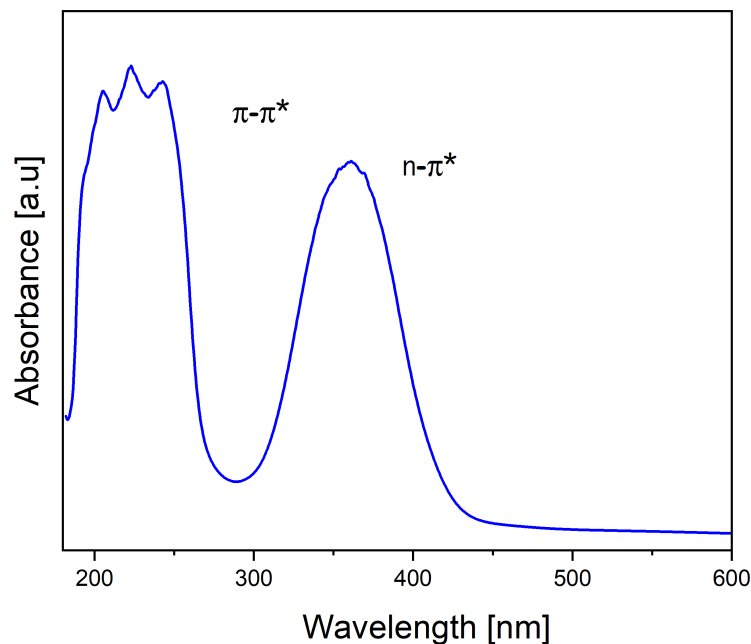
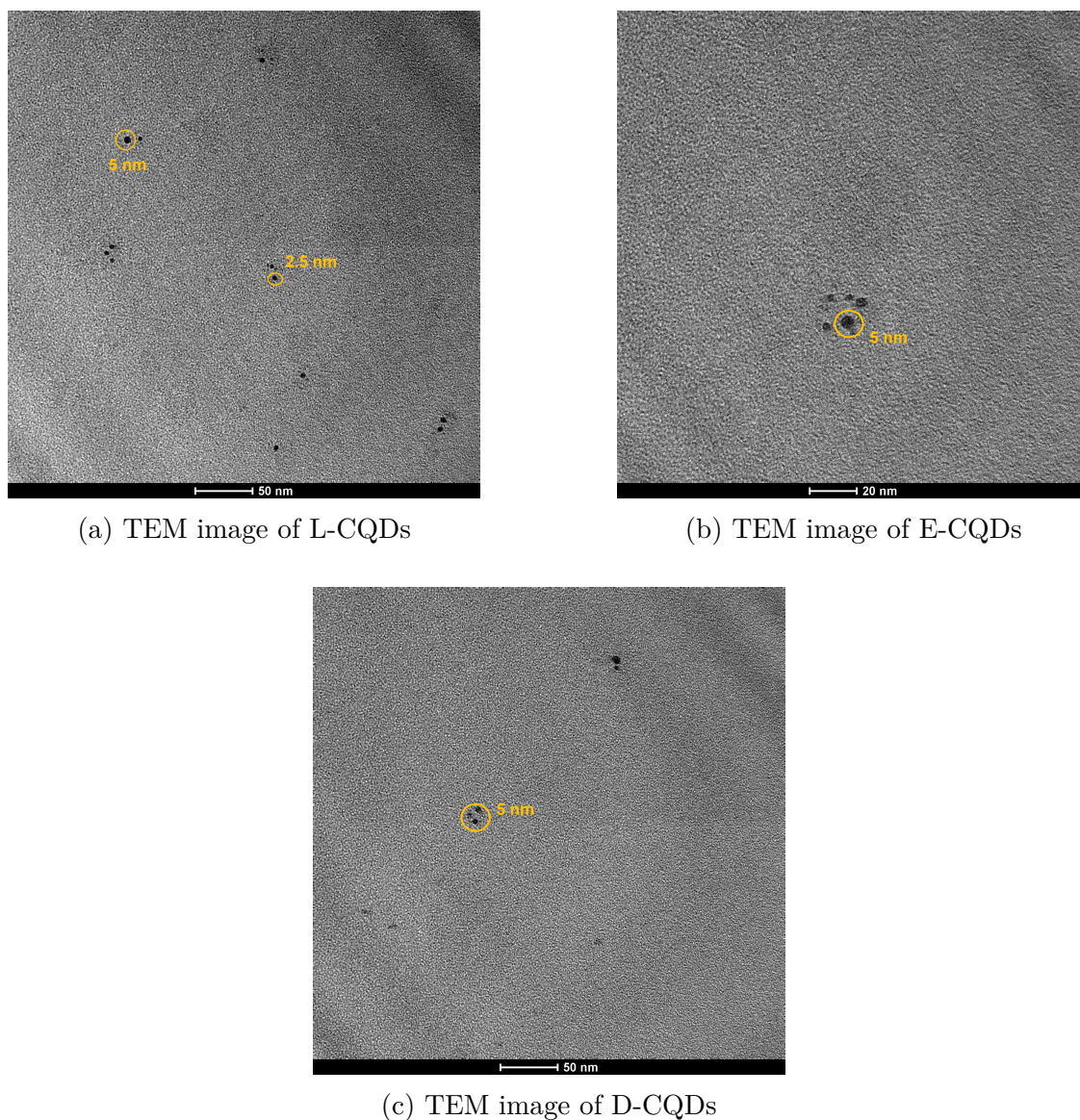


Figure 4.4: UV–Vis absorption spectra of synthesized carbon dots with diethylenetriamine

4.2 Structural Analysis of CQDs

4.2.1 Transmission Electron Microscopy Analysis

The morphology and particle size of the L-CQDs, E-CQDs and D-CQDs, where characterized by TEM, and the results are presented in Figure 4.5a, 4.5b and 4.5c, respectively. The images shows that CQDs are well-dispersed and spherical, with no notable agglomeration. The average size of these L-CQDs is around 4 nm. Similarly, E-CQDs present a 5 nm of size. Finally, D-CQDs exhibit 4 nm. This indicates that regardless of precursor used (L-cysteine, ethylenediamine, or diethylenetriamine), the resulting CQDs exhibit a uniform size of around 5 nm. This suggesting that the synthesis process was robust and controlled, consistently achieving particles of uniform size. The similarity in size can be important for applications where the CQDs size affects their properties [125].



(a) TEM image of L-CQDs

(b) TEM image of E-CQDs

(c) TEM image of D-CQDs

Figure 4.5: TEM of CQDs obtained from a) L-cysteine (L-CQDs), b) ethylenediamine (ECQDs), and c) Diethylenetriamine (D-CQDs)

4.2.2 Structural Analysis of CQDs by FT-IR

Fourier Transform Infrared Spectroscopy (FT-IR) was used to identify the functional groups of the functional groups present in the different CQDs based on the peaks values in the region of IR radiation

L-CQDs FT-IR

FT-IR spectra of LCYS, CA, and L-CQDs shown in Figure 4.6 exhibits various characteristic bands, which evidenced the different interactions. Additionally, in the Table 4.1, are

shown the assignments of the band of the spectra. The broadband around $3500\text{-}3200\text{ cm}^{-1}$ corresponds to O–H and N–H stretching vibrations, indicative of hydroxyl and amine groups. This is consistent with the spectra of the precursors (LCYS, CA) and L-CQDs, which also exhibit broad O–H stretches in this region.

The absorption band at 2950 cm^{-1} occurring in all samples indicates the presence of C–H vibrations of aliphatic compounds. For LCYS, a weak band around $2500\text{-}2000\text{ cm}^{-1}$ can be attributed to S–H stretching vibrations, which are prominently observed in the CQDs FT-IR spectrum, suggesting potential interactions or modifications of the thiol group during the synthesis process.

In the region of $1700\text{-}1600\text{ cm}^{-1}$, the L-CQDs spectrum exhibit bands that can be assigned to C=O stretching vibrations. These bands may arise from both amide and carboxylic groups, reflecting contributions from both LCYS and CA. The presence of these bands confirms the integration of these functional groups into the CQDs structure.

The bands between $1400\text{-}1300\text{ cm}^{-1}$ are associated with C–H and O–H deformations, common in both LCYS and CA, suggesting that these functional groups are retained in the CQDs. Additionally, the region of $1200\text{-}1000\text{ cm}^{-1}$ shows bands corresponding to C–O and C–N stretching vibrations, indicating the presence of these functionalities in the CQDs. The C–N stretching suggests the incorporation of nitrogen-containing groups from LCYS.

Notably, the bands in the region of $700\text{-}600\text{ cm}^{-1}$ are indicative of C–S stretching vibrations. This confirms that the sulfur-containing groups from LCYS are preserved in the CQDs.

Table 4.1: Assignments of IR bands spectra of L-CQDs

L-Cysteine	Samples		Wavenumber cm^{-1}
	Citric Acid	L-Cysteine CQDs	
O-H or N-H stretch	OH stretch	O-H and N-H stretch	3500-3200
C-H aliphatic stretch	C-H aliphatic stretch	C-H aliphatic stretch	2950
S-H (weak) stretch		S-H (weak) stretch	2500-2270
C=O stretch	C=O stretch	C=O stretch	1700-1600
N-H bending		N-H bending	1600-1500
C-H bend		C-H bend	1400-1300
C-N stretch	C-O stretch	C-N stretch	1200-1000
C-S stretch		C-S stretch	700-600

The FT-IR spectra demonstrate that the L-CQDs retain key functional groups from their precursors, including O–H, N–H, C=O, C–H, C–N, and C–S bonds. This suggests successful incorporation of these functional groups into the CQDs, which could influence their chemical and optical properties. The most of bands are presented in the L-CQDs synthesis are associated with the literature [116, 115, 126, 127].

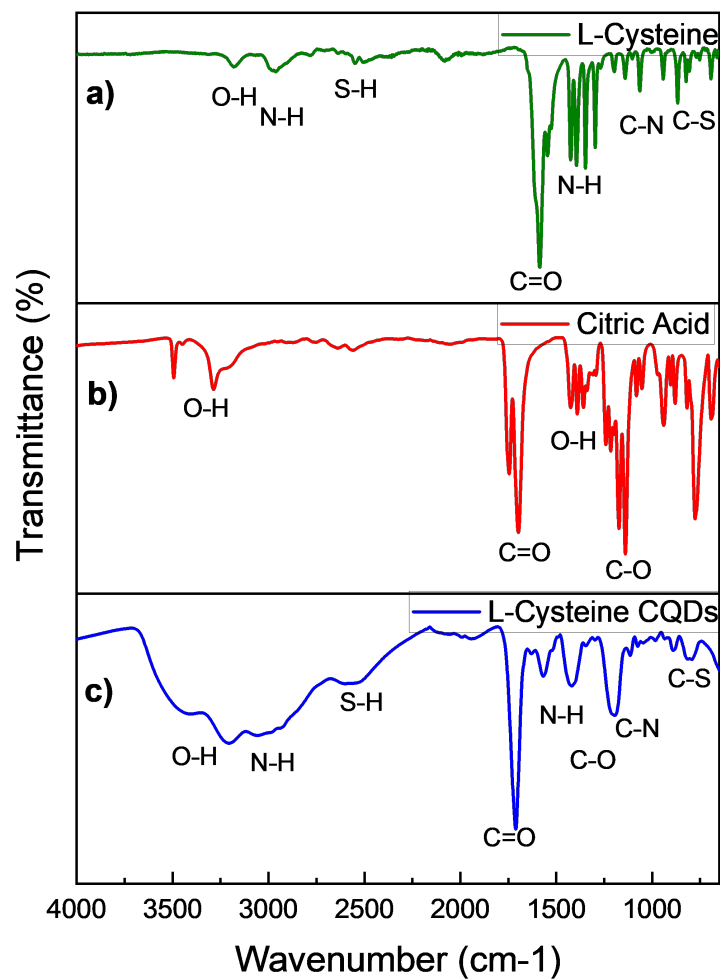


Figure 4.6: FT-IR spectra of a) L-Cysteine reference, b) citric acid reference and c) L-Cysteine CQDs

E-CQDs FT-IR

Several characteristic bands of EDA, AC, and E-CQDs are observed in the Figure 4.7.

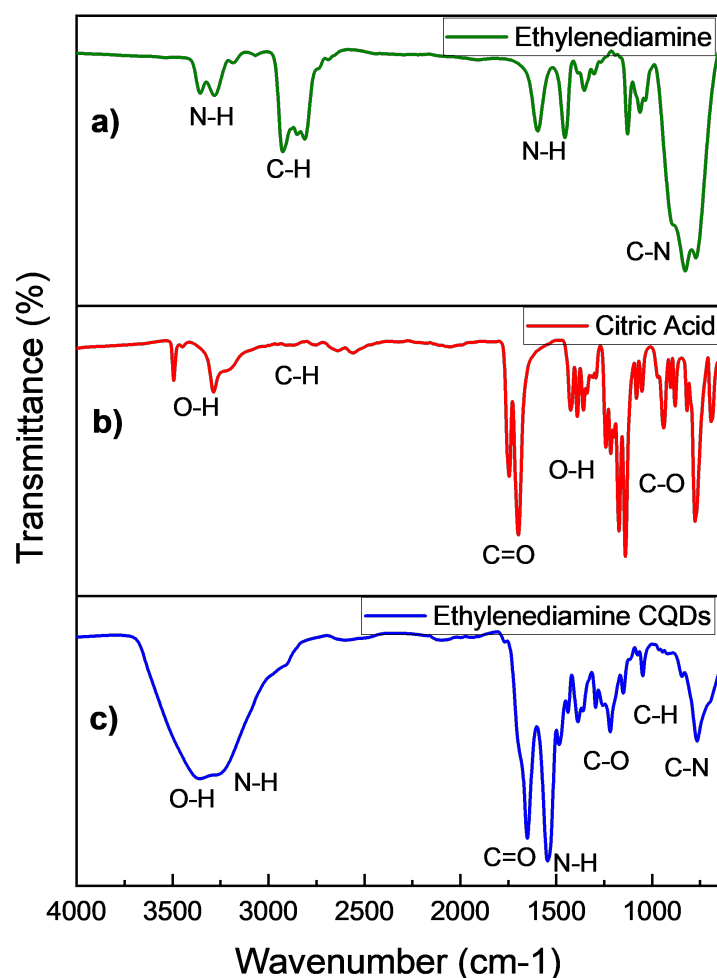


Figure 4.7: FT-IR Spectra of a) ethylenediamine reference, b) citric acid reference and c) ethylenediamine CQDs

In Table 4.2, are exhibited the band values of the spectras. The broad band around $3500\text{-}3200\text{ cm}^{-1}$ corresponds to O–H and N–H stretching vibrations, indicating the presence of hydroxyl and amine groups. This observation suggests with the spectra of the precursors, EDA and CA, both of which exhibit broad O–H stretches in this region.

Table 4.2: Assignments of IR spectra of E-CQDs

Ethylenediamine	Samples		Wavenumber cm ⁻¹
	Citric Acid	Ethylenediamine CQDs	
N-H stretch	OH stretch	O-H and N-H stretch	3500-3200
C-H aliphatic stretch	C-H aliphatic stretch	C-H aliphatic stretch	2950-3100
	C=O stretch	C=O stretch	1750-1600
N-H bending		N-H bending	1600-1500
C-H bend	C-O stretch	C-H bend and C-O stretch	1400-1300
C-N stretch	C-O stretch	C-O stretch and C-N stretch	1200-1000

Absorption bands at approximately 2950-3100 cm⁻¹ suggest the presence of C–H stretching vibrations of aliphatic compounds, which are consistent across all samples. In the region of 1700-1600 cm⁻¹, the E-CQDs display bands that can be attributed to C=O stretching vibrations. These bands may arise from both amide and carboxylic groups, suggesting contributions from both ethylenediamine and citric acid. This confirms the integration of these functional groups into the CQDs structure.

The bands between 1400-1300 cm⁻¹ are associated with C–H bend and C–O stretch, which are common in both EDA and CA indicating the retention of these functional groups in the CQDs. Additionally, the region of 1200-1000 cm⁻¹ shows bands corresponding to C–O and C–N stretching vibrations, signifying the presence of these functionalities in the CQDs. The C–N stretching bands suggest the incorporation of nitrogen-containing groups from ethylenediamine. The literature reports bands that closely match the majority of those observed in the synthesis of E-CQDs [118, 122, 128, 129, 130, 131].

D-CQDs

In the FT-IR spectra of DETA, CA, and D-CQDs, various characteristic bands are observed in the Figure 4.8. As shown in Table 4.3, the broad band around 3500-3200 cm⁻¹ corresponds to the O–H and N–H stretching vibrations, indicative of hydroxyl and amine groups. This is consistent with the spectra of the precursors, DETA and CA, which also exhibit broad O–H stretches in this region.

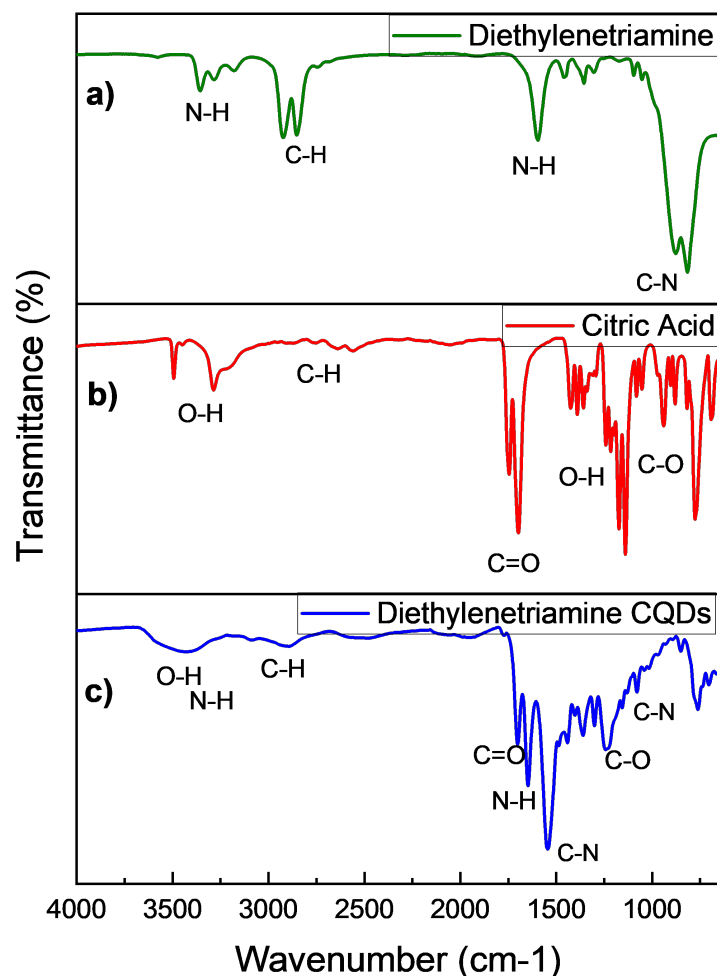


Figure 4.8: FT-IR Spectra of a) diethylenetriamine reference, b) citric acid reference and c) diethylenetriamine CQDs

Absorption bands at 2930-3000 cm⁻¹ in all samples indicate the presence of C-H vibrations of aliphatic compounds. In the case of diethylenetriamine, bands around 1600-1500 cm⁻¹ can be attributed to N-H bending and C-N stretching vibrations, which are prominently observed in the CQDs spectrum, suggesting the presence of amine groups that have not undergone significant modification during the synthesis process.

In the region of 1750 cm⁻¹, D-CQDs exhibit bands that can be assigned to C=O stretching vibrations. These bands may arise from both amide and carboxylic groups, reflecting contributions from both precursors, DETA and CA. The presence of these bands confirms the integration of these functional groups into the structure of the CQDs.

Table 4.3: Assignments of IR spectra bands of D-CQDs

Diethylenetriamine	Samples		Wavenumber cm^{-1}
	Citric Acid	Diethylenetriamine CQDs	
N-H stretch	OH stretch	O-H and N-H stretch	3500-3200
C-H aliphatic stretch	C-H aliphatic stretch	C-H aliphatic stretch	2930-3000
	C=O stretch	C=O stretch	1750-1600
N-H bending and C-N stretch		N-H bending and C-N stretch	1600-1500
	C-O stretch	C-O stretch	1400-1300
	C-O stretch	C-O stretch and C-N stretch	1200-1000

The bands between $1400\text{-}1300\text{ cm}^{-1}$ are associated with C–H and O–H deformations, common in both diethylenetriamine and citric acid. This suggests that these functional groups are retained in the CQDs. Additionally, the region of $1200\text{-}1000\text{ cm}^{-1}$ shows bands corresponding to C–O and C–N stretching vibrations, indicating the presence of these functionalities in the CQDs. The C–N stretch suggests the incorporation of nitrogen-containing groups from diethylenetriamine.

The FT-IR spectra demonstrate that D-CQDs retain key functional groups from their precursors, including O–H, N–H, C=O, C–H, and C–N. This suggests a successful incorporation of these functional groups into the CQDs. Addition, this analysis suggests that during the synthesis of CQDs from DETA and CA, chemical reactions have occurred, leading to the formation of new functionalities, primarily amides, which were not present in the original precursors [132, 133, 134, 135].

4.3 Stability of CQDs

4.3.1 Stability with concentration of CQDs

The stability in concentration of CQDs ensures that they maintain their original characteristics, allowing experiments and applications to be replicate. Based in this study was only performed on the synthesis that exhibited notable emission peak at 365 nm, specifically L-CQDs, D-CQDs and E-CQDs.

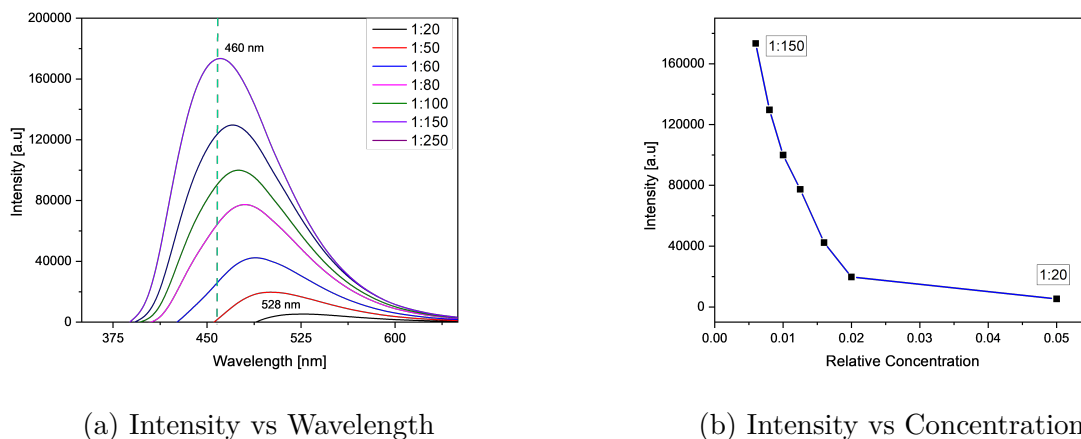


Figure 4.9: Fluorescence spectra of L-CQDs at different dilutions

L-CQDs

The fluorescence spectra shown in Figure 4.9, the emission behavior of CQDs functionalized with L-cysteine is observed with respect to their concentration. The results show that fluorescence intensities vary with different dilutions of the CQDs, from 1:20 (less diluted) to 1:250 (more diluted). The study suggests that higher dilutions (1:250) of CQDs functionalized with L-cysteine exhibit greater fluorescence intensity. Additionally, as the concentration of CQDs decreases (from 1:20 to 1:250), a redshift into longer wavelengths is observed. This can be seen in the shift of the maximum emission wavelength from 460 nm to 528 nm.

D-CQDs

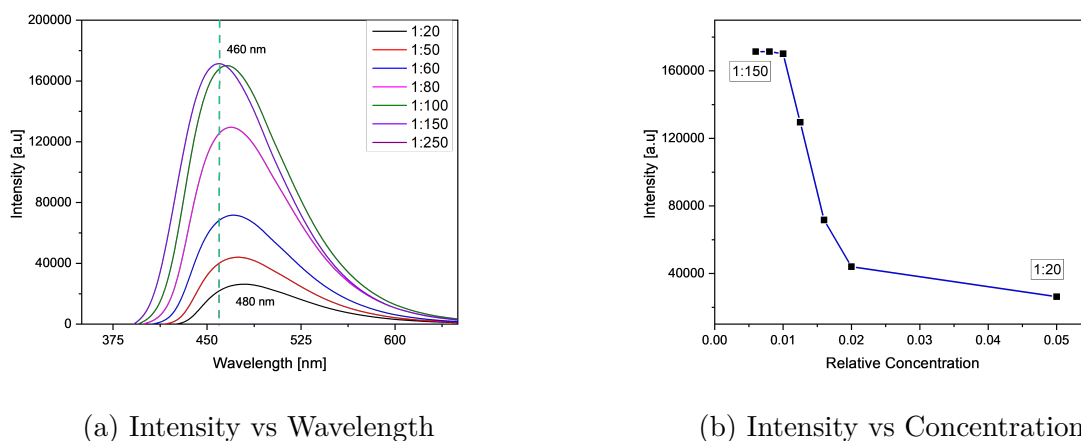


Figure 4.10: Fluorescence Spectroscopy to different dilutions of Diethylenetriamine CQDs

As in the case of L-CQDs, Figure 4.10 shows fluorescence spectra CQDs functionalized with

diethylenetriamine for several dilutions, from 1:20 (less diluted) to 1:150 (more diluted). As illustrated in L-CQDs, a redshift towards longer wavelengths is observed. This is manifested in the shift of the maximum emission wavelength from 460 nm to 480 nm. Fluorescence intensity increases with dilution, being higher at 1:150 and lower at 1:20, suggesting that the reduction of self-absorption and quenching phenomena in more diluted solutions improves emission. This behavior is consistent with previous studies showing that concentration affects fluorescence intensity as a result of these mechanisms, highlighting the importance of concentration in the optical properties of D-CQDs.

In many fluorescent organic molecules, when they are aggregated or concentrated at high levels, their fluorescence decreases [136]. This phenomenon is known as aggregation-induced quenching. The same effect has been commonly observed in CQDs [137]. Aggregation induced quenching, also called **aggregation-caused quenching (ACQ)**, is the phenomenon in some light-emitting materials where the light emission by the luminophores is drastically reduced or even totally extinguished by their aggregation or clustering. This contrasts with their behavior in the monodisperse state, where the molecules are separated and emission. In traditional luminophores, strong and planar intermolecular interactions in the aggregated state can lead to the formation of non-radiative excitonic states or facilitate non-radiative energy transfer between aggregated molecules. These interactions can cause the excited energy to dissipate as heat rather than being emitted as light, resulting in weakened or extinguished emission in the aggregated state [138].

Most CQDs experiment a decrease in luminescence intensity as concentration increases, due to quenching and reabsorption effects at high concentrations, which occur once a low concentration threshold is exceeded. The fluorescence quenching effect induced by the aggregation of small luminescent organic molecules with flat aromatic ring structures can be explained as follows: when these molecules are close enough, their planar polycyclic aromatic ring structure causes them to orient due to strong $\pi - \pi$ stacking intermolecular interactions. This overlap allows the photoexcited state to return to the ground state through a non-radiative transition, resulting in luminescence quenching [136]. However, due to the structural complexity of CQDs, various quenching mechanisms may be present, which are difficult to distinguish. In the case of small organic fluorophore molecules, aggregation is often prevented by introducing steric hindrances or controlling molecular conformation.

E-CQDs

Otherwise, the Figure 4.11 shows fluorescence spectra of carbon quantum dots synthesized with ethylenediamine and shows a behavior opposite to that of diethylenetriamine and

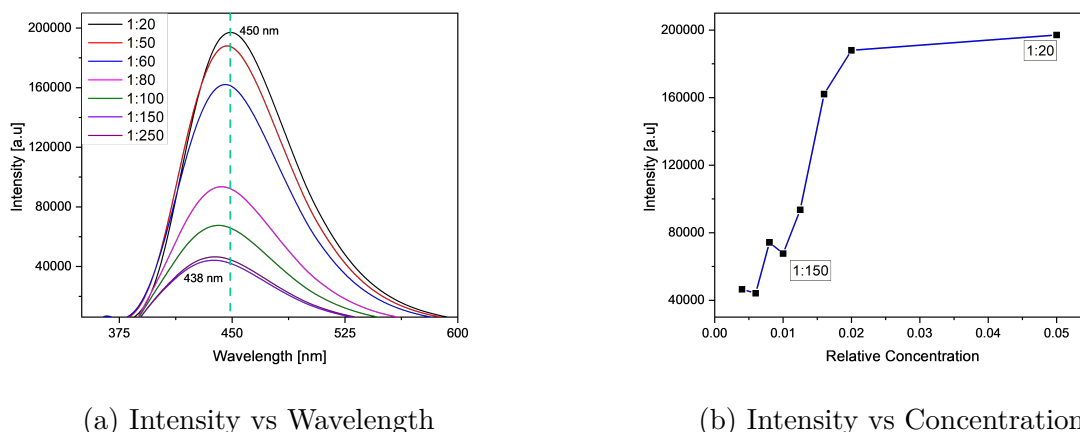


Figure 4.11: Fluorescence Spectroscopy to different dilutions of Ethylenediamine CQDs

l-cystein due to for dilutions ranging from 1:20 (less diluted) to 1:250 (more diluted). The maximum fluorescence is observed around 450 nm. Unlike another CQDs, the fluorescence intensity is higher in less diluted solutions (1:20) and decreases as the solution becomes more diluted (1:250).

This behavior can be explained by **aggregation-induced emission (AIE)**. This process refers in which fluorophores emit weakly in very dilute solutions but radiate strongly in an aggregated form. In small organic molecules, AIE is achieved by restricting intramolecular rotation and vibration or through highly twisted structures that weaken intermolecular $\pi - \pi$ stacking. In CQDs, similar AIE phenomena involve aggregation-induced fluorescence enhancement with red shifts in the emission wavelength. It has been reported that aggregation increases the conjugation of surface luminophores, decreases the band gap, and results in a red shift with increased concentration [136, 139]. AIE in CQDs has captured the attention of research because of its fascinating aspects, such as its sensitivity to changes in pH and solvent polarity, large Stokes shift, high photostability, and biocompatibility. These characteristics make CDs ideal for various applications [140].

4.3.2 Stability with Time

This study was only performed on the synthesis that exhibited emission peak at 365 nm, and the L-CQDs and D-CQDs.

First, in the Figure 4.12 shows a series of fluorescence spectra of L-CQDs measured at different time intervals (1, 3, 7, 12, and 15 days). The fluorescence intensity, peaking around 450-460 nm, is highest on the first day. Over time, there is a gradual decline in fluorescence intensity, with the largest decrease observed between the 1st and 15th days.

The spectral curve shape remains consistent throughout the measurements, though the overall intensity decreases as time progresses, indicating a loss of fluorescence efficiency or stability of the carbon quantum dots over time. The emission peak position stays relatively constant near 450-460 nm without significant shifts, suggesting that the main optical properties are maintained despite the reduction in intensity.

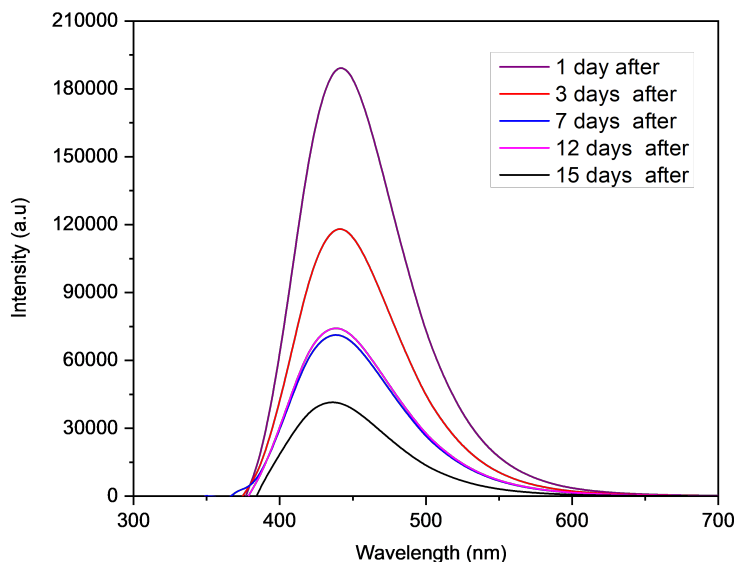


Figure 4.12: PL spectra of L-CQDs at different days

A set of fluorescence spectra measured at different time intervals (1, 3, 7, and 15 days) of D-CQDs is shown in the figure 4.13. The fluorescence intensity progressively decreases over time, with the peak consistently around 450 nm. Initially, the first day shows a strong fluorescence intensity, but the highest intensity is observed on the third day. After that, the intensity significantly decreases by the seventh day and continues to reduce more gradually by the fifteenth day. Despite the decrease in intensity, the emission peak remains consistent throughout the measurements.

The Figures 4.12 and 4.13 illustrate a decrease in the fluorescence intensity of the material over time while maintaining a similar curve shape and peak wavelength (450 nm and 470 nm, respectively). In the Figure 4.12, the intensity gradually decreases from the first day to the fifteenth day. In the Figure 4.13, the intensity is highest on the third day and then significantly decreases by the seventh and fifteenth days. This behavior suggests a degradation process of the fluorescent emitting centers, possibly due to the formation of non-radiative defects or the decomposition of active components. Understanding this

process is crucial for evaluating the temporal stability and efficiency of fluorescent materials in practical applications [141].

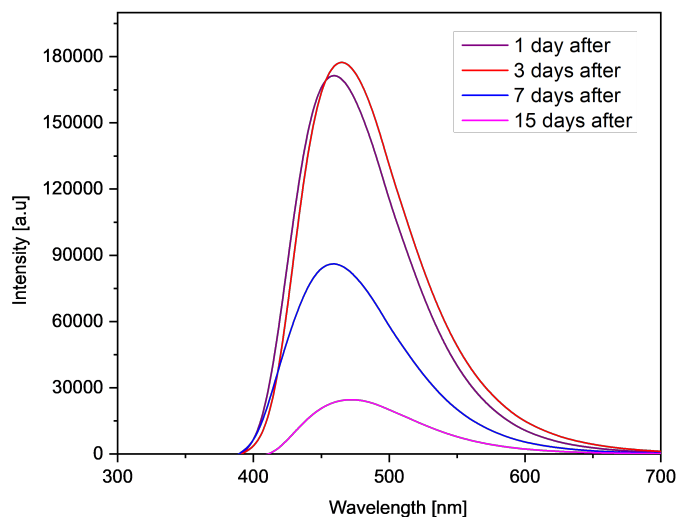


Figure 4.13: PL spectra of D-CQDs at different days

4.4 Selectivity and Sensing Study of CQDs

4.4.1 Selectivity Study

The selectivity of the prepared L-CQDs, E-CQDs, and D-CQDs for specific metal ions was examined by mixing the CQDs with various ion solutions (Al^{3+} , Fe^{3+} , K^+ , Cd^{2+} , Co^{2+} , Hg^{2+} , and Pb^{2+}), each ion solutions at concentration of 50 ppm.

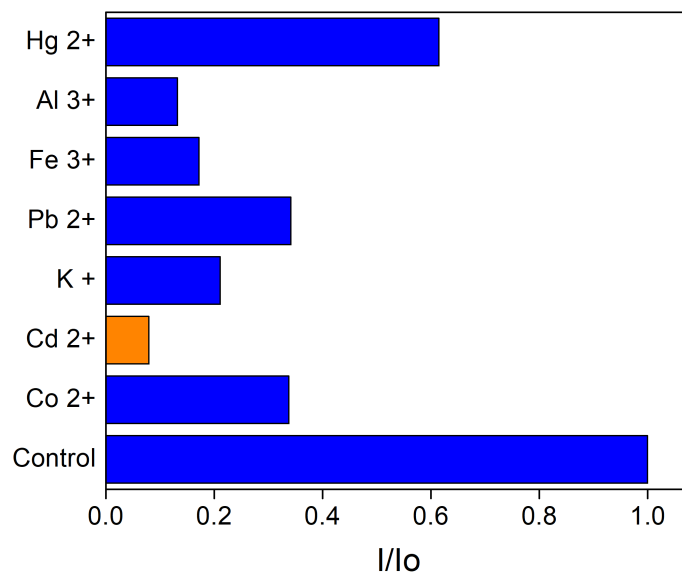


Figure 4.14: I/I₀ ratio of L-CQDs in the presence of 50 ppm of various metal ions

Figure 4.14 illustrates that the fluorescent L-CQDs do not exhibit sensitivity towards a single ion but rather demonstrate a heterogeneous response across various ionic species. The results reveal a pronounced response to Cd²⁺, followed by Al³⁺, Fe³⁺, and K⁺, while the sensitivity is notably lower for ions such as Co²⁺, Pb²⁺, and Hg²⁺. These findings indicate that the L-CQDs-based fluorescence sensor lacks high specificity for any individual ion but possesses the capability to detect multiple ionic species with varying degrees of sensitivity.

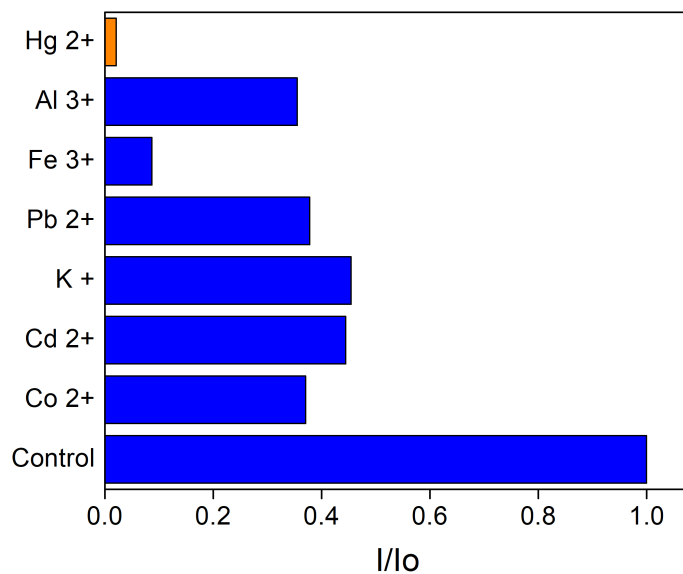


Figure 4.15: I/I_0 ratio of E-CQDs in the presence of 50 ppm of various metal ions

Conversely, the evaluation of fluorescence quenching effects induced by various metal ions on E-CQDs, as illustrated in Figure 4.15, revealed a substantially greater quenching effect for Hg^{2+} compared to other ionic species. The fluorescence emission intensity of the E-CQDs decreased by more than 90% upon exposure to the Hg^{2+} solution.

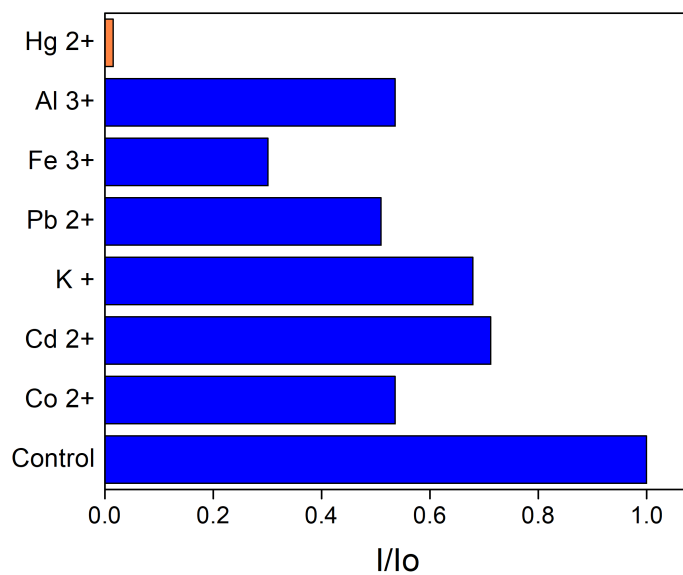


Figure 4.16: I/I_0 ratio of D-CQDs in the presence of 50 ppm of various metal ions

As illustrated in Figure 4.16, the introduction of Hg^{2+} to diethylenetriamine-derived CQDs (D-CQDs) resulted in a significant fluorescence quenching effect (exceeding 90%), whereas other metal ions induced only minimal quenching. These results demonstrate that D-CQDs exhibit excellent sensing capabilities, characterized by high selectivity for Hg^{2+} detection.

It is important to note that ethylenediamine and diethylenetriamine contains primary amine groups ($-\text{NH}_2$) that can form strong coordination bonds with mercury ions. Hg^{2+} exhibits a high affinity for nitrogen-based electron donors, resulting in robust interactions with the amine groups present in CQDs functionalized with ethylenediamine. This strong coordination between Hg^{2+} and the surface-bound amine groups of the E-CQDs is likely responsible for the observed selective fluorescence quenching. Additionally, the formation constant of Hg^{2+} complexes with amine ligands is typically higher than those of complexes formed with other metal ions, including alkali metals (e.g. K^+), alkaline earth metals (e.g. Ca^{2+}), and various transition metals. This superior complexation affinity implies that mercury ions will preferentially coordinate with the amine groups of ethylenediamine and diethylenetriamine functionalized CQDs, even in the presence of competing metal cations [142].

The thiol group ($-\text{SH}$) exhibits weak acidity but demonstrates remarkably strong complexation with numerous metal ions. It shares characteristics with neutral soft donors, forming particularly stable complexes with soft metal ions such as $\text{Cd}(\text{II})$ and $\text{Hg}(\text{II})$ [142]. Cd^{2+} possesses an ionic radius and charge that facilitate effective interactions with the available coordination sites on the surface of CQDs. According to the Hard and Soft Acids and Bases (HSAB) theory, Cd^{2+} , classified as a soft acid, preferentially interacts with soft bases such as thiols. This preferential interaction explains the strong affinity observed between Cd^{2+} and the thiol-functionalized CQDs [58].

4.4.2 Sensing with different metals

Sensing of Pb^{2+} ions by L-CQDs

To conduct a sensitivity study, the fluorescence response of L-CQDs was examined against various concentrations of Pb^{2+} , and the results are presented in Figure 4.17. It is observed that the fluorescence intensity of L-CQDs decreases as the concentration of Pb^{2+} increases, indicating that the degree of fluorescence quenching increases proportionally with the concentration of Pb^{2+} . Additionally, the solutions fluorescence intensity is noted at $\lambda_{em} = 434$ nm (emission wavelength).

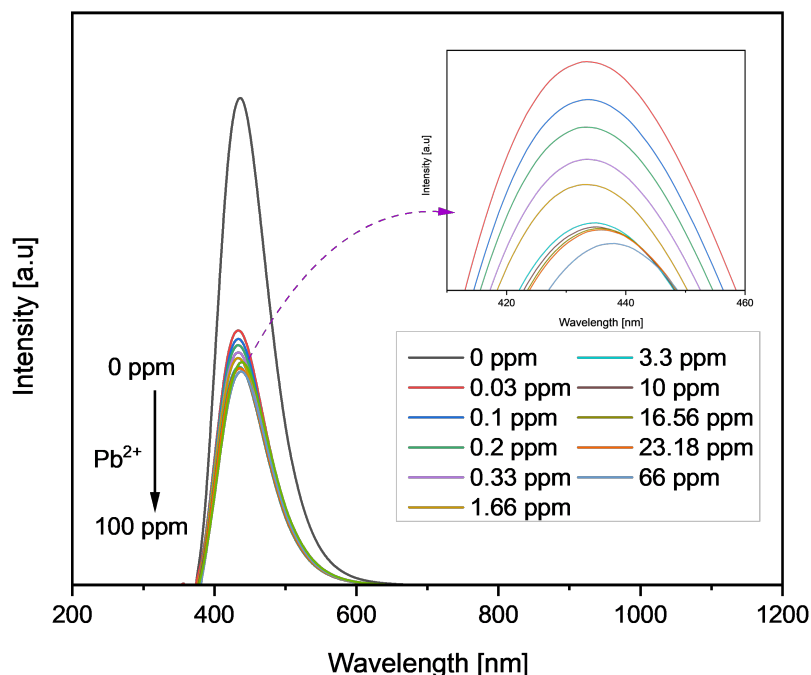
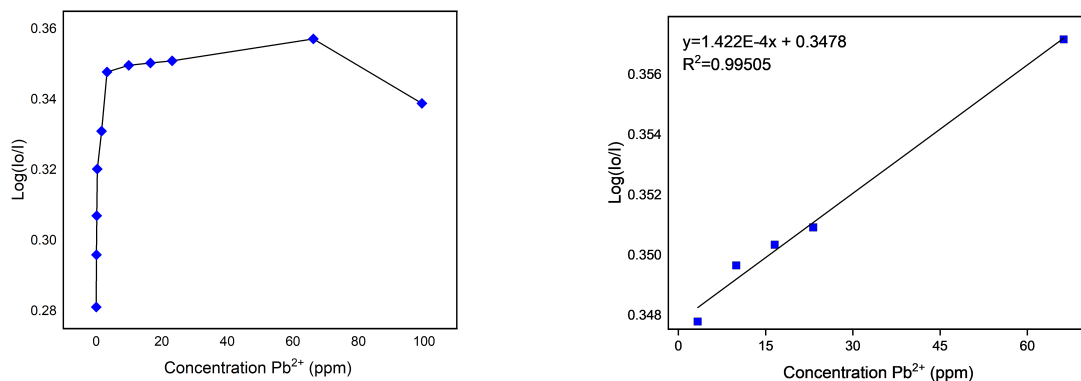


Figure 4.17: PL spectra of L-CQDs in the presence of Pb^{2+} ion in a concentration range of 0-66 ppm

The quenching effect, expressed as $\text{Log}(I_0-I)$, exhibited an excellent linear correlation ($R^2 = 0.995$) when plotted against Pb^{2+} concentration within the range of 0 to 66 ppm (Fig. 4.18b b). As the concentration of lead increases, the value of $\text{Log}(I_0-I)$ decreases (Fig. 4.18b a). This reduction in intensity (I) at high concentrations is a common phenomenon attributed to self-quenching, which can result from an increased frequency of molecular collisions presented in other systems, for example in the study of Ag^+ , the fluorescence of nitrogen-doped graphene quantum dots was quenched significantly through the charge transfer process[143]. Furthermore, the detection limit (LOD) for Pb^{2+} using L-CQDs was determined by analyzing the relationship between lead ion concentration and fluorescence intensity at 434 nm. Employing the equations 3.2 and 3.3, the LOD was calculated to be 5.63 ppm and LOQ was 18.79 ppm.

Sensing of Cd^{2+} ions by L-CQDs

To assess the sensitivity of L-CQDs towards Cd^{2+} , their fluorescence response were evaluated across a range of Cd^{2+} concentrations (0-100 ppm), as illustrated in Figure 4.19. The results demonstrate an inverse relationship between $\text{Cd}(\text{II})$ concentration and L-CQDs fluorescence intensity, consistent with the previous observations. This relationship indicates



(a) The non-linear trend of Pb^{2+} (ppm) and $\text{Log}(I_o/I)$ for concentrations between 0 and 100 ppm. (b) A linear relationship between the concentration of Pb^{2+} (ppm) and $\text{Log}(I_o/I)$ for low concentrations (0 to 60 ppm).

Figure 4.18: Fluorescence Spectroscopy to different dilutions of Ethylenediamine CQDs

that the degree of fluorescence quenching is proportional to the $Cd(II)$ concentration. All fluorescence intensity measurements were conducted at an emission wavelength of 425 nm.

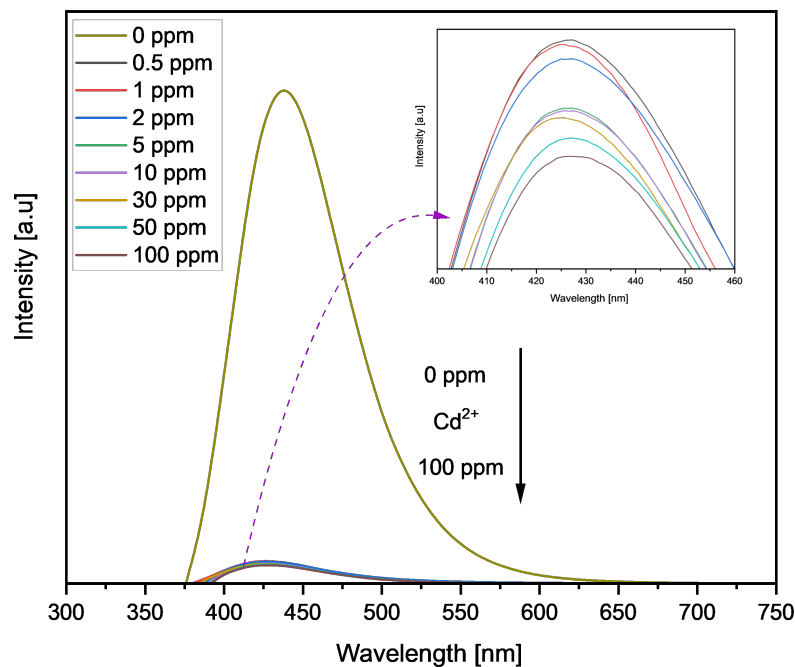
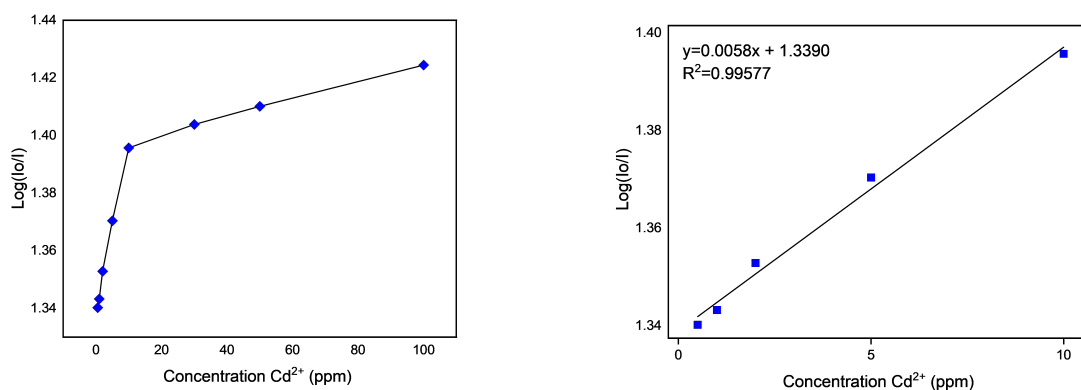


Figure 4.19: PL spectra of L-CQDs in the presence of Cd^{2+} ion (0-100 ppm)

The quenching effect, represented by $\text{Log}(I_o/I)$, exhibited an excellent linear correlation



(a) Non-linear trend of Cd²⁺ (ppm) and (b) Linear relationship between the concentration Log(I_o-I) for concentrations between 0 and 100 ppm and of Cd²⁺ (ppm) and Log(I_o-I) for low concentrations (0 to 10 ppm)

Figure 4.20: Fluorescence Spectroscopy to different dilutions of L-CQDs in a concentration range of 1-100 ppm

($R^2 = 0.995$) when plotted against Cd²⁺ concentration within the range of 0 to 10 ppm (Fig. 4.20b). As the cadmium concentration increased, the Log(I_o-I) value decreased (Fig.4.20a). The detection limit (LOD) for Cd²⁺ using L-CQDs was determined by analyzing the relationship between cadmium ion concentration and fluorescence intensity at 425 nm. Utilizing equations 3.2 and 3.3, the LOD and limit of quantification (LOQ) were calculated to be 0.8158 ppm and 2.7194 ppm, respectively.

According to the World Health Organization (WHO), the maximum concentration allowed of inorganic Cd²⁺ ions in drinking water is 0.003 ppm [144], demonstrated this sensor can not be successfully used to monitor the concentration of Cd²⁺ ions. For this purpose, in a previous study, sulfur co-doped carbon dots were synthesized via a hydrothermal process and employed for Cd²⁺ detection, yielding a limit of detection (LOD) of 0.00379 ppm [145]. Another study demonstrated that nitrogen and sulfur co-doped CQDs, synthesized using scallion as the carbon source, can function as effective fluorescent probes for Cd²⁺ ion detection and living cell imaging applications. These CQDs exhibited a linear response range for Cd²⁺ detection: 0.1–3.0 μM and 5.0–30.0 μM. The limit of detection achieved in this study was 15.0 nM, which is equivalent to 0.0031 ppm [146].

According to Pearson's Hard and Soft Acids and Bases (HSAB) theory, the affinity of metals for nitrogen and sulfur can be explained by the interaction between soft acids and soft bases. In this context, CQDs functionalized with nitrogen and sulfur act as soft bases, while Cd²⁺ ions act as soft acids. This complementary acid-base character facilitates strong interactions. The observed fluorescence quenching effect is attributed to

the interaction between cadmium ions and the surface functional groups of the nitrogen and sulfur co-doped carbon dots. Specifically, the cadmium ions potentially coordinate with the sulfhydryl (-SH), hydroxyl (-OH), and amide (-CONH₂) groups present on the L-CQDs, leading to aggregation and subsequent fluorescence quenching [146, 147].

Sensing of Hg²⁺ ions by E-CQDs

To evaluate the sensitivity of E-CQDs towards Hg²⁺, their fluorescence response was analyzed over a range of Hg²⁺ concentrations (0-100 ppm). Various concentrations of Hg²⁺ were introduced to the E-CQDs solution. As the concentration of mercury(II) ions increased from 0 to 100 ppm, the fluorescence intensity of E-CQDs at 450 nm decreased gradually (Figure 4.21).

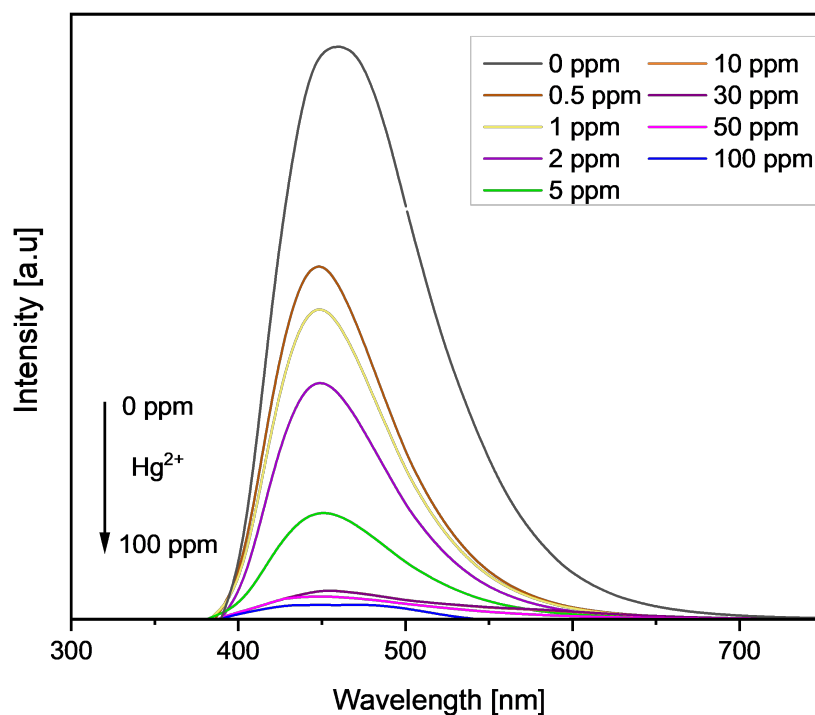
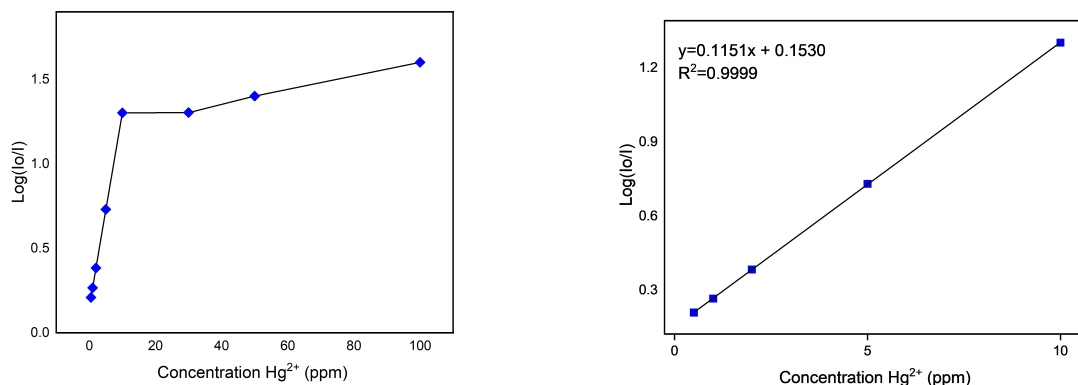


Figure 4.21: PL spectra of E-CQDs in the presence of Hg²⁺ ion in a range of 0-100 ppm

The quenching effect, represented by $\text{Log}(I_0-I)$, exhibited an excellent linear correlation ($R^2 = 0.999$) when plotted against Hg²⁺ concentration within the range of 0 to 10 ppm (Figure 4.22a). As the cadmium concentration increased, $\text{Log}(I_0-I)$ value decreased (Figure 4.22b). The LOD for Hg²⁺ using E-CQDs was determined by analyzing the relationship between mercury ion concentration and fluorescence intensity at 450 nm. Utilizing equations 3.2



(a) Non-linear trend of Hg^{2+} (ppm) and (b) Linear relationship between the concentration $\text{Log}(I_o-I)$ for concentrations between 0 and 100 of Hg^{2+} (ppm) and $\text{Log}(I_o-I)$ for low concentrations (0 to 10 ppm).

Figure 4.22: The relationship between fluorescence intensity ratio $\text{Log}(I_o-I)$ of E-CQDs and mercury (II) concentration

and 3.3, the LOD and limit of quantification (LOQ) were calculated to be 0.3597 ppm and 1.1990 ppm, respectively.

Sensing of Hg^{2+} ions by D-CQDs

Based on the fluorescent properties of D-CQDs, different concentrations of Hg^{2+} solution were added to the aqueous solution of D-CQDs to measure the fluorescence emission intensity and study the sensitivity of the CQDs chemosensor. As shown in Figure 4.23, the fluorescence intensity of the D-CQDs around $\lambda_{em} = 450\text{nm}$ gradually decreased as the Hg^{2+} concentration increased, indicating that the addition of Hg^{2+} effectively quenched the fluorescence of the D-CQDs.

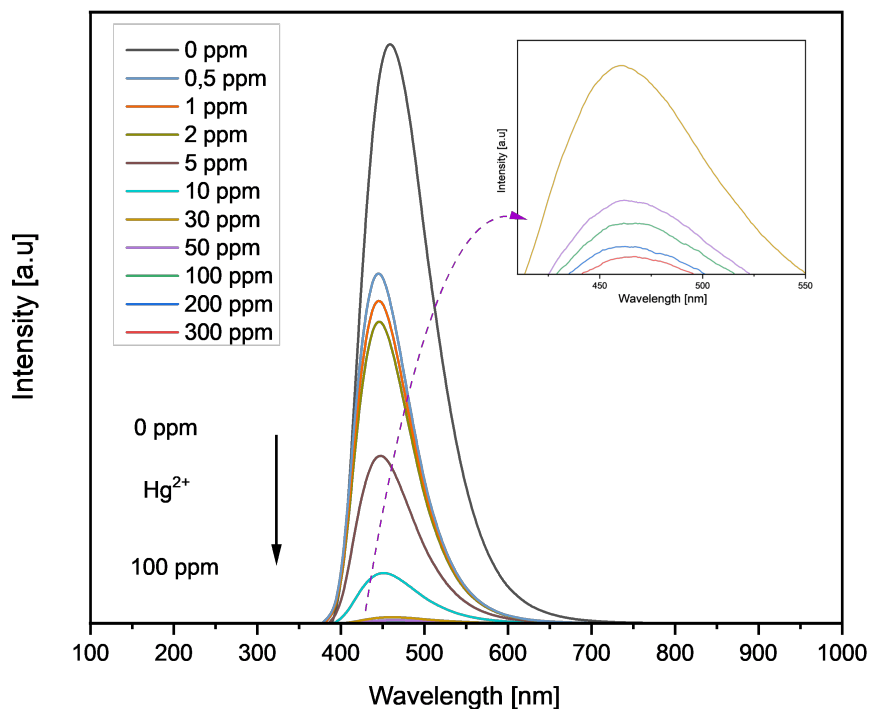
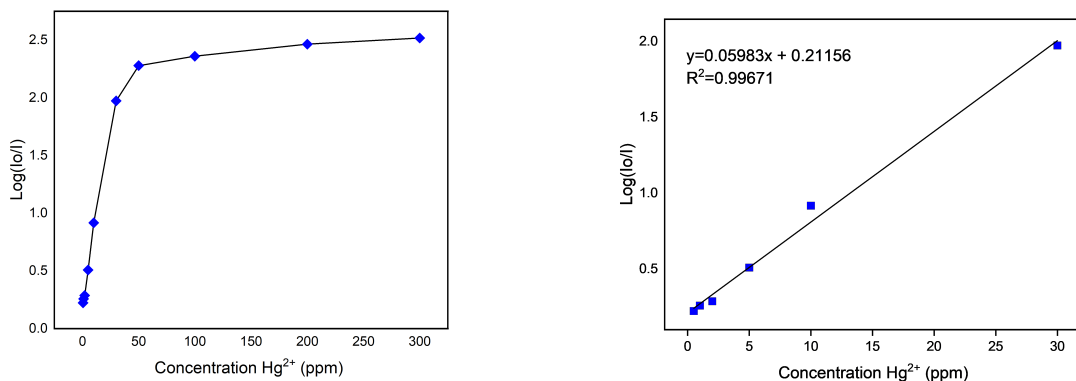


Figure 4.23: PL spectra D-CQDs in the presence of Hg^{2+} ion in a concentration range 0-300 ppm

A good linear correlation over the range from 0 to 30 ppm with a correlation coefficient R^2 0.997 was obtained (Figure 4.24b). The limit of detection was estimated to be and de LOQ. Notably, the obtained detection limit of the D-CQDs sensor for Hg^{2+} was much lower than those previously reported for other fluorescent probes [119]. These results indicate that our sensing system exhibits superior sensitivity compared to previously reported systems, suggesting that the D-CQDs-based sensor may be highly useful for environmental applications in mercury detection. The LOD and LOQ is calculated to be 1.5970 ppm and 5.3234 ppm respectively.

As observed in the results, the detection limits were not optimal to detect ions in water due to the preliminary nature of this study. However, with further analytical studies, it is possible to achieve better detection limits. This is evidenced by the presented in Figures 4.19, 4.21, and 4.23, which show a clear difference in quenching that warrants more detailed analysis. It is important to note that the main focus of our research was to examine the selectivity and sensitivity of the sensor in comparison to its precursors, taking into account the heteroatoms present. The evaluation demonstrated that sensitivity varies depending



(a) The non-linear trend of Hg^{2+} (ppm) and $\text{Log}(I_o/I)$ for concentrations between 0 and 300 ppm.

(b) A linear relationship between the concentration of Hg^{2+} (ppm) and $\text{Log}(I_o/I)$ for low concentrations (0 to 30 ppm)

Figure 4.24: Fluorescence Spectroscopy to different dilutions of Diethylenetriamine CQDs

on the heteroatoms (S, N, and O). Moving forward, our study will focus on stabilizing the CQDs to further enhance their performance. However, these CQDs can be used in agricultural and industrial wastewater.

4.5 Computational Chemical Calculations

4.5.1 Geometry optimization of CQDs and CQDs with Hg^{2+}

The representations of the CQDs without modifiers (C) and with N (N-CQDs), O (O-CQDs), and S (S-CQDs) modifiers, and with the incorporation of Hg^{2+} , after being optimized using the CAM B3LYP method, can be observed in the respective Figure 4.25 and Figure 4.26 .

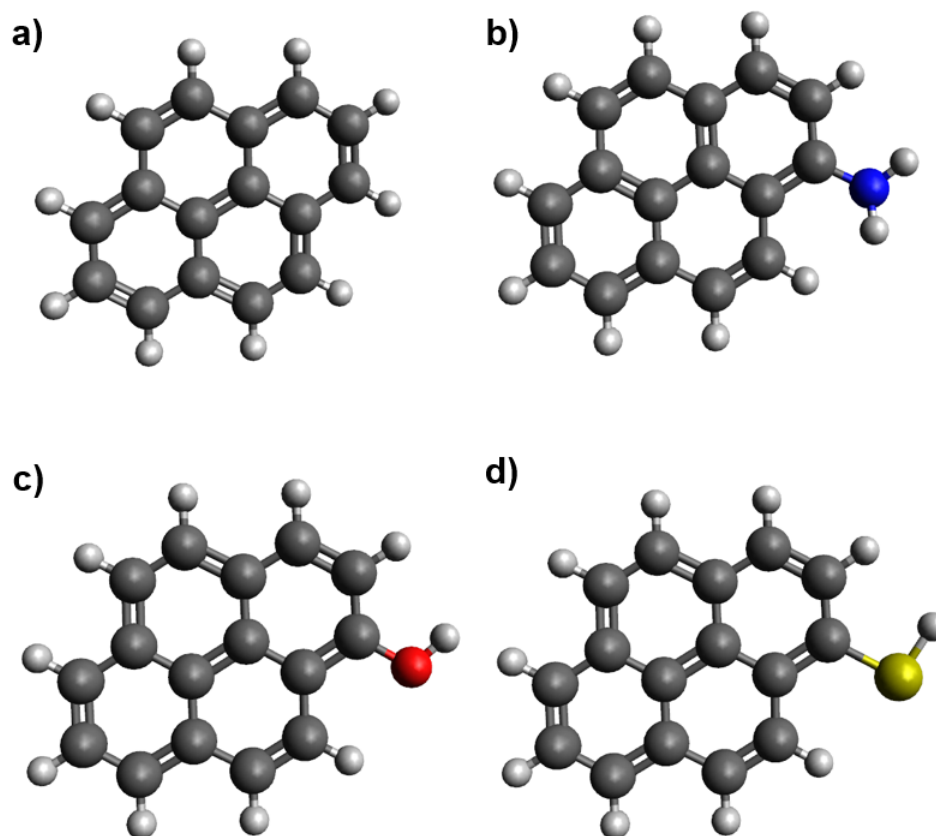


Figure 4.25: The 4 CQDs models with different structural features a) Only Carbon (C) b) N-Modifier (N-CQDs) c) O-Modifier (O-CQDs) and d) S-Modifier (S-CQDs) optimized by CAM B3LYP

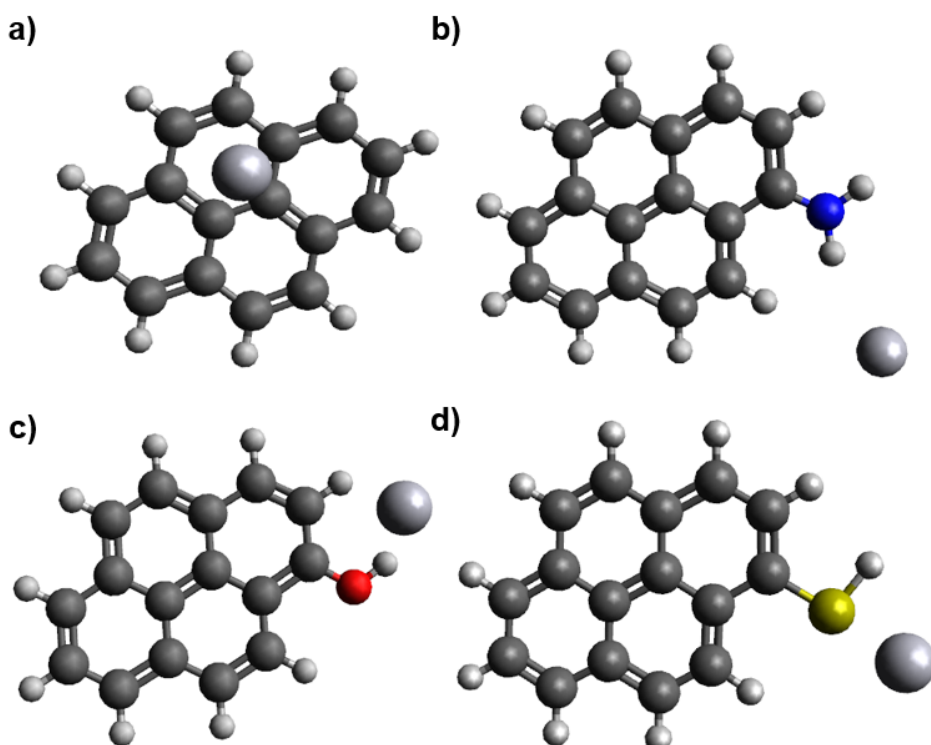


Figure 4.26: The 4 CQDs models with Hg^{2+} a) Only Carbon b) N-Modifier c) O-Modifier and d) S-Modifier optimized by CAM B3LYP

Table 4.4 exhibits the distances between Hg atom and different types of functionalized models: C-QDs, N-QDs, O-QDs, and S-QDs. These results allow us to conclude that there is no coordination of the metal, but only weak interactions could be proposed. Therefore, it mostly follows the van der Waals radius, except for carbon C-QDs (4.946 Å) and S-QDs (3.24711 Å). With carbon, there is only a very weak interaction. The case of sulfur is interesting because a shorter distance with mercury is observed, suggesting a slightly stronger interaction.

Distance Hg and Structure (Å)				
Structure	C-QDs	N-QDs	O-QDs	S-QDs
	4.946	3.6714	3.70648	3.24711

Table 4.4: Distances between Hg and CQDs model structure

In addition, the HOMO (highest occupied molecular orbital) and LUMO (lowest unoccupied molecular orbital) energies of the theoretical structures with and without the interaction with Hg^{2+} are presented in Table 4.5.

Frontier molecular orbital energies (Ev)				
Structure without Hg ²⁺	C-QDs	N-QDs	O-QDs	S-QDs
HOMO	-6.83602	-6.29451	-6.29451	-6.6537
LUMO	-0.66747	-0.45394	-0.51776	-0.7607
ΔE	-6.16854	-5.84056	-5.77675	-5.893
Structure with Hg ²⁺	C-QDs Hg ²⁺	N-QDs Hg ²⁺	O-QDs Hg ²⁺	S-QDs Hg ²⁺
HOMO	-14.429	-14.3852	-14.0498	-14.1739
LUMO	-12.0658	-10.9699	-11.4679	-11.188
ΔE	-2.36311	-3.41527	-2.58195	-2.9859

Table 4.5: HOMO-LUMO energy levels and band gaps for different CQDs with and without Hg²⁺ ions

When comparing the structures before and after interaction with Hg²⁺, all show a decrease in ΔE . This suggests that the interaction with Hg²⁺ significantly affects the energy gap, possibly making the material more conductive or altering its optical properties. Experimental and theoretical results corroborated this idea.

The sensitivity of a sensor, particularly one that operates through electron transfer, can be greatly modified by the HOMO-LUMO energy gap. The smaller the energy gap, the more easily electrons can be excited and transferred to an analyte, leading to high charge transfer from the analyte to the electrode, resulting in high detection sensitivity. Additionally, due to less energy is required to excite and move the electrons, the sensor is likely to have a much faster response time. This ease of electronic excitation can provide greater sensitivity for detecting lower concentrations of the analyte [148, 149].

However, sensitivity is also influenced by other factors, such as interaction energy. The interaction energy (E_i , shown in Table 4.6, is a crucial parameter that represents the energy required to form a stable complex between the CQDs and Hg²⁺. It is a measure of how strongly the CQDs bind to Hg²⁺ ions, which directly influences the system's ability to detect mercury.

The basic equation to calculate (E_i) is:

$$E_i = E_{\text{Structure with}} - (E_{\text{Structure}} + E_{\text{Hg}}) \quad (4.1)$$

Where:

- $E_{\text{Structure with Hg}}$ is the total energy of the Structure with Hg.

- $E_{\text{Structure}}$ is the total energy of the structure alone.
- E_{Hg} is the total energy of mercury alone.

Structure	Final Energy (kJ/mol)	Structure	Final Energy (kJ/mol)	Ei (kJ/mol)
C-QDs	-2017559.035	C-QDs-Hg	-1616425	-996.293
N-QDs	-2163072.232	N-QDs-Hg	-1761774	-1160.915
O-QDs	-2215175.755	O-QDs-Hg	-1813961	-1077.313
S-QDs	-3063161.444	S-QDs-Hg	-2661943	-1080.584
Hg	-400137.5971			

Table 4.6: Energy of Interaction for different CQDs with and without Hg²⁺ ions

From these results, a theoretical order of preferential interaction with Hg²⁺ can be constructed: $E(\text{C}) < E(\text{O}) < E(\text{S}) < E(\text{N})$. This suggests that introducing nitrogen or sulfur groups would always lead to a greater interaction with Hg²⁺ and should be thus present when thinking about the design of mercury detection.

4.5.2 UV-Vis calculations

The different models with different heteroatoms of nitrogen, sulfur and oxygen were constructed from the structure that have only carbon and once optimized, which are the vertical transition using the optimized geometry of the ground state using TDDFT/CAM-B3LYP-D4 method. The absorption spectra of each theoretical model were compared with L-CQDS, E-CQDS and D-CQDS experimental spectra.

L-CQDs experimental vs CQDs theoretical

The experimental UV-Vis spectra of L-CQDs and computational spectra of N-CQDs, O-CQDs, S-CQDs, and C-CQDs are presented in Figure 4.27, depicted in blue, red, orange, and gray, respectively. Comparison of these spectra suggests that nitrogen contributes most significantly to absorbance, followed by oxygen, and then sulfur. The theoretical structures exhibit common signals with the experimental spectrum. This analysis indicates that the band at 340 nm in L-CQDs is predominantly influenced by nitrogen. However, the presence of oxygen and sulfur may contribute to a more comprehensive spectral relationship.

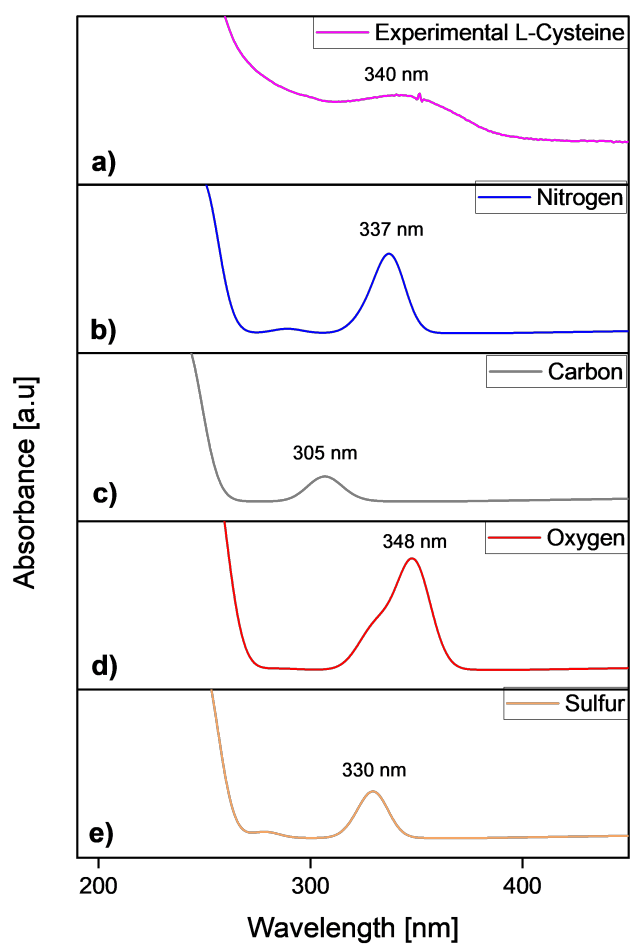


Figure 4.27: UV-Vis spectra for L-CQDS a) experimental result b) nitrogen, c) carbon, d) oxygen and e) sulfur in structure

E-CQDs experimental vs CQDs theoretical

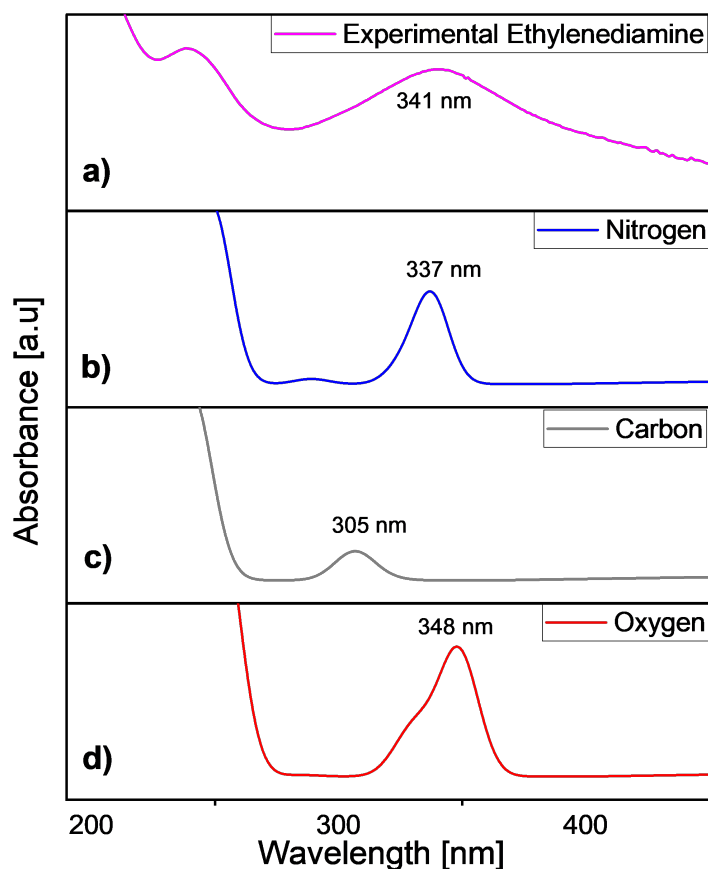


Figure 4.28: UV-Vis spectra for E-CQDS a) experimental result b) nitrogen, c) carbon and d) oxygen in structure

D-CQDs experimental vs CQDs theoretical

In ECQDs spectrum, presented in Figure 4.28, nitrogen remains as the main absorbance contributor, particularly at the 341 nm band. Finally, Figure 4.29 highlights a red-shifted absorption peak (358 nm) in DCQDs, attributed to the presence of diethylenetriamine functional groups, such as amines, which significantly alter CQD absorption. Simplified models with nitrogen and oxygen also exhibit UV absorption but are less red-shifted, underscoring the impact of more complex functional groups. Each functional group in carbon structures directly affects the optical properties of CQDs. The use of L-cysteine in CQD synthesis induces a shift in absorption, suggesting that the amino and thiol groups in L-cysteine interact with the carbon matrix to modify optical properties. Ethylenediamine, being smaller, does not cause as red-shifted absorption as diethylenetriamine, which interacts more effectively with the carbon matrix due to its larger size and more amino groups,

resulting in significant absorption influence. In summary, the theoretical results are consistent with the experimental findings. Strategically, it is advantageous to prioritize nitrogen groups for improved absorption. While oxygen groups yield high absorption intensity, they exhibit lower energetic affinity. Conversely, sulfur groups display favorable affinity but lower absorption intensity. Thus, nitrogen groups appear to be the most effective for functionalizing carbon dots to increase their absorption properties

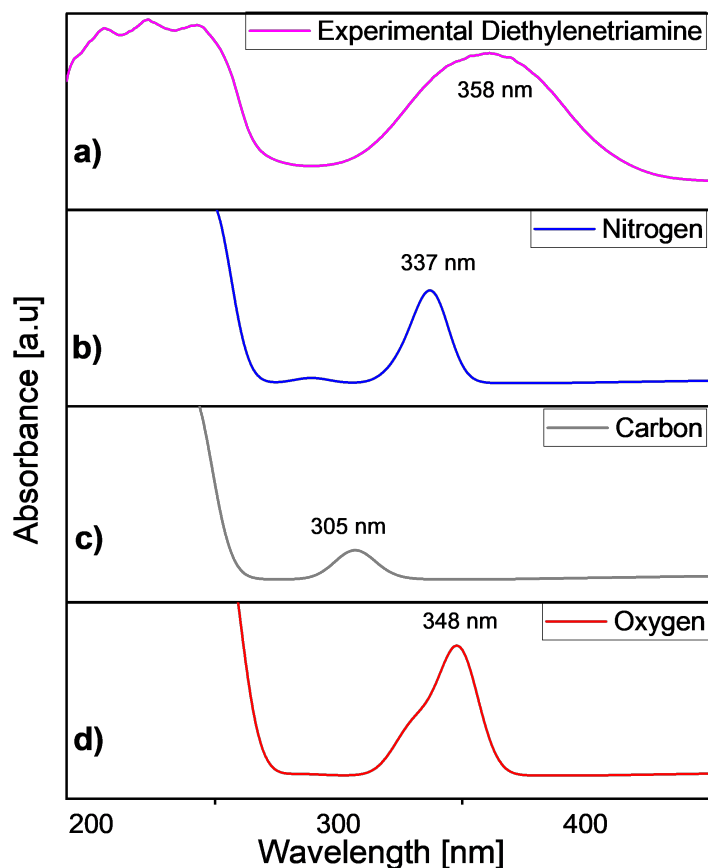


Figure 4.29: UV-Vis spectra for D-CQDS a) experimental result b) nitrogen, c) carbon and d) oxygen in structure

Each functional groups in carbon structures has a direct effect on the optical properties of CQDs. The use of L-cysteine in the synthesis of CQDs induces a shift in absorption, suggesting that the functional groups in L-cysteine (amino and thiol) interact with the carbon matrix to modify the optical properties. Additionally, ethylenediamine, being a relatively small compound, does not cause as red-shifted absorption as diethylenetriamine, which can interact with the carbon matrix to a greater extent due to its larger size. The greater number of amino groups and the length of diethylenetriamine allow it to interact more

effectively with the carbon matrix, resulting in a significant influence on absorption. Furthermore, the experimental absorption peak aligns with the calculated absorption spectrum results of the N-CQD absorption peaks. These results are consistent with the literature. According to the Jianguang et. al, [150] the optical properties of GQDs co-doped with three configurations (N and B, P, and S) were calculated using TDDFT. Through the analysis of electronic transitions, it was found that the effect of nitrogen in adjusting the electronic structure of co-doped GQDs is more significant than another heteroatoms.

4.5.3 Fluorescence analysis

The emission spectra using the optimized geometry of the excited state via the TDDFT/CAM-B3LYP-D4 method. Each theoretical model were compared with the experimental spectra of L-CQDS, E-CQDS, and D-CQDS.

L-CQDS experimental vs CQDs theoretical

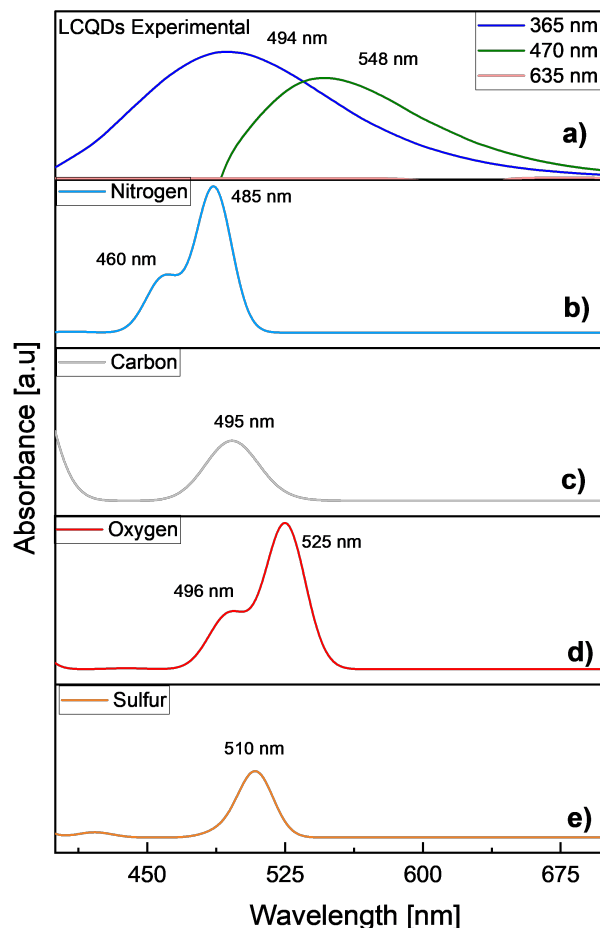


Figure 4.30: PL spectra for L-CQDS a) experimental result b) nitrogen, c) carbon, d) oxygen and e) sulfur in structure

The emission spectrum of CQDs synthesized by L-cysteine and theoretical simplified models is shown in Figure 4.30. Individual models with respective functional groups exhibited blue-green emission peaks, which reveal the contribution toward different spectral regions. The multiplicity of emission peaks of L-cysteine CQDs (494 and 548 nm) implied complex interactions between functional groups of L-cysteine and the carbon, which the creation of various emission sites or charge transfer effects should possibly bring. The additional emission states are induced or some are modified by the amino and thiol groups in L-cysteine.

E-CQDS experimental vs CQDs theoretical

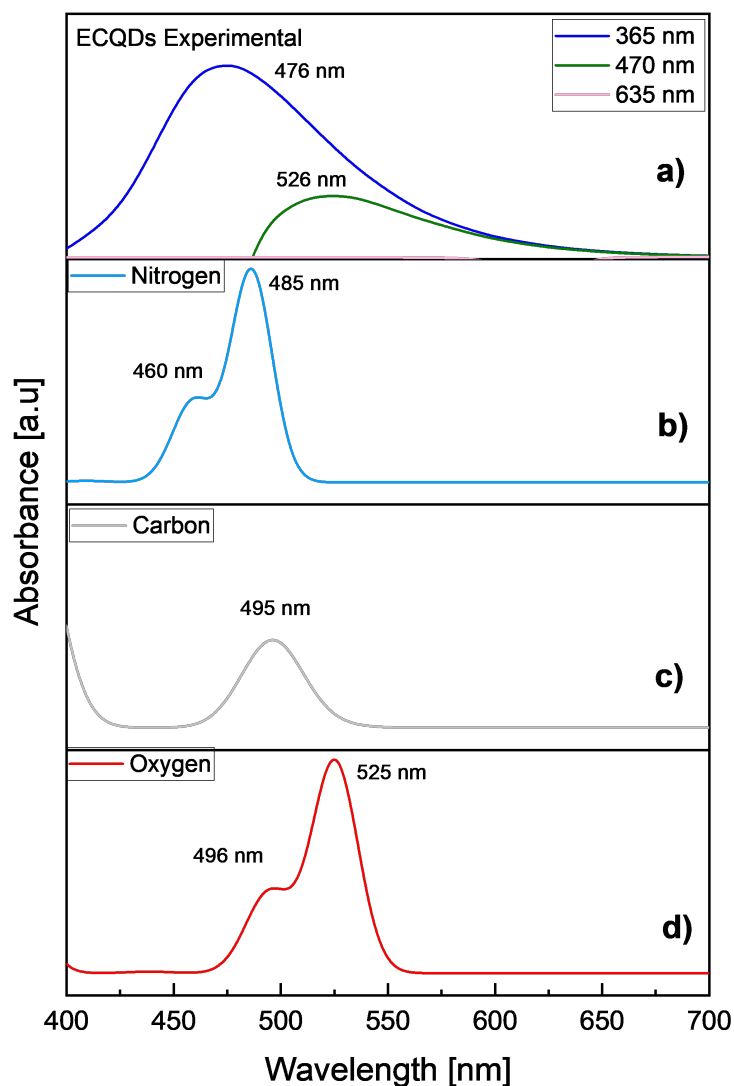


Figure 4.31: PL spectra for E-CQDS a) experimental result b) nitrogen, c) carbon and d) oxygen in structure

The E-CQDs have a broad emission spectrum with two peaks, the first located at 476 nm and the second at 526 nm. Theoretical models consisting of certain functional groups with nitrogen, pure carbon, and oxygen show emission peaks in the blue-green region of the spectrum, but these are more consistent compared to the experimental CQDs. The emission maximum at 476 nm in ethylenediamine CQDs can be attributed to electronic transitions due to the amino groups. The fact that another peak appears at 526 nm when

excited at 470 nm suggests that the CQDs may have more than one emission center or that there is some energy transfer effect.

D-CQDS experimental vs CQDs theoretical

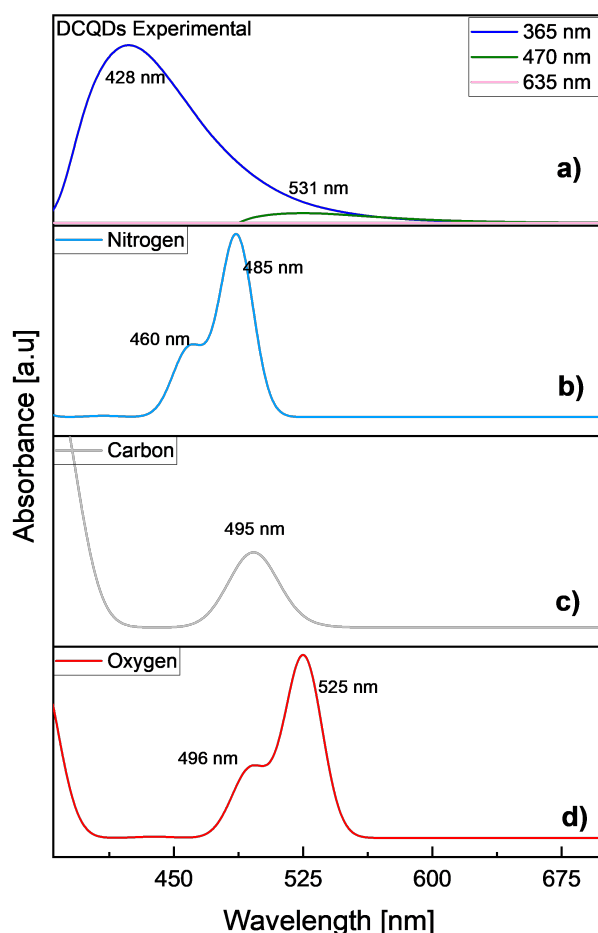


Figure 4.32: PL spectra for D-CQDS a) experimental result b) nitrogen, c) carbon and d) oxygen in structure

Finally, D-CQDS synthesized with diethylenetriamine has a relatively broad emission spectrum with two peaks at 428 nm and 531 nm, which covers an emission range from blue to green. It is hypothesized that the different amino groups in diethylenetriamine modify the carbon precursor to create more emission states or alter existing ones. The theoretical models that include particular functional groups in combination with nitrogen, pure carbon, and oxygen result in emission maxima in the blue-green range of the spectrum, though with less shift and structure compared to the experimental CQDs. In addition, the

emission peak at 428 nm in experimental spectra can be attributed to some characteristic electronic transition supported by the amino groups, while the other peak at 531 nm reveals the presence of another emitting species or some type of energy transfer occurring in the D-CQDS.

The electron-donating amino groups not only create a significant red shift in the absorption and PL spectra of CQDs but also importantly maintain the strong oscillator strengths of the main radiative transitions [151]. It can be said that the separation determines the Stokes shift of the emission of CQDs, which increases with the increasing amount of amino functional groups on the surface of the CQDs in the present study.

4.6 Stability of CQDs with Polymers

As observed in the previous study of stability of CQDs, they lose their fluorescence emission capability over time. Photochemical stability is one of the most important parameters that determine the usefulness of fluorophores in various applications. Therefore, it is crucial to find strategies to stabilize CQDs. Therefore, it would be a significant advancement if CQDs could be encapsulated or protected with a polymer capable of restricting non-specific interactions and eliminating interferences in the graphitic electronic transition between their planes. Specially to fluorescent property, CQDs are stable when they are embedded in a polymer matrix [135].

4.6.1 Stability of LCQDs with polymers into a 1:1 ratio

In the first study, CQDs were added to the suspension solution of polymer poly(N-vinyl caprolactam-co-PEGDA) (VCL-co-PEGDA) previously synthesized [152] and the solution polymer of Poly(N-isopropylacrylamide) (NIPA) in a ratio 1:1. The CQDs functionalized with L-cysteine into to polymers matrix was studied, comparing the results with the individual study of L-CQDs. In the VCL-co-PEGDA, Figure 4.33a, high fluorescence intensity was observed at 2 hours, which significantly decreased after 3 days but increased again at 8 days, suggesting a possible reconfiguration or stabilization within the matrix.

In the same way, in a NIPA polymer (Figure 4.33b) CQDs show an increase fluorescence during the time, Initially, at 2 hours, the fluorescence intensity is high with a peak at 435 nm. Over time, a blue shift to 449 nm and a decrease in fluorescence intensity are observed at 3 and 8 days, suggesting a dynamic interaction and stabilization between the L-CQDs and the NIPA matrix. In contrast, in both context, the L-CQDs without the polymer matrix show a more linear and consistent decrease in fluorescence intensity

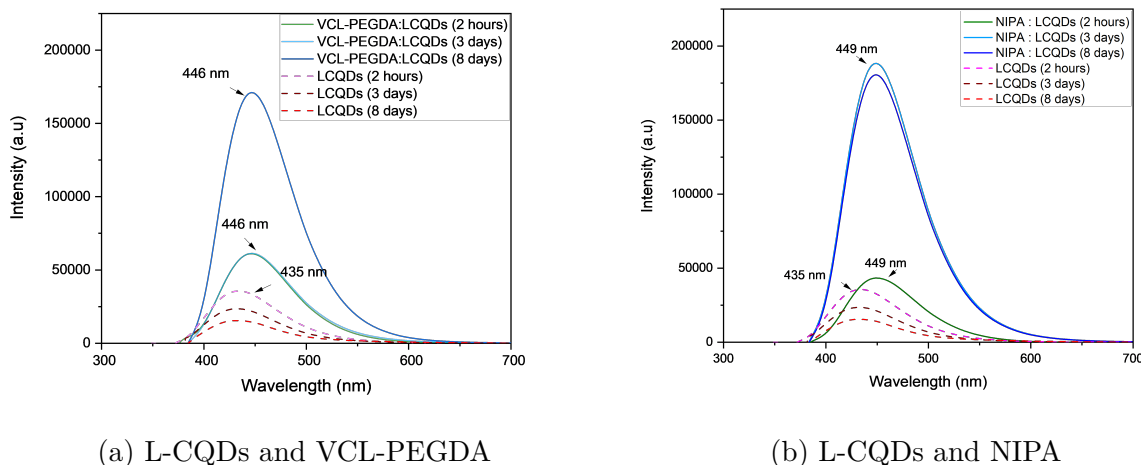


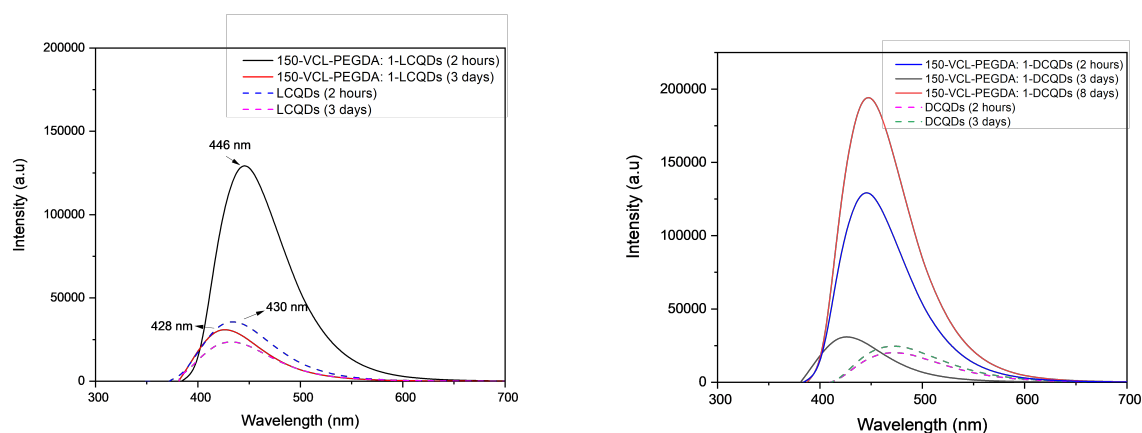
Figure 4.33: Effect of concentration in L-Cysteine-CQDs: Relation 1:1 (left) and 1:150 (right) during 8 days

over time (from 2 hours to 8 days). These results highlight the influence of the VCL-co-PEGDA and NIPA polymer in modulating the fluorescent properties of L-CQDs, likely due to specific interactions between the polymer and the quantum dots that affect their environment and, consequently, their emission.

4.6.2 Stability of L-CQDs and D-CQDs with VCL-co-PEGDA into 1:150 ratio polymer: CQDs

In this study, the incorporation a new D-CQDS and the modification of their ratios respect with VCL-co-PEGDA were compared. Figure 4.34a shows the PL spectra of incorporation of LCQDs into the VCL-co-PEG polymer matrix. The results reveals that significantly affects their fluorescence emission. Initially, at 2 hours, the fluorescence intensity is high with a peak at 446 nm. Over time, a peak shift to 430 nm and a decrease in fluorescence intensity are observed at 3 days, suggesting a dynamic interaction and stabilization between the L-CQDs and the VCL-co-PEGDA matrix. In contrast, the L-CQDs without the polymer matrix show a more linear and consistent decrease in fluorescence intensity over time. These results highlight the influence of the VCL-co-PEGDA polymer in modulating the fluorescent properties of L-CQDs at a 1:150 ratio, likely due to specific interactions between the polymer and the CQDs that affect their environment and, consequently, their emission.

This suggests that the quantity of polymer in the VCL PEG matrix is critical to the fluorescence emission from the L-CQDs. At the 1:1 ratio, one can observe dynamic reorganization, which ought to favor increasing emission over time, while at the 1:150 ratio, the



(a) L-CQDs and VCL-co-PEGDA with ratio 1:150 (b) D-CQDs and VCL-co-PEGDA with ratio 1:150

Figure 4.34: Effect of concentration on a ratio 1:150 with L-CQDs (left) and D-CQDs (right) in VCL-co-PEGDA

higher amount of polymer seems to quench the fluorescence, therefore more pronounced decay. This finding is not found in the literature and points to the importance of the L-CQDs interacting with the polymer matrix in regulating the optical properties.

On the other hand, in the Figure 4.34b, D-CQDs incorporate to VCL-co-PEGDA matrix in a relation 1:150. Initially, at 2 hours, a high fluorescence intensity with a peak around 449 nm is observed. After 3 days, the fluorescence intensity decreases significantly, maintaining a similar peak, but after 8 days, a significant increase in fluorescence intensity is noted. This behavior suggests a dynamic interaction between the D-CQDs and the VCL-PEGDA polymer matrix, with a possible reconfiguration that favors greater fluorescence emission over time. At both time intervals (2 hours and 3 days), the D-CQDs show lower fluorescence intensity compared to the results obtained in the polymer matrix and a more linear and consistent decay.

In comparison to what was found for L-CQDs in a 1:150 ratio of VCL-PEG to L-CQDs, where fluorescence loss was sustained, the fluorescence of D-CQDs in VCL-PEGDA increases over 8 days. It has been suggested that these differences in contrast depend not only on the type of CQD but also on the specific polymer matrix, possibly as a result of differences in molecular interactions and stabilization within the polymer matrix.

4.6.3 TEM Analysis of L-CQDs nanofibers

Figure 4.35 shows the TEM image of the L-CQDs, revealing numerous particles with sizes

ranging from 5 to 7 nanometers. These features are typical for the morphology and size of CQDs (less 10 nm). Additionally, the TEM image indicates that not many particles were observed, suggesting that these particles might not be the only ones exhibiting PL activity. It is important to mention that this composite was made specifically for proved the L-CQDs incorporation, and no post-study testing was conducted. The primary objective was to determine the size of the CQDs, corroborate with L-CQDs in solution and demonstrate their ability to be embedded in a polymer. According to the literature [153, 154, 155] reveals several instances of nanofibers incorporating CQDs for biomedical applications. Therefore, further study of this polymer is suggested for future research because this material has not been reported with this type of CQDs.

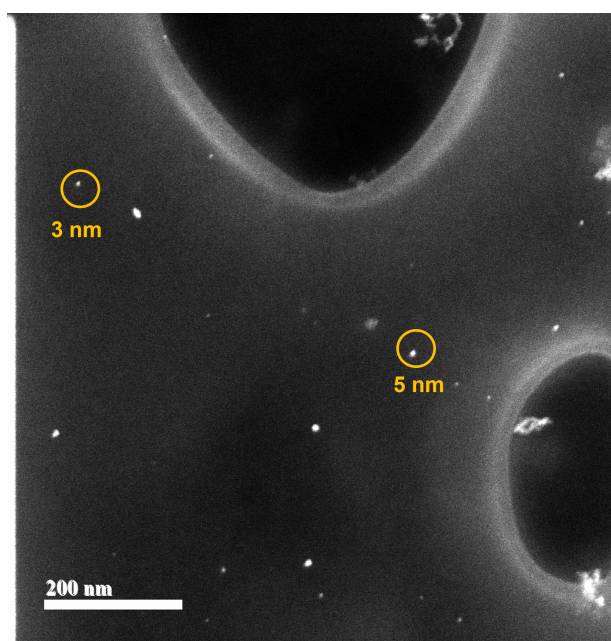


Figure 4.35: Transmission electron microscope (TEM) image Polycaprolactone embedded L-CQDs

4.6.4 D-CQDs-Incorporated PEGDA Film for Selective Sensing of Hg^{2+} ions

The fluorescence response of the hydrogel to varying concentrations of Hg^{2+} was investigated, as shown in the Figure 4.37. The results indicate that the fluorescence intensity of the hydrogel decreases continuously with increasing Hg^{2+} concentration, demonstrating that the degree of fluorescence quenching increases proportionally with the Hg^{2+} concentration.

Figure 4.37 shows the quenching effect of a polymer with D-CQDs in the presence of dif-

ferent concentrations (0-10 ppm) of Hg^{2+} . As the concentration of Hg^{2+} increases, the fluorescence intensity decreases, indicating effective quenching. Although the experiments were not conducted using specialized equipment for performing fluorescence tests on solids, the current results appear reliable due to the consistency of the observed trends, the potential repeatability of the assays, and their coherence with existing scientific literature. To enhance the accuracy and confidence in the results, the use of specialized equipment such as a fluorescence spectrophotometer, a confocal fluorescence microscopy system, or time-resolved spectroscopy platforms is recommended.

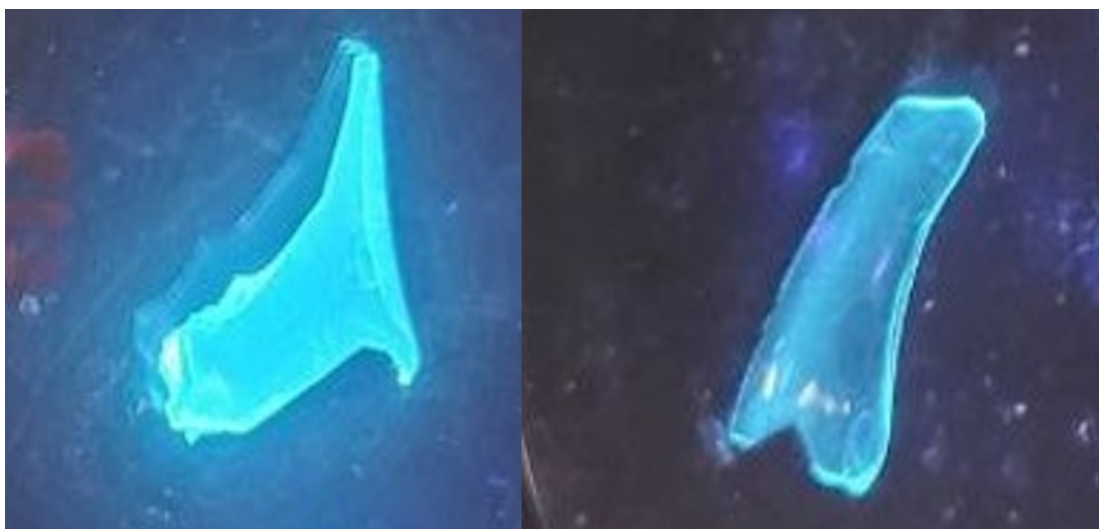


Figure 4.36: a) Fluorescence response of D-CQDs PEGDA Film and b) D-CQDs PEGDA Film with Hg^{2+} under 365 nm light

Additionally, the quenching effect was observed qualitative. In Figure 4.36, we see the polymer with D-CQDS exhibiting luminescence under a wavelength of 365 nm. In In Figure 4.36a, we see the same polymer after being exposed to a Hg^{2+} solution (10 ppm). This demonstrates the decrease in fluorescence, indicating that the polymer with the CQDs is capturing the Hg^{2+} ions.

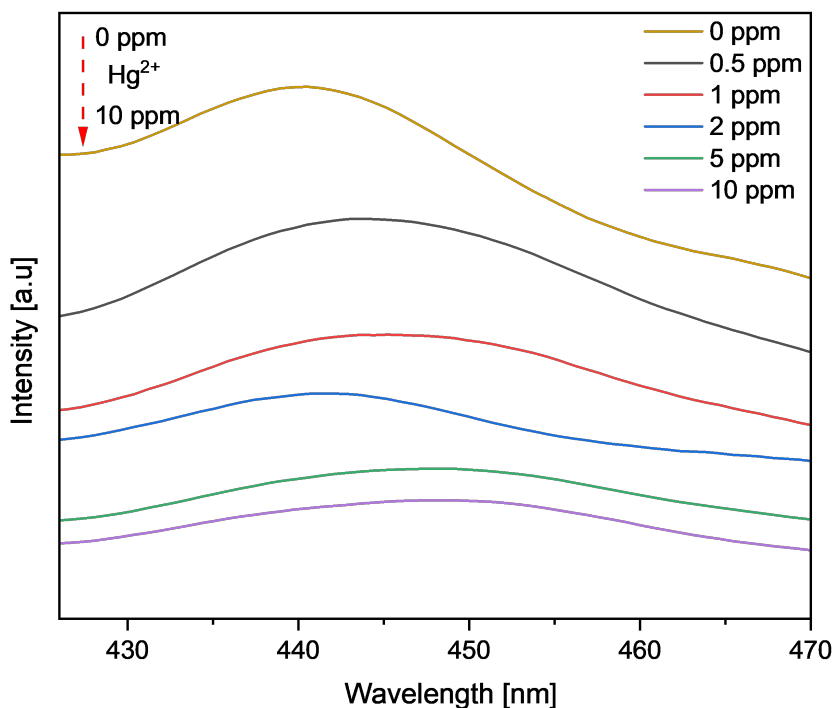


Figure 4.37: The fluorescence intensity spectra of D-CQDs with Polyethylene Glycol diacrylate in the presence of Hg^{2+} ion (0-10 ppm)

4.6.5 Characterization of D-CQDs-PEGDA Film

Figure 4.38 shows the FT-IR spectra of raw PEGDA (green line), D-CQDs (green line) and PEGDA-D-CQDs (red line). This spectrum has been considered to verify the presence of expected functional groups. The spectrum of D-CQDs itself showed characteristic peaks: O–H or N–H stretching vibration close to 3000 cm^{-1} , C=C or C=O stretching vibration between $1500\text{--}1600\text{ cm}^{-1}$, and C–O or C–N stretching vibration close to 1100 cm^{-1} . In contrast, the spectrum of pure PEGDA showed the presence of a C=O stretching vibration at 1720 cm^{-1} , indicative of the carbonyl group from diacrylate; a C–H stretching vibration between $2850\text{--}2950\text{ cm}^{-1}$, characteristic of aliphatic chains; and a C–O–C stretching vibration around 1100 cm^{-1} , indicative of the ether linkage.

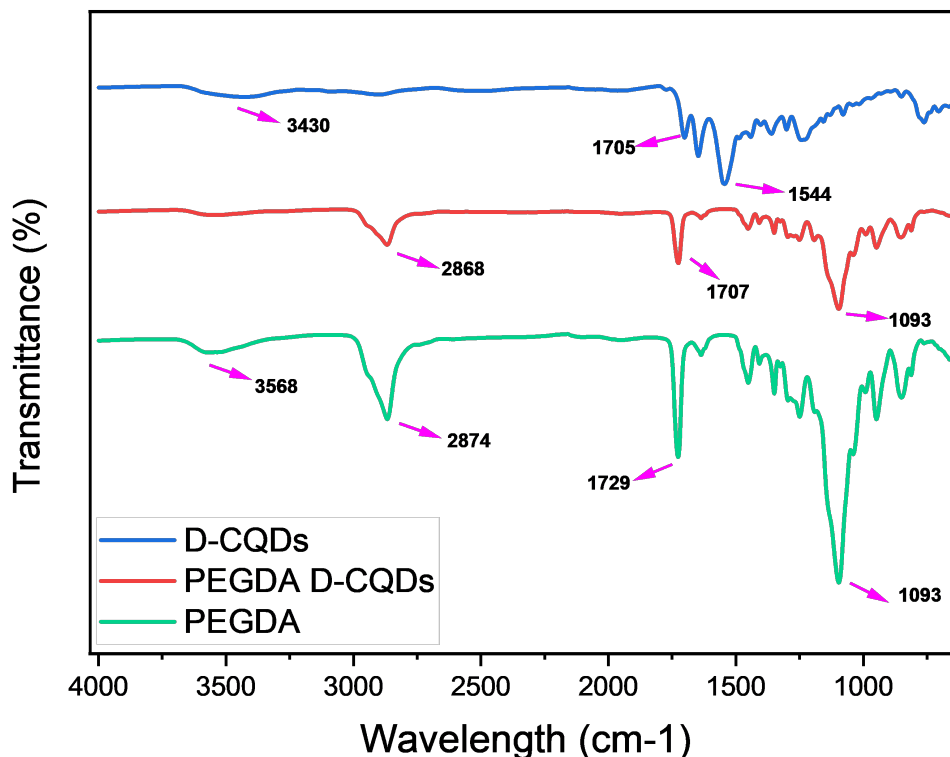


Figure 4.38: FTIR spectra of D-CQDs, PEGDA and D-CQDs-PEGDA film

In the spectrum of PEGDA-D-CQDs, any significant shifts or changes in intensity in the peaks corresponding to the C=O stretching vibration at 1720 cm^{-1} was observed suggesting the interaction with the D-CQDs. Additionally, new peaks or changes in the $1500\text{--}1600\text{ cm}^{-1}$ region reflect interactions with functional groups on D-CQDs, while changes in the region around 1100 cm^{-1} indicate interactions involving C–O–C or C–N bonds. Moreover, a broad peak observed in the $4000\text{--}3000\text{ cm}^{-1}$ region of pure PEGDA, which can be attributed to O–H stretching, showed less pronounced or different peaks for D-CQDs. The composite may show peaks similar to both components, indicating the presence of both.

The comprehensive FTIR spectra thus provide confirmation of the envisioned composite material resulting from both PEGDA and D-CQDs, with significant interactions between these two components evident through shifts in peaks and alterations in their intensities throughout the spectra.

Chapter 5

Conclusions and Recommendations

5.1 Conclusions

The research results have led to the following conclusions:

1. Among the six synthesis processes conducted using cinnamic acid, allicin, 2-mercaptoethanol, L-cysteine, ethylenediamine, and diethylenetriamine as precursors, only three CQDs with observable emission properties. These successful syntheses resulted in the production of L-CQDs, E-CQDs, and D-CQDs. **L-CQDs, E-CQDs and D-CQDs.**
2. UV-ViS showed the characteristic transitions for **L-CQDs, E-CQDs and D-CQDs.**
3. FT-IR results confirmed the chemical structures of CQDs synthesized from each precursor, revealing the differences in the structures of the heteroatoms.
4. TEM analysis reveals that the size of CQDS ranges from 3 to 5 nm.
5. **L-CQDS and D-CQDS** demonstrated, through concentration studies, that they suffer from aggregation-caused quenching, while **E-CQDS** exhibit aggregation-induced emission. The major effect of concentration was observed for **LCQDs and D-CQDS at a 1-CQDs:150-H₂O** ratio, and for **E-CQDS at a 1-CQDs:20-H₂O** ratio.
6. To stabilize CQDs over time, they were incorporated into polymer matrices. For the first time, the incorporation into VCL-PEGDA and NIPA demonstrated an increase in the fluorescent properties of the CQDs. It was revealed that fluorescence increased over time within these matrices.
7. Selectivity studies of CQDs against Al³⁺, Fe³⁺, K⁺, Cd²⁺, Co²⁺, Hg²⁺ revealed a sensitivity to Cd²⁺ for L-CQDS and to Hg²⁺ for E-CQDS and D-CQDS.

8. The fluorescence quenching effect of L-CQDs showed a linear correlation with Pb^{2+} concentrations ($R = 0.995$, $\text{LOD} = 5.63$ ppm, $\text{LOQ} = 18.79$ ppm) and Cd^{2+} ($R = 0.995$, $\text{LOD} = 0.8158$ ppm, $\text{LOQ} = 2.7194$ ppm). E-CQDs also demonstrated sensitivity towards Hg^{2+} , with a linear correlation ($R^2 = 0.999$, $\text{LOD} = 0.3597$ ppm, $\text{LOQ} = 1.1990$ ppm). The sensor based on D-CQDs showed sensitivity to Hg^{2+} ($R^2 = 0.997$, $\text{LOD} = 1.5970$ ppm, $\text{LOQ} = 5.3234$ ppm), making it useful for environmental applications. Qualitative fluorescence quenching in polymers with D-CQDS was also observed, indicating effective Hg^{2+} capture, although the use of specialized equipment is recommended for greater precision.
9. The structural analysis with FT-IR demonstrated the incorporation of D-CQDS into PEGDA. This new composite demonstrated that the PEGDA hydrogel film with Hg^{2+} is highly selective and sensitive, also showing great potential as a stabilizing matrix for D-CQDS
10. The band gaps of theoretical models revealed small values, which are ideal for sensor applications.
11. The computational studies revealed that the functional groups in carbon structures affect the optical properties of CQDs. L-cysteine modifies absorption due to its amino and thiol groups, while diethylenetriamine, with its larger size and greater number of amino groups, interacts more intensely with the carbon matrix, causing a greater shift in absorption.

5.2 Recommendations for future work

1. For ion selectivity studies, it is recommended to include anions and also to combine two or more ions in a single study.
2. For the detection limit study, it is recommended to work with lower concentrations than those previously used, as there is a wide range that can be explored, potentially achieving much lower detection levels.
3. Incorporation of CQDs into VCL-PEGDA and NIPA polymers revealed an increase in fluorescence over time. It is recommended to conduct kinetic studies on this phenomenon, as it could be of interest for various applications and has not been previously observed.
4. The incorporation of L-CQDS into polycaprolactone via electrospinning to produce nanofibers can be a potential application in the field of biomedicine. This study

demonstrated the incorporation of L-CQDS into this polymer, with the objective solely focused on microscopy studies. Therefore, this new composite has significant potential for further exploitation.

5. For theoretical studies, it is recommended to use models that closely match the experimental ones. With models more similar in size to the experimental ones, greater correlation with experimental results can be achieved, and electronic studies can be explored in greater depth.

Bibliography

- [1] A. James, "Water pollution," in *Encyclopedia of Physical Science and Technology (Third Edition)*, 3rd ed., R. A. Meyers, Ed. New York: Academic Press, 2003, pp. 699–719. [Online]. Available: <https://www.sciencedirect.com/science/article/pii/B0122274105008206>
- [2] M. I. Lone, Z.-l. He, P. J. Stoffella, and X.-e. Yang, "Phytoremediation of heavy metal polluted soils and water: progresses and perspectives," *Journal of Zhejiang University Science B*, vol. 9, no. 3, pp. 210–220, 2008.
- [3] L. A. Malik, A. Bashir, A. Qureashi, and A. H. Pandith, "Detection and removal of heavy metal ions: a review," *Environmental Chemistry Letters*, vol. 17, pp. 1495–1521, 2019.
- [4] G. Perenlei, T. W. Tee, N. A. Yusof, and G. J. Kheng, "Voltammetric detection of potassium ferricyanide mediated by multi-walled carbon nanotube/titanium dioxide composite modified glassy carbon electrode," *International Journal of Electrochemical Science*, vol. 6, no. 2, pp. 520–531, 2011.
- [5] M. B. Gumpu, S. Sethuraman, U. M. Krishnan, and J. B. B. Rayappan, "A review on detection of heavy metal ions in water – an electrochemical approach," *Sensors and Actuators B: Chemical*, vol. 213, pp. 515–533, 2015. [Online]. Available: <https://www.sciencedirect.com/science/article/pii/S092540051500307X>
- [6] M. Li, H. Gou, I. Al-Ogaidi, and N. Wu, "Nanostructured Sensors for Detection of Heavy Metals: A Review," *ACS Sustainable Chemistry & Engineering*, vol. 1, no. 7, pp. 713–723, 7 2013.
- [7] U. Resch-Genger, M. Grabolle, S. Cavaliere-Jaricot, R. Nitschke, and T. Nann, "Quantum dots versus organic dyes as fluorescent labels," *Nature Methods*, vol. 5, no. 9, pp. 763–775, 9 2008.

- [8] M. L. Liu, B. B. Chen, C. M. Li, and C. Z. Huang, "Carbon dots: synthesis, formation mechanism, fluorescence origin and sensing applications," *Green Chemistry*, vol. 21, no. 3, pp. 449–471, 2019.
- [9] W. L. Armarego, *Nanomaterials*. Elsevier, 2022, pp. 586–630.
- [10] A. Kumar, K. Kaladharan, and F.-G. Tseng, "Nanomaterials: Surface functionalization, modification, and applications," *Nanomaterials and Their Biomedical Applications*, pp. 405–438, 2021.
- [11] S. A. M. Ealia and M. P. Saravanakumar, "A review on the classification, characterisation, synthesis of nanoparticles and their application," in *IOP conference series: materials science and engineering*, vol. 263, no. 3, IOP Publishing. IOP Publishing, 2017, p. 032019.
- [12] M. S. Mauter and M. Elimelech, "Environmental applications of carbon-based nanomaterials," *Environmental Science & Technology*, vol. 42, pp. 5843–5859, 8 2008.
- [13] I. Khan, K. Saeed, and I. Khan, "Nanoparticles: Properties, applications and toxicities," *Arabian Journal of Chemistry*, vol. 12, pp. 908–931, 11 2019.
- [14] K. Pan and Q. Zhong, "Organic nanoparticles in foods: Fabrication, characterization, and utilization," *Annual Review of Food Science and Technology*, vol. 7, pp. 245–266, 2 2016.
- [15] N. Toshima and T. Yonezawa, "Bimetallic nanoparticles—novel materials for chemical and physical applications," *New Journal of Chemistry*, vol. 22, pp. 1179–1201, 1998.
- [16] M. A. Nascimento, J. C. Cruz, G. D. Rodrigues, A. F. de Oliveira, and R. P. Lopes, "Synthesis of polymetallic nanoparticles from spent lithium-ion batteries and application in the removal of reactive blue 4 dye," *Journal of Cleaner Production*, vol. 202, pp. 264–272, 11 2018.
- [17] V. Mody, R. Siwale, A. Singh, and H. Mody, "Introduction to metallic nanoparticles," *Journal of Pharmacy And Bioallied Sciences*, vol. 2, p. 282, 2010.
- [18] S. Thomas, B. S. P. Harshita, P. Mishra, and S. Talegaonkar, "Ceramic nanoparticles: Fabrication methods and applications in drug delivery," *Current Pharmaceutical Design*, vol. 21, pp. 6165–6188, 12 2015.
- [19] R. K. Goyal, *Nanomaterials and nanocomposites: synthesis, properties, characterization techniques, and applications*. CRC Press, 2017.

- [20] T. Edvinsson, "Optical quantum confinement and photocatalytic properties in two-, one- and zero-dimensional nanostructures," *Royal Society Open Science*, vol. 5, p. 180387, 9 2018.
- [21] T. N. C. for Chemistry, "Quantum dots – seeds of nanoscience," *The Nobel Prize in Chemistry 2023*, 6 2023.
- [22] T. Maxwell, M. G. N. Campos, S. Smith, M. Doomra, Z. Thwin, and S. Santra, *Quantum dots*. Elsevier, 1 2019, pp. 243–265.
- [23] A. I. Ekimov and A. A. Onushchenko, "Quantum size effect in three-dimensional microscopic semiconductor crystals," *JETP Letters*, vol. 118, pp. S15–S17, 12 1981.
- [24] E. E. AL, "Interband light absorption in a semiconductor sphere." *Fiz Tekh Poluprovodn (Leningrad)*, vol. 16, pp. 772–775, 1982.
- [25] L. E. Brus, "A simple model for the ionization potential, electron affinity, and aqueous redox potentials of small semiconductor crystallites," *The Journal of Chemical Physics*, vol. 79, pp. 5566–5571, 12 1983.
- [26] C. B. Murray, D. J. Norris, and M. G. Bawendi, "Synthesis and characterization of nearly monodisperse cde (e = sulfur, selenium, tellurium) semiconductor nanocrystallites," *Journal of the American Chemical Society*, vol. 115, pp. 8706–8715, 9 1993.
- [27] R. Koole, E. Groeneveld, D. Vanmaekelbergh, A. Meijerink, and C. D. M. Donegá, *Size effects on semiconductor nanoparticles*. Springer-Verlag Berlin Heidelberg, 9 2014, vol. 9783662448236, pp. 13–51.
- [28] X. Xu, R. Ray, Y. Gu, H. J. Ploehn, L. Gearheart, K. Raker, and W. A. Scrivens, "Electrophoretic Analysis and Purification of Fluorescent Single-Walled Carbon Nanotube Fragments," *Journal of the American Chemical Society*, vol. 126, no. 40, pp. 12736–12737, 10 2004.
- [29] A. Cayuela, M. L. Soriano, C. Carrillo-Carrión, and M. Valcárcel, "Semiconductor and carbon-based fluorescent nanodots: the need for consistency," *Chemical Communications*, vol. 52, no. 7, pp. 1311–1326, 2016.
- [30] S. Y. Lim, W. Shen, and Z. Gao, "Carbon quantum dots and their applications," *Chem. Soc. Rev.*, vol. 44, pp. 362–381, 2015. [Online]. Available: <http://dx.doi.org/10.1039/C4CS00269E>
- [31] P. K. Yadav, S. Chandra, V. Kumar, D. Kumar, and S. H. Hasan, "Carbon quantum dots: Synthesis, structure, properties, and catalytic applications

- for organic synthesis,” *Catalysts*, vol. 13, no. 2, 2023. [Online]. Available: <https://www.mdpi.com/2073-4344/13/2/422>
- [32] H. Yu, R. Shi, Y. Zhao, G. I. N. Waterhouse, L. Wu, C. Tung, and T. Zhang, “Smart utilization of carbon dots in semiconductor photocatalysis,” *Advanced Materials*, vol. 28, pp. 9454–9477, 11 2016.
- [33] K. Hola, Y. Zhang, Y. Wang, E. P. Giannelis, R. Zboril, and A. L. Rogach, “Carbon dots—emerging light emitters for bioimaging, cancer therapy and optoelectronics,” *Nano Today*, vol. 9, no. 5, pp. 590–603, 2014.
- [34] Y. Li, Z.-Z. Huang, Y. Weng, and H. Tan, “Pyrophosphate ion-responsive alginate hydrogel as an effective fluorescent sensing platform for alkaline phosphatase detection,” *Chemical Communications*, vol. 55, no. 76, pp. 11 450–11 453, 2019.
- [35] X. Sun and Y. Lei, “Fluorescent carbon dots and their sensing applications,” *TrAC Trends in Analytical Chemistry*, vol. 89, pp. 163–180, 2017.
- [36] A. Nair, J. T. Haponiuk, S. Thomas, and S. Gopi, “Natural carbon-based quantum dots and their applications in drug delivery: A review,” *Biomedicine & Pharmacotherapy*, vol. 132, p. 110834, 2020.
- [37] L. Tian, Z. Li, P. Wang, X. Zhai, X. Wang, and T. Li, “Carbon quantum dots for advanced electrocatalysis,” *Journal of Energy Chemistry*, vol. 55, pp. 279–294, 2021.
- [38] S. C. Ray, A. Saha, N. R. Jana, and R. Sarkar, “Fluorescent carbon nanoparticles: Synthesis, characterization, and bioimaging application,” *Journal of Physical Chemistry C*, vol. 113, no. 43, pp. 18 546–18 551, 2009.
- [39] D. Ozyurt, M. Al Kobaisi, R. K. Hocking, and B. Fox, “Properties, synthesis, and applications of carbon dots: A review,” *Carbon Trends*, vol. 12, p. 100276, 2023.
- [40] H. Wang, J. Shen, Y. Li, Z. Wei, G. Cao, Z. Gai, K. Hong, P. Banerjee, and S. Zhou, “Magnetic iron oxide–fluorescent carbon dots integrated nanoparticles for dual-modal imaging, near-infrared light-responsive drug carrier and photothermal therapy,” *Biomater. Sci.*, vol. 2, pp. 915–923, 2014.
- [41] P. Roy, P.-C. Chen, A. P. Periasamy, Y.-N. Chen, and H.-T. Chang, “Photoluminescent carbon nanodots: synthesis, physicochemical properties and analytical applications,” *Materials Today*, vol. 18, no. 8, pp. 447–458, 2015.

- [42] A. Sciortino, A. Cannizzo, and F. Messina, “Carbon Nanodots: A Review—From the Current Understanding of the Fundamental Photophysics to the Full Control of the Optical Response,” *C*, vol. 4, no. 4, p. 67, 12 2018.
- [43] K. Hola, A. B. Bourlinos, O. Kozak, K. Berka, K. M. Siskova, M. Havrdova, J. Tucek, K. Safarova, M. Otyepka, E. P. Giannelis, and R. Zboril, “Photoluminescence effects of graphitic core size and surface functional groups in carbon dots: COO- induced red-shift emission,” *Carbon*, vol. 70, pp. 279–286, 4 2014.
- [44] F. Yuan, S. Li, Z. Fan, X. Meng, L. Fan, and S. Yang, “Shining carbon dots: Synthesis and biomedical and optoelectronic applications,” *Nano Today*, vol. 11, no. 5, pp. 565–586, 2016.
- [45] C. Ding, A. Zhu, and Y. Tian, “Functional surface engineering of C-dots for fluorescent biosensing and in vivo bioimaging,” *Accounts of Chemical Research*, vol. 47, no. 1, pp. 20–30, 1 2014.
- [46] J. Zuo, T. Jiang, X. Zhao, X. Xiong, S. Xiao, and Z. Zhu, “Preparation and application of fluorescent carbon dots,” *Journal of Nanomaterials*, vol. 2015, no. 1, p. 787862, 2015.
- [47] M. Farshbaf, S. Davaran, F. Rahimi, N. Annabi, R. Salehi, and A. Akbarzadeh, “Carbon quantum dots: recent progresses on synthesis, surface modification and applications,” *Artificial Cells, Nanomedicine, and Biotechnology*, vol. 46, no. 7, pp. 1331–1348, 2018, pMID: 28933188. [Online]. Available: <https://doi.org/10.1080/21691401.2017.1377725>
- [48] X. Wang, Y. Feng, P. Dong, and J. Huang, “A mini review on carbon quantum dots: Preparation, properties, and electrocatalytic application,” *Frontiers in Chemistry*, vol. 7, 2019. [Online]. Available: <https://www.frontiersin.org/journals/chemistry/articles/10.3389/fchem.2019.00671>
- [49] F. Ghezzi, R. Donnini, A. Sansonetti, U. Giovanella, B. La Ferla, and B. Vercelli, “Nitrogen-Doped Carbon Quantum Dots for Biosensing Applications: The Effect of the Thermal Treatments on Electrochemical and Optical Properties,” *Molecules*, vol. 28, no. 1, 1 2023.
- [50] H. Ahmad, R. A. Khan, B. H. Koo, and A. Alsalmeh, “Systematic study of physicochemical and electrochemical properties of carbon nanomaterials,” *RSC Advances*, vol. 12, no. 24, pp. 15 593–15 600, 5 2022.

- [51] S. Dinç and R. G. Özmelleş, “Carbon dots applications in electrochemical and electrochemiluminescence sensors: Some examples of pathogen sensors,” *Turkish Journal of Analytical Chemistry*, vol. 2, no. 1, pp. 37–46, 2020.
- [52] Y. Wang and A. Hu, “Carbon quantum dots: Synthesis, properties and applications,” *Journal of Materials Chemistry C*, vol. 2, no. 34, pp. 6921–6939, 9 2014.
- [53] J. Jana, Y.-L. T. Ngo, J. S. Chung, and S. H. Hur, “Contribution of carbon dot nanoparticles in electrocatalysis: Development in energy conversion process,” *Journal of Electrochemical Science and Technology*, vol. 11, no. 3, pp. 220–237, 2020.
- [54] S. Miao, K. Liang, J. Zhu, B. Yang, D. Zhao, and B. Kong, “Hetero-atom-doped carbon dots: Doping strategies, properties and applications,” *Nano Today*, vol. 33, p. 100879, 2020.
- [55] Q. Xu, T. Kuang, Y. Liu, L. Cai, X. Peng, T. S. Sreeprasad, P. Zhao, Z. Yu, and N. Li, “Heteroatom-doped carbon dots: synthesis, characterization, properties, photoluminescence mechanism and biological applications,” *Journal of Materials Chemistry B*, vol. 4, no. 45, pp. 7204–7219, 2016.
- [56] P. Dharmalingam, V. Ramanan, G. G. Karthikeyan, N. S. Palani, R. Ilangovan, and P. Ramamurthy, “A study on the electrochemical performance of nitrogen and oxygen co-doped carbon dots derived from a green precursor for supercapacitor applications,” *Journal of Materials Science: Materials in Electronics*, vol. 28, no. 24, pp. 18 489–18 496, 12 2017.
- [57] F. Yan, Z. Sun, H. Zhang, X. Sun, Y. Jiang, and Z. Bai, “The fluorescence mechanism of carbon dots, and methods for tuning their emission color: a review,” *Microchimica Acta*, vol. 186, pp. 1–37, 2019.
- [58] H. Shabbir, E. Csapó, and M. Wojnicki, “Carbon quantum dots: The role of surface functional groups and proposed mechanisms for metal ion sensing,” *Inorganics*, vol. 11, no. 6, 2023. [Online]. Available: <https://www.mdpi.com/2304-6740/11/6/262>
- [59] H. J. Yoo, B. E. Kwak, and D. H. Kim, “Competition of the roles of π -conjugated domain between emission center and quenching origin in the photoluminescence of carbon dots depending on the interparticle separation,” *Carbon*, vol. 183, pp. 560–570, 10 2021.
- [60] O. D. Neikov and N. A. Yefimov, “Nanopowders,” in *Handbook of Non-Ferrous Metal Powders*. Elsevier, 2019, pp. 271–311.

- [61] K. Barrientos, J. P. Arango, M. S. Moncada, J. Placido, J. Patiño, S. L. Macías, C. Maldonado, S. Torijano, S. Bustamante, M. E. Londoño, and M. Jaramillo, “Carbon dot-based biosensors for the detection of communicable and non -communicable diseases,” *Talanta*, vol. 251, p. 123791, 2023. [Online]. Available: <https://www.sciencedirect.com/science/article/pii/S0039914022005872>
- [62] S. Yang, Y. Li, L. Chen, H. Wang, L. Shang, P. He, H. Dong, G. Wang, and G. Ding, “Fabrication of carbon-based quantum dots via a “bottom-up” approach: Topology, chirality, and free radical processes in “building blocks”,” *Small*, vol. 19, no. 31, p. 2205957, 2023.
- [63] B. Gayen, S. Palchoudhury, and J. Chowdhury, “Carbon dots: A mystic star in the world of nanoscience,” *Journal of Nanomaterials*, vol. 2019, no. 1, p. 3451307, 2019. [Online]. Available: <https://onlinelibrary.wiley.com/doi/abs/10.1155/2019/3451307>
- [64] O. Mkhari, T. D. Ntuli, N. J. Coville, E. N. Nxumalo, and M. S. Maubane-Nkadimeng, “Supported carbon-dots: A review,” *Journal of Luminescence*, vol. 255, p. 119552, 2023.
- [65] M. Langer, M. Paloncýová, M. Medveď, M. Pykal, D. Nachtigallová, B. Shi, A. J. Aquino, H. Lischka, and M. Otyepka, “Progress and challenges in understanding of photoluminescence properties of carbon dots based on theoretical computations,” *Applied Materials Today*, vol. 22, p. 100924, 2021.
- [66] V. Magesh, A. K. Sundramoorthy, and D. Ganapathy, “Recent advances on synthesis and potential applications of carbon quantum dots,” *Frontiers in materials*, vol. 9, p. 906838, 2022.
- [67] V. L. John, Y. Nair, and T. Vinod, “Doping and surface modification of carbon quantum dots for enhanced functionalities and related applications,” *Particle & Particle Systems Characterization*, vol. 38, no. 11, p. 2100170, 2021.
- [68] T. J. Pillar-Little, N. Wanninayake, L. Nease, D. K. Heidary, E. C. Glazer, and D. Y. Kim, “Superior photodynamic effect of carbon quantum dots through both type I and type II pathways: Detailed comparison study of top-down-synthesized and bottom-up-synthesized carbon quantum dots,” *Carbon*, vol. 140, pp. 616–623, 12 2018.
- [69] R. M. El-Shabasy, M. Farouk Elsadek, B. Mohamed Ahmed, M. Fawzy Farahat, K. N. Mosleh, and M. M. Taher, “Recent developments in carbon quantum dots:

- properties, fabrication techniques, and bio-applications,” *Processes*, vol. 9, no. 2, p. 388, 2021.
- [70] I. Singh, R. Arora, H. Dhiman, and R. Pahwa, “Carbon quantum dots: Synthesis, characterization and biomedical applications,” *Turk. J. Pharm. Sci*, vol. 15, no. 2, pp. 219–230, 2018.
- [71] A. Sharma and J. Das, “Small molecules derived carbon dots: synthesis and applications in sensing, catalysis, imaging, and biomedicine,” *Journal of nanobiotechnology*, vol. 17, no. 1, p. 92, 2019.
- [72] D. Ghosh, K. Sarkar, P. Devi, K.-H. Kim, and P. Kumar, “Current and future perspectives of carbon and graphene quantum dots: From synthesis to strategy for building optoelectronic and energy devices,” *Renewable and Sustainable Energy Reviews*, vol. 135, p. 110391, 2021.
- [73] Y. X. Gan, A. H. Jayatissa, Z. Yu, X. Chen, and M. Li, “Hydrothermal synthesis of nanomaterials,” *Journal of Nanomaterials*, vol. 2020, 2020.
- [74] A. V. Bandura and S. N. Lvov, “The ionization constant of water over wide ranges of temperature and density,” *Journal of Physical and Chemical Reference Data*, vol. 35, pp. 15–30, 2006.
- [75] M. Sevilla and A. Fuertes, “The production of carbon materials by hydrothermal carbonization of cellulose,” *Carbon*, vol. 47, pp. 2281–2289, 8 2009.
- [76] M. R. Hasan, N. Saha, T. Quaid, and M. T. Reza, “Formation of carbon quantum dots via hydrothermal carbonization: Investigate the effect of precursors,” *Energies*, vol. 14, 2 2021.
- [77] N. Nammahachak, K. K. Aup-Ngoen, P. Asanithi, M. Horpratum, S. Chuangchote, S. Ratanaphan, and W. Surareungchai, “Hydrothermal synthesis of carbon quantum dots with size tunability via heterogeneous nucleation,” *RSC Advances*, vol. 12, pp. 31 729–31 733, 11 2022.
- [78] J. Tang, J. Zhang, Y. Zhang, Y. Xiao, Y. Shi, Y. Chen, L. Ding, and W. Xu, “Influence of Group Modification at the Edges of Carbon Quantum Dots on Fluorescent Emission,” *Nanoscale Research Letters*, vol. 14, no. 1, 12 2019.
- [79] W. You, W. Zou, S. Jiang, J. Zhang, Y. Ge, G. Lu, D. W. Bahnemann, and J. H. Pan, “Fluorescent carbon quantum dots with controllable physicochemical properties

- fantastic for emerging applications: A review,” *Carbon Neutralization*, vol. 3, no. 2, pp. 245–284, 3 2024.
- [80] R. Wang, K.-Q. Lu, Z.-R. Tang, and Y.-J. Xu, “Recent progress in carbon quantum dots: synthesis, properties and applications in photocatalysis,” *Journal of Materials Chemistry A*, vol. 5, no. 8, pp. 3717–3734, 2017.
- [81] H. Ding, S. B. Yu, J. S. Wei, and H. M. Xiong, “Full-color light-emitting carbon dots with a surface-state-controlled luminescence mechanism,” *ACS Nano*, vol. 10, no. 1, pp. 484–491, 1 2016.
- [82] L. Bao, Z. L. Zhang, Z. Q. Tian, L. Zhang, C. Liu, Y. Lin, B. Qi, and D. W. Pang, “Electrochemical tuning of luminescent carbon nanodots: From preparation to luminescence mechanism,” *Advanced Materials*, vol. 23, no. 48, pp. 5801–5806, 12 2011.
- [83] S. Hu, R. Tian, L. Wu, Q. Zhao, J. Yang, J. Liu, and S. Cao, “Chemical regulation of carbon quantum dots from synthesis to photocatalytic activity,” *Chemistry - An Asian Journal*, vol. 8, no. 5, pp. 1035–1041, 5 2013.
- [84] Y. Sun, M. Zhang, B. Bhandari, and C. Yang, “Recent development of carbon quantum dots: biological toxicity, antibacterial properties and application in foods,” *Food Reviews International*, vol. 38, no. 7, pp. 1513–1532, 2022.
- [85] H. Ding, X. H. Li, X. B. Chen, J. S. Wei, X. B. Li, and H. M. Xiong, “Surface states of carbon dots and their influences on luminescence,” *Journal of Applied Physics*, vol. 127, no. 23, 6 2020.
- [86] B. D. Mansuriya and Z. Altintas, “Carbon dots: Classification, properties, synthesis, characterization, and applications in health care—an updated review (2018–2021),” *Nanomaterials*, vol. 11, no. 10, p. 2525, 2021.
- [87] H.-L. Yang, L.-F. Bai, Z.-R. Geng, H. Chen, L.-T. Xu, Y.-C. Xie, D.-J. Wang, H.-W. Gu, and X.-M. Wang, “Carbon quantum dots: Preparation, optical properties, and biomedical applications,” *Materials Today Advances*, vol. 18, p. 100376, 6 2023.
- [88] S. Chapman, M. Dobrovolskaia, K. Farahani, A. Goodwin, A. Joshi, H. Lee, T. Meade, M. Pomper, K. Ptak, J. Rao, R. Singh, S. Sridhar, S. Stern, A. Wang, J. B. Weaver, G. Woloschak, and L. Yang, “Nanoparticles for cancer imaging: The good, the bad, and the promise,” *Nano Today*, vol. 8, pp. 454–460, 2013.

- [89] Z. M. Markovic, B. Z. Ristic, K. M. Arsikin, D. G. Klisic, L. M. Harhaji-Trajkovic, B. M. Todorovic-Markovic, D. P. Kepic, T. K. Kravic-Stevovic, S. P. Jovanovic, M. M. Milenkovic, D. D. Milivojevic, V. Z. Bumbasirevic, M. D. Dramicanin, and V. S. Trajkovic, "Graphene quantum dots as autophagy-inducing photodynamic agents," *Biomaterials*, vol. 33, pp. 7084–7092, 10 2012.
- [90] M. Han, S. Zhu, S. Lu, Y. Song, T. Feng, S. Tao, J. Liu, and B. Yang, "Recent progress on the photocatalysis of carbon dots: Classification, mechanism and applications," *Nano Today*, vol. 19, pp. 201–218, 4 2018.
- [91] J. R. Lakowicz, *Instrumentation for Fluorescence Spectroscopy*. Springer US, 2006, pp. 27–61.
- [92] A. López-Beltrán, C. Iriarte-Mesa, C. Murru, F. J. Chao-Mujica, A. L. Corcho-Valdés, L. Morales-Álvarez, L. F. Desdín-García, J. Deschamps, and M. Antuch, "Design of fluorescent carbon dots (cds) for the selective detection of metal-containing ions," *Chemistry—A European Journal*, vol. 29, no. 31, p. e202300188, 2023.
- [93] M. K. Homer, D. Y. Kuo, F. Y. Dou, and B. M. Cossairt, "Photoinduced charge transfer from quantum dots measured by cyclic voltammetry," *Journal of the American Chemical Society*, vol. 144, pp. 14 226–14 234, 8 2022.
- [94] L. Wu, C. Huang, B. P. Emery, A. C. Sedgwick, S. D. Bull, X.-P. He, H. Tian, J. Yoon, J. L. Sessler, and T. D. James, "Förster resonance energy transfer (fret)-based small-molecule sensors and imaging agents," *Chemical Society Reviews*, vol. 49, no. 15, pp. 5110–5139, 2020.
- [95] M. Formica, V. Fusi, L. Giorgi, and M. Micheloni, "New fluorescent chemosensors for metal ions in solution," *Coordination Chemistry Reviews*, vol. 256, no. 1-2, pp. 170–192, 2012.
- [96] J. Tang, Y. Zhang, Y. Liu, D. Liu, H. Qin, and N. Lian, "Carbon quantum dots as a fluorophore for "inner filter effect" detection of metronidazole in pharmaceutical preparations," *RSC Advances*, vol. 9, pp. 38 174–38 182, 2019.
- [97] A. Kaur, K. Pandey, R. Kaur, N. Vashishat, and M. Kaur, "Nanocomposites of carbon quantum dots and graphene quantum dots: environmental applications as sensors," *Chemosensors*, vol. 10, no. 9, p. 367, 2022.
- [98] N. Tomczak, D. Jańczewski, M. Han, and G. J. Vancso, "Designer polymer–quantum dot architectures," *Progress in Polymer Science*, vol. 34, no. 5, pp. 393–430, 2009.

- [99] Q. Wu, X. Wang, S. A. Rasaki, T. Thomas, C. Wang, C. Zhang, and M. Yang, "Yellow-emitting carbon-dots-impregnated carboxy methyl cellulose/poly-vinyl-alcohol and chitosan: stable, freestanding, enhanced-quenching Cu²⁺ ions sensor," *Journal of Materials Chemistry C*, vol. 6, no. 16, pp. 4508–4515, 2018.
- [100] C. Wang, T. Hu, Y. Chen, Y. Xu, and Q. Song, "Polymer-Assisted Self-Assembly of Multicolor Carbon Dots as Solid-State Phosphors for Fabrication of Warm, High-Quality, and Temperature-Responsive White-Light-Emitting Devices," *ACS Applied Materials & Interfaces*, vol. 11, no. 25, pp. 22 332–22 338, 6 2019.
- [101] D. L. Zhao, S. Das, and T.-S. Chung, "Carbon Quantum Dots Grafted Antifouling Membranes for Osmotic Power Generation via Pressure-Retarded Osmosis Process," *Environmental Science & Technology*, vol. 51, no. 23, pp. 14 016–14 023, 12 2017.
- [102] Z. Yuan, X. Wu, Y. Jiang, Y. Li, J. Huang, L. Hao, J. Zhang, and J. Wang, "Carbon dots-incorporated composite membrane towards enhanced organic solvent nanofiltration performance," *Journal of Membrane Science*, vol. 549, pp. 1–11, 3 2018.
- [103] H. Koulivand, A. Shahbazi, V. Vatanpour, and M. Rahmandoust, "Development of carbon dot-modified polyethersulfone membranes for enhancement of nanofiltration, permeation and antifouling performance," *Separation and Purification Technology*, vol. 230, p. 115895, 1 2020.
- [104] X. Xu, G. Xu, F. Wei, Y. Cen, M. Shi, X. Cheng, Y. Chai, M. Sohail, and Q. Hu, "Carbon dots coated with molecularly imprinted polymers: A facile bioprobe for fluorescent determination of caffeic acid," *Journal of Colloid and Interface Science*, vol. 529, pp. 568–574, 11 2018.
- [105] V. Rimal, S. Shishodia, and P. K. Srivastava, "Novel synthesis of high-thermal stability carbon dots and nanocomposites from oleic acid as an organic substrate," *Applied Nanoscience*, vol. 10, no. 2, pp. 455–464, 2 2020.
- [106] L. Janus, M. Piątkowski, J. Radwan-Pragłowska, and A. Sierakowska, "Carbon Quantum Dots (CQDs) prepared from waste biomass as a new class of biomaterials with luminescent properties," *Inzynieria Mineralna*, vol. 2020, no. 2, pp. 57–62, 2020.
- [107] M. Zufajri, S. Sudewi, S. Ismulyati, A. Rasool, M. Adlim, and G. G. Huang, "Carbon dot/polymer composites with various precursors and their sensing applications: A review," *Coatings*, vol. 11, no. 9, 2021. [Online]. Available: <https://www.mdpi.com/2079-6412/11/9/1100>

- [108] W. A. Laftah, S. Hashim, and A. N. Ibrahim, "Polymer hydrogels: A review," *Polymer-Plastics Technology and Engineering*, vol. 50, no. 14, pp. 1475–1486, 2011.
- [109] S. Kanungo, N. Gupta, R. Rawat, B. Jain, A. Solanki, A. Panday, P. Das, and S. Ganguly, "Doped carbon quantum dots reinforced hydrogels for sustained delivery of molecular cargo," *Journal of Functional Biomaterials*, vol. 14, no. 3, p. 166, 2023.
- [110] J. Zhang, J. Jin, J. Wan, S. Jiang, Y. Wu, W. Wang, X. Gong, and H. Wang, "Quantum dots-based hydrogels for sensing applications," *Chemical Engineering Journal*, vol. 408, p. 127351, 2021.
- [111] T. Wang, A. Wang, R. Wang, Z. Liu, Y. Sun, G. Shan, Y. Chen, and Y. Liu, "Carbon dots with molecular fluorescence and their application as a "turn-off" fluorescent probe for ferricyanide detection," *Scientific Reports*, vol. 9, 12 2019.
- [112] H. Boaz and G. K. Rollefson, "The quenching of fluorescence. deviations from the stern-volmer law," *Journal of the American Chemical Society*, vol. 72, pp. 3435–3443, 8 1950.
- [113] M. E. K. Wahba, N. El-Enany, and F. Belal, "Application of the stern–volmer equation for studying the spectrofluorimetric quenching reaction of eosin with clindamycin hydrochloride in its pure form and pharmaceutical preparations," *Analytical Methods*, vol. 7, pp. 10 445–10 451, 2015.
- [114] F. Neese, "Software update: The orca program system—version 5.0," *Wiley Interdisciplinary Reviews: Computational Molecular Science*, vol. 12, no. 5, p. e1606, 2022.
- [115] D. Xiao, R. Pan, S. Li, J. He, M. Qi, S. Kong, Y. Gu, R. Lin, and H. He, "Porous carbon quantum dots: One step green synthesis vial-cysteine and applications in metal ion detection," *RSC Advances*, vol. 5, no. 3, pp. 2039–2046, 2015.
- [116] Y. Mao, C. Zhao, S. Ge, T. Luo, J. Chen, J. Liu, F. Xi, and J. Liu, "Gram-scale synthesis of nitrogen doped graphene quantum dots for sensitive detection of mercury ions and L-cysteine," *RSC Advances*, vol. 9, no. 57, pp. 32 977–32 983, 2019.
- [117] P. Duan, B. Zhi, L. Coburn, C. L. Haynes, and K. Schmidt-Rohr, "A molecular fluorophore in citric acid/ethylenediamine carbon dots identified and quantified by multinuclear solid-state nuclear magnetic resonance," *Magnetic Resonance in Chemistry*, vol. 58, pp. 1130–1138, 11 2020.

- [118] M. Zhang, X. Long, Y. Ma, and S. Wu, "Re-discussion on the essence of the ultra-bright fluorescent carbon dots synthesized by citric acid and ethylenediamine," *Optical Materials*, vol. 135, 1 2023.
- [119] J. He, H. Zhang, J. Zou, Y. Liu, J. Zhuang, Y. Xiao, and B. Lei, "Carbon dots-based fluorescent probe for "off-on" sensing of Hg(II) and I-," *Biosensors and Bioelectronics*, vol. 79, pp. 531–535, 5 2016.
- [120] N. Ibrayev, R. Dzhanabekova, E. Seliverstova, and G. Amanzholova, "Optical properties of N- and S-doped carbon dots based on citric acid and L-cysteine," *Fullerenes, Nanotubes and Carbon Nanostructures*, vol. 30, no. 1, pp. 22–26, 1 2022.
- [121] F. Gao, S. Ma, J. Li, K. Dai, X. Xiao, D. Zhao, and W. Gong, "Rational design of high quality citric acid-derived carbon dots by selecting efficient chemical structure motifs," *Carbon*, vol. 112, pp. 131–141, 2 2017.
- [122] W. J. Niu, Y. Li, R. H. Zhu, D. Shan, Y. R. Fan, and X. J. Zhang, "Ethylenediamine-assisted hydrothermal synthesis of nitrogen-doped carbon quantum dots as fluorescent probes for sensitive biosensing and bioimaging," *Sensors and Actuators, B: Chemical*, vol. 218, pp. 229–236, 5 2015.
- [123] S. Devi, A. Kaur, S. Sarkar, S. Vohra, and S. Tyagi, "Synthesis and characterization of highly luminescent N-doped carbon quantum dots for metal ion sensing," *Integrated Ferroelectrics*, vol. 186, no. 1, pp. 32–39, 1 2018.
- [124] W. Fawaz, J. Hasian, and I. Alghoraibi, "Synthesis and physicochemical characterization of carbon quantum dots produced from folic acid," *Scientific Reports*, vol. 13, no. 1, 12 2023.
- [125] K. Linehan and H. Doyle, "Size controlled synthesis of carbon quantum dots using hydride reducing agents," *J. Mater. Chem. C*, vol. 2, pp. 6025–6031, 2014.
- [126] Y. Wei, L. Chen, S. Zhao, X. Liu, Y. Yang, J. Du, Q. Li, and S. Yu, "Green-emissive carbon quantum dots with high fluorescence quantum yield: Preparation and cell imaging," *Frontiers of Materials Science*, vol. 15, pp. 253–265, 6 2021.
- [127] Y. Zhang, L. Hu, Y. Sun, C. Zhu, R. Li, N. Liu, H. Huang, Y. Liu, C. Huang, and Z. Kang, "One-step synthesis of chiral carbon quantum dots and their enantioselective recognition," *RSC Advances*, vol. 6, pp. 59 956–59 960, 2016.
- [128] X. D. Mai, T. T. K. Chi, T. C. Nguyen, and V. T. Ta, "Scalable synthesis of highly photoluminescence carbon quantum dots," *Materials Letters*, vol. 268, 6 2020.

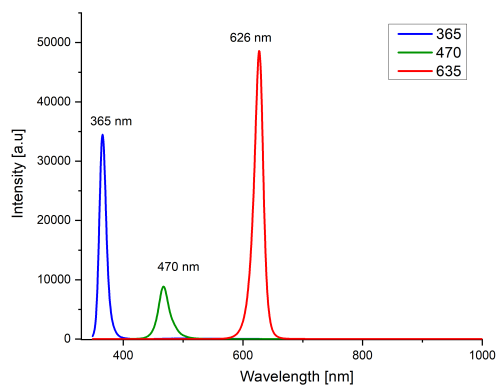
- [129] Z. Li, H. Yu, T. Bian, Y. Zhao, C. Zhou, L. Shang, Y. Liu, L. Z. Wu, C. H. Tung, and T. Zhang, “Highly luminescent nitrogen-doped carbon quantum dots as effective fluorescent probes for mercuric and iodide ions,” *Journal of Materials Chemistry C*, vol. 3, pp. 1922–1928, 3 2015.
- [130] Y. Liu, Y. Zhang, J. Niu, L. Nie, S. Huang, H. Liu, S. Yuan, and Q. Zhou, “Selective fluorescent probe for sensitive determination of bisphenol a based on molecularly imprinted polymers decorated carbon dots derived from citric acid and ethylenediamine,” *Chemosphere*, vol. 324, 5 2023.
- [131] S. K. Tammina, D. Yang, S. Koppala, C. Cheng, and Y. Yang, “Highly photoluminescent n, p doped carbon quantum dots as a fluorescent sensor for the detection of dopamine and temperature,” *Journal of Photochemistry and Photobiology B: Biology*, vol. 194, pp. 61–70, 5 2019.
- [132] J. Yang, Y. Yang, L. Su, X. Tao, J. Zhang, Y. Chen, and L. Yang, “Diethylenetriamine- β -cd-modified carbon quantum dots for selective fluorescence sensing of hg²⁺ and fe³⁺ and cellular imaging,” *Spectrochimica Acta Part A: Molecular and Biomolecular Spectroscopy*, vol. 291, p. 122364, 4 2023.
- [133] T. Han, T. Yan, Y. Li, W. Cao, X. Pang, Q. Huang, and Q. Wei, “Eco-friendly synthesis of electrochemiluminescent nitrogen-doped carbon quantum dots from diethylene triamine pentacetate and their application for protein detection,” *Carbon*, vol. 91, pp. 144–152, 5 2015.
- [134] A. Aghamali, M. Khosravi, H. Hamishehkar, N. Modirshahla, and M. A. Behnajady, “Synthesis and characterization of high efficient photoluminescent sunlight driven photocatalyst of n-carbon quantum dots,” *Journal of Luminescence*, vol. 201, pp. 265–274, 9 2018.
- [135] W. Zhang, L. Shi, Y. Liu, X. Meng, H. Xu, Y. Xu, B. Liu, X. Fang, H. B. Li, and T. Ding, “Supramolecular interactions via hydrogen bonding contributing to citric acid derived carbon dots with high quantum yield and sensitive photoluminescence,” *RSC Advances*, vol. 7, pp. 20 345–20 353, 2017.
- [136] Y. Ru, G. I. Waterhouse, and S. Lu, “Aggregation in carbon dots: Special issue: Emerging investigators,” *Aggregate*, vol. 3, no. 6, p. e296, 2022.
- [137] J. R. Adsetts, S. Hoesterey, C. Gao, D. A. Love, and Z. Ding, “Electrochemiluminescence and photoluminescence of carbon quantum dots controlled by aggregation-

- induced emission, aggregation-caused quenching, and interfacial reactions,” *Langmuir*, vol. 36, pp. 14 432–14 442, 12 2020.
- [138] Z. Zhao, H. Zhang, J. W. Lam, and B. Z. Tang, “Aggregation-induced emission: new vistas at the aggregate level,” *Angewandte Chemie International Edition*, vol. 59, no. 25, pp. 9888–9907, 2020.
- [139] Z. X. Liu, Z. L. Wu, M. X. Gao, H. Liu, and C. Z. Huang, “Carbon dots with aggregation induced emission enhancement for visual permittivity detection,” *Chemical Communications*, vol. 52, pp. 2063–2066, 2016.
- [140] F. Arshad, A. Pal, and M. P. Sk, “Review—aggregation-induced emission in carbon dots for potential applications,” *ECS Journal of Solid State Science and Technology*, vol. 10, p. 021001, 2 2021.
- [141] S. Dua, P. Kumar, B. Pani, A. Kaur, M. Khanna, and G. Bhatt, “Stability of carbon quantum dots: a critical review,” *RSC advances*, vol. 13, no. 20, pp. 13 845–13 861, 2023.
- [142] R. D. Hancock and A. E. Martell, “Ligand design for selective complexation of metal ions in aqueous solution,” *Chemical Reviews*, vol. 89, no. 8, pp. 1875–1914, 1989.
- [143] R. Tabaraki and A. Nateghi, “Nitrogen- Doped Graphene Quantum Dots: ”turn-off” Fluorescent Probe for Detection of Ag⁺ Ions,” *Journal of Fluorescence*, vol. 26, no. 1, pp. 297–305, 1 2016.
- [144] World Health Organization, *Guidelines for Drinking-Water Quality*, 4th ed., Geneva, Ed. World Health Organization, 2017.
- [145] M. Tang, X. Liu, N. Zhang, J. Pang, Y. Zou, F. Chai, H. Wu, and L. Chen, “Synthesis of nitrogen and sulfur codoped carbon dots and application for fluorescence detection of cd (ii) in real water samples,” *Analytical Methods*, vol. 11, no. 40, pp. 5214–5221, 2019.
- [146] D. Gu, L. Hong, L. Zhang, H. Liu, and S. Shang, “Nitrogen and sulfur co-doped highly luminescent carbon dots for sensitive detection of Cd (II) ions and living cell imaging applications,” *Journal of Photochemistry and Photobiology B: Biology*, vol. 186, pp. 144–151, 9 2018.
- [147] K. Jlassi, K. Eid, M. H. Sliem, A. M. Abdullah, M. M. Chehimi, and I. Krupa, “Rational synthesis, characterization, and application of environmentally friendly

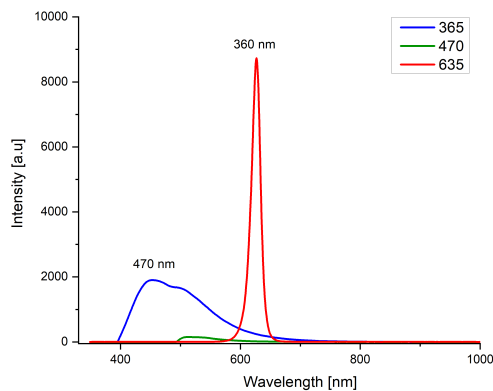
- (polymer–carbon dot) hybrid composite film for fast and efficient UV-assisted Cd²⁺ removal from water,” *Environmental Sciences Europe*, vol. 32, no. 1, 12 2020.
- [148] M. Noei, “Different electronic sensitivity of bn and aln nanoclusters to so₂ gas: Dft studies,” *Vacuum*, vol. 135, pp. 44–49, 1 2017.
- [149] H. Sajid, T. Mahmood, and K. Ayub, “High sensitivity of polypyrrole sensor for uric acid over urea, acetamide and sulfonamide: A density functional theory study,” *Synthetic Metals*, vol. 235, pp. 49–60, 1 2018.
- [150] J. Feng, Q. Guo, N. Song, H. Liu, H. Dong, Y. Chen, L. Yu, and L. Dong, “Density functional theory study on optical and electronic properties of co-doped graphene quantum dots based on different nitrogen doping patterns,” *Diamond and Related Materials*, vol. 113, 3 2021.
- [151] E. V. Kundelev, N. V. Tepliakov, M. Y. Leonov, V. G. Maslov, A. V. Baranov, A. V. Fedorov, I. D. Rukhlenko, and A. L. Rogach, “Amino functionalization of carbon dots leads to red emission enhancement,” *Journal of Physical Chemistry Letters*, vol. 10, pp. 5111–5116, 9 2019.
- [152] R. H. J. Fernanda, “Biocompatible thermo-responsive poly(vcl-co-pegda) hydrogels for controlled drug delivery systems,” B.S. Thesis, Chemistry Science and Engineering, Yachay Tech, 2020.
- [153] M. Ghorghi, M. Rafienia, V. Nasirian, F. S. Bitaraf, A. M. Gharravi, and A. Zarrabi, “Electrospun captopril-loaded pcl -carbon quantum dots nanocomposite scaffold: Fabrication, characterization, and in vitro studies,” *Polymers for Advanced Technologies*, vol. 31, pp. 3302–3315, 12 2020.
- [154] C. Yan, Y. Ren, X. Sun, L. Jin, X. Liu, H. Chen, K. Wang, M. Yu, and Y. Zhao, “Photoluminescent functionalized carbon quantum dots loaded electroactive silk fibroin/pla nanofibrous bioactive scaffolds for cardiac tissue engineering,” *Journal of Photochemistry and Photobiology B: Biology*, vol. 202, p. 111680, 1 2020.
- [155] S. Rastegar, M. Mehdikhani, A. Bigham, E. Poorazizi, and M. Rafienia, “Poly glycerol sebacate/ polycaprolactone/ carbon quantum dots fibrous scaffold as a multi-functional platform for cardiac tissue engineering,” *Materials Chemistry and Physics*, vol. 266, p. 124543, 7 2021.

Appendices

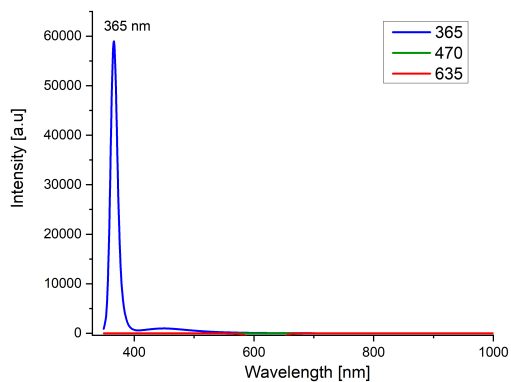
Appendix 1. Spectras of allicine (A-CQDs), cinnamic acid (CN-CQDs) and 2-mercaptoethanol (M-CQDs) synthesis



(a) PL spectra CN-CQDs



(b) PL spectra A-CQDs



(c) PL spectra M-CQDs